

Jet radius dependence of dijet momentum balance and suppression in Pb+Pb collisions at 5.02 TeV with the ATLAS detector

G. Aad *et al.*^{*}
(ATLAS Collaboration)



(Received 29 July 2024; accepted 22 October 2024; published 25 November 2024)

This paper describes a measurement of the jet radius dependence of the dijet momentum balance between leading back-to-back jets in 1.72 nb^{-1} of Pb+Pb collisions collected in 2018 and 255 pb^{-1} of pp collisions collected in 2017 by the ATLAS detector at the LHC. Both datasets were collected at $\sqrt{s_{\text{NN}}} = 5.02 \text{ TeV}$. Jets are reconstructed using the anti- k_t algorithm with jet radius parameters $R = 0.2, 0.3, 0.4, 0.5$, and 0.6 . The dijet momentum balance distributions are constructed for leading jets with transverse momentum p_T from 100 to 562 GeV for $R = 0.2, 0.3$, and 0.4 jets, and from 158 to 562 GeV for $R = 0.5$ and 0.6 jets. The absolutely normalized dijet momentum balance distributions are constructed to compare measurements of the dijet yields in Pb+Pb collisions directly to the dijet cross sections in pp collisions. For all jet radii considered here, there is a suppression of more balanced dijets in Pb+Pb collisions compared with pp collisions, while for more imbalanced dijets there is an enhancement. There is a jet radius dependence to the dijet yields, being stronger for more imbalanced dijets than for more balanced dijets. Additionally, jet pair nuclear modification factors are measured. The subleading jet yields are found to be more suppressed than leading jet yields in dijets. A jet radius dependence of the pair nuclear modification factors is observed, with the suppression decreasing with increasing jet radius. These measurements provide new constraints on jet quenching scenarios in the quark-gluon plasma.

DOI: [10.1103/PhysRevC.110.054912](https://doi.org/10.1103/PhysRevC.110.054912)

I. INTRODUCTION

The physics aim of the heavy-ion program at the Large Hadron Collider (LHC) [1–3] and the BNL Relativistic Heavy Ion Collider (RHIC) [4–8] is to produce the quark-gluon plasma (QGP) and measure its properties. The QGP is an ultrahot and ultradense state of matter in which quarks and gluons are no longer confined in color-neutral hadrons (for a recent review, see Ref. [9]). To understand the properties of the QGP at short distances, high transverse momentum (p_T) probes such as jets are used [10,11]. Jets traversing the QGP experience *jet quenching*, characterized by a reduction in the overall jet energy compared with expectations from pp collisions. This phenomenon is understood to arise from radiative and collisional energy loss, reducing the jet p_T by moving the energy of the initial parton to wider angles, with some of it ending up outside the predefined jet cone [12]. Jet quenching is typically quantified by the overall rate of

jets in a given centrality¹ interval in Pb+Pb collisions and at a given p_T compared with geometric expectations based on measured cross sections in pp , commonly known as the *nuclear modification factor*,

$$R_{AA} = \frac{1}{N_{\text{evt}}^{AA}} \frac{dN_{\text{jet}}^{AA}}{dp_T} \left/ \left(\langle T_{AA} \rangle \frac{d\sigma_{\text{jet}}^{pp}}{dp_T} \right) \right., \quad (1)$$

where N_{evt}^{AA} is the total number of minimum-bias Pb+Pb events and $\langle T_{AA} \rangle$ is the mean nuclear thickness function [13] for the centrality interval. This normalization accounts for the geometric enhancement in hard scattering rates in Pb+Pb collisions with respect to pp collisions. The jet yield in Pb+Pb collisions is N_{jet}^{AA} , and the jet cross section in pp collisions is σ_{jet}^{pp} , both measured as a function of the jet p_T . In the most central Pb+Pb collisions, R_{AA} is observed to be approximately 0.5, dependent on the jet p_T and jet radius, up to a p_T of approximately 1 TeV [14–17]. Measurements of the suppression of jets of different radii are of great interest to understand where the lost energy is with respect to the jet axis, how the energy is distributed among the jet particles, and to measure the possible response of the QGP to the presence of the jet

^{*}Full author list given at the end of the article.

Published by the American Physical Society under the terms of the Creative Commons Attribution 4.0 International license. Further distribution of this work must maintain attribution to the author(s) and the published article's title, journal citation, and DOI. Open access publication funded by CERN.

¹Centrality characterizes the degree to which the colliding nuclei overlap. The most central collisions have a large overlap and the highest particle multiplicities, while the most peripheral collisions have only a minimal overlap and have particle multiplicities closer to those of pp collisions at the same nucleon-nucleon collision energy.

[18,19]. For $p_T > 400$ GeV in central collisions, CMS has measured no significant dependence of the jet R_{AA} on the jet radius [15]. At much lower momentum ($p_T < 100$ GeV), measurements from ATLAS [20] found a modest decrease in jet quenching (an increased jet yield) with increasing jet radius. In contrast, recent measurements from ALICE [21] in a similar momentum region suggest that jet quenching *increases* with increasing jet radius. For recent reviews of jet quenching, see Refs. [11,22].

Jets are largely produced in pairs in $2 \rightarrow 2$ partonic scattering processes. The quantum chromodynamics (QCD) evolution of the partons after the scattering gives rise to back-to-back jets, referred to here as “dijets.” The two jets are expected to experience asymmetric energy loss due to traversing unequal path lengths in the QGP [23], driven by the geometry of the overlapping nuclei and the relative orientation of the jet trajectories through the QGP. Measurements of the azimuthal anisotropy of jets [24] have shown that the geometry of the overlapping nuclei affects the relative rates of jets measured in Pb+Pb collisions. Additionally, jets are also expected to experience jet-by-jet fluctuations in the energy-loss process [25]. While single jets can be used to study jet quenching, dijets can also be used as a complementary probe. The measurement of the p_T balance of dijets provides a way to constrain the relative importance of fluctuations and geometry in jet quenching. The shape modification of jets in dijets has been less studied than for single jets, where the jet shape is the distribution of charged-particle transverse momentum as a function of the angular distance to the jet axis. Studying jet shapes, CMS observed a redistribution of the charged-particle transverse momentum with an enhancement at larger angular distances with respect to the jet axis, when comparing Pb+Pb to pp collisions [26]. In this context, measurements of the jet radius dependence of the dijet balance are especially interesting and can provide different sensitivity to the location of the lost energy than is available with single jet measurements.

To compare the transverse momenta of the two jets that comprise a dijet, the leading dijet momentum balance

$$x_J \equiv p_{T,2}/p_{T,1} \quad (2)$$

is measured. The leading dijet is constructed using the two highest- p_T jets out of the set of jets in an event, $p_{T,1}$ is the transverse momentum of the highest- p_T (leading) jet, and $p_{T,2}$, of the second-highest- p_T (subleading) jet.

In pp collisions, the showering process in vacuum and higher-order scattering processes can lead to imbalanced dijet transverse momenta. However, the most probable situation is that the jets are nearly balanced in p_T [27,28]. Previous dijet measurements in Pb+Pb collisions have shown that jets are more likely to be more imbalanced in Pb+Pb collisions than in pp collisions [27–30].

Early dijet publications reported only the dijet momentum balance normalized by the measured dijet yields [27,29,30], to study the changes in the shape of the x_J distribution as a function of the heavy-ion collision centrality. Reference [28] addressed the absolute rate at which $R = 0.4$ dijets are produced in Pb+Pb collisions, assessing whether leading dijets are suppressed at levels similar to those for inclusive jets [14]. This paper extends the studies of Ref. [28] by varying the jet ra-

dius parameter, with leading dijets being measured in Pb+Pb and pp collisions at $\sqrt{s_{NN}} = 5.02$ TeV. The measurements use 1.72 nb^{-1} of Pb+Pb collisions collected in 2018 and 255 pb^{-1} of pp data collected in 2017 with the ATLAS detector [31] at the LHC.

Jets are reconstructed using the anti- k_t algorithm [32] with radius parameters $R = 0.2, 0.3, 0.4, 0.5$, and 0.6 . The analysis is conducted independently for each of the jet radius values. In each case, the leading dijets are constructed from the two highest- p_T jets in the event and are required to have the two jets nearly back-to-back in azimuth with $|\phi_1 - \phi_2| > 7\pi/8$ and $|y| < 2.1$.² Leading jets are reported with p_T values from 100 to 562 GeV for $R = 0.2, 0.3$, and 0.4 and from 158 to 562 GeV for $R = 0.5$ and 0.6 . To be consistent with Refs. [27,28], subleading jets are reported down to x_J values of 0.32 for each leading jet p_T selection. Events in which the two highest- p_T jets do not meet the selection criteria are discarded.

The primary observable for this measurement is the two-dimensional yield of leading dijets (N_{pair}) meeting the selection criteria described above:

$$\frac{d^2N_{\text{pair}}}{dp_{T,1}dp_{T,2}}. \quad (3)$$

Analogously to R_{AA} in Eq. (1), the pair nuclear modification factors for dijets as a function of the leading and subleading jet p_T can be defined as

$$R_{AA}^{\text{pair}}(p_{T,1}) = \frac{\frac{1}{\langle T_{AA} \rangle N_{\text{evt}}^{AA}} \int_{0.32 \times p_{T,1}}^{p_{T,1}} \frac{d^2N_{\text{pair}}^{AA}}{dp_{T,1}dp_{T,2}} dp_{T,2}}{\frac{1}{L_{pp}} \int_{0.32 \times p_{T,1}}^{p_{T,1}} \frac{d^2N_{\text{pair}}^{pp}}{dp_{T,1}dp_{T,2}} dp_{T,2}}, \quad (4)$$

and

$$R_{AA}^{\text{pair}}(p_{T,2}) = \frac{\frac{1}{\langle T_{AA} \rangle N_{\text{evt}}^{AA}} \int_{p_{T,2}}^{p_{T,2}/0.32} \frac{d^2N_{\text{pair}}^{AA}}{dp_{T,1}dp_{T,2}} dp_{T,1}}{\frac{1}{L_{pp}} \int_{p_{T,2}}^{p_{T,2}/0.32} \frac{d^2N_{\text{pair}}^{pp}}{dp_{T,1}dp_{T,2}} dp_{T,1}}, \quad (5)$$

where $\langle T_{AA} \rangle$ and N_{evt}^{AA} are defined the same way as in Eq. (1), L_{pp} is the integrated luminosity of the pp collisions [33], and N_{pair}^{pp} and N_{pair}^{AA} are the dijet yields in pp and Pb+Pb collisions, respectively. By integrating over $p_{T,2}$ ($p_{T,1}$), one can access information from $R_{AA}^{\text{pair}}(p_{T,1})$ [$R_{AA}^{\text{pair}}(p_{T,2})$] about the differential rate of dijet production in leading (subleading) jet p_T bins. Comparison of these two quantities at a fixed jet p_T provides information about the suppression of leading and

²ATLAS uses a right-handed coordinate system with its origin at the nominal interaction point (IP) in the center of the detector, and the z axis along the beam pipe. The x axis points from the IP to the center of the LHC ring, and the y axis points upward. Cylindrical coordinates (r, ϕ) are used in the transverse plane, ϕ being the azimuthal angle around the z axis. The pseudorapidity is defined in terms of the polar angle θ as $\eta = -\ln \tan(\theta/2)$. The rapidity is defined as $y = 0.5 \ln[(E + p_z)/(E - p_z)]$ where E and p_z are the energy and z component of the momentum along the beam direction, respectively. Transverse momentum and transverse energy are defined as $p_T = p \sin \theta$ and $E_T = E \sin \theta$, respectively. The angular distance between two objects with relative differences $\Delta\eta$ in pseudorapidity and $\Delta\phi$ in azimuth is given by $\Delta R = [(\Delta\eta)^2 + (\Delta\phi)^2]^{1/2}$.

subleading jets in a dijet. These quantities were first shown in Ref. [28].

Additionally, projections of the two-dimensional ($p_{T,1}$, $p_{T,2}$) distributions can be used to construct x_J distributions as a function of $p_{T,1}$ and $p_{T,2}$. The x_J values, as defined in Eq. (2), are reported for $0.32 < x_J < 1.0$ for selections in $p_{T,1}$. This paper presents results of the *absolutely normalized* x_J distributions in pp collisions:

$$\frac{1}{L_{pp}} \frac{dN_{\text{pair}}^{pp}}{dx_J} \quad (6)$$

and in Pb+Pb collisions:

$$\frac{1}{\langle T_{AA} \rangle N_{\text{evt}}^{AA}} \frac{dN_{\text{pair}}^{AA}}{dx_J}. \quad (7)$$

Similarly, the *dijet-yield-normalized* x_J distributions are defined as

$$\frac{1}{N_{\text{pair}}} \frac{dN_{\text{pair}}}{dx_J}, \quad (8)$$

with a normalization that was used in previous dijet measurements [27–30].

The absolutely normalized x_J distributions allow a direct comparison between the dijet rates measured in Pb+Pb and pp collisions. This comparison is quantified by the ratio:

$$J_{AA} \equiv \frac{1}{\langle T_{AA} \rangle N_{\text{evt}}^{AA}} \frac{dN_{\text{pair}}^{AA}}{dx_J} \Bigg/ \left(\frac{1}{L_{pp}} \frac{dN_{\text{pair}}^{pp}}{dx_J} \right). \quad (9)$$

Finally, the absolutely normalized x_J distributions can be integrated over the measurement range of $0.32 < x_J < 1.0$ (and the corresponding ranges in $p_{T,1}$ and $p_{T,2}$) to construct the absolutely normalized dijet yields in Pb+Pb collisions:

$$\frac{1}{\langle T_{AA} \rangle N_{\text{evt}}^{AA}} \int_{0.32 \times p_{T,1}}^{p_{T,1}} \frac{d^2 N_{\text{pair}}^{AA}}{dp_{T,1} dp_{T,2}}, \quad (10)$$

and the dijet cross sections in pp collisions:

$$\frac{1}{L_{pp}} \int_{0.32 \times p_{T,1}}^{p_{T,1}} \frac{d^2 N_{\text{pair}}^{pp}}{dp_{T,1} dp_{T,2}}. \quad (11)$$

II. ATLAS DETECTOR

The ATLAS detector [31] at the LHC is a multipurpose particle detector with a forward–backward symmetric cylindrical geometry and a near- 4π coverage in solid angle. It consists of an inner tracking detector surrounded by a thin superconducting solenoid, electromagnetic and hadron calorimeters, and a muon spectrometer. The inner-detector system is immersed in a 2 T axial magnetic field and provides charged-particle tracking in $|\eta| < 2.5$. The high-granularity silicon pixel detector covers the vertex region and typically provides four measurements per track, with the first hit typically being in the insertable B-layer installed before Run 2 [34,35]. It is followed by the silicon microstrip tracker (SCT), which usually provides eight measurements per track. These silicon detectors are complemented by the transition radiation tracker, a drift-tube-based detector, which surrounds the SCT and has coverage up to $|\eta| = 2.0$.

The calorimeter system covers the pseudorapidity range $|\eta| < 4.9$. In the region $|\eta| < 3.2$, electromagnetic calorimetry is provided by barrel and endcap high-granularity lead/liquid-argon (LAr) calorimeters, with an additional thin LAr presampler covering $|\eta| < 1.8$ to correct for energy loss in material upstream of the calorimeters. Hadronic calorimetry is provided by the steel and scintillator-tile calorimeter, segmented into three barrel structures in $|\eta| < 1.7$, and two copper-LAr hadronic endcap calorimeters. The solid angle coverage is completed with copper-LAr and tungsten-LAr calorimeter modules (FCal), covering the forward regions of $3.1 < |\eta| < 4.9$. Minimum-bias trigger scintillators detect charged particles over $2.1 < |\eta| < 3.9$ using two hodoscopes of 12 counters, positioned at $z = \pm 3.6$ m along the beamline from the center of the ATLAS detector, which are used for the minimum bias triggers and data samples. The zero-degree calorimeters (ZDCs) consist of layers of alternating quartz rods and tungsten plates and are located symmetrically at $z = \pm 140$ m and cover $|\eta| \geq 8.3$. In Pb+Pb collisions, the ZDCs primarily measure “spectator” neutrons: neutrons that do not interact hadronically when the incident nuclei collide.

An extensive software suite [36] is used in simulation, in reconstruction and analysis of real and simulated events, in detector operations, and in the trigger and data acquisition systems of the experiment. Events of interest are selected for recording and offline analysis by the first-level (L1) trigger system implemented in custom hardware, followed by selections made by algorithms implemented in software in the high-level trigger (HLT) [37–39]. The L1 trigger identifies jet candidates by applying a sliding-window algorithm and selecting events above an E_T threshold of 30 GeV. These events are then passed to the HLT trigger, which uses a jet reconstruction and background subtraction procedure similar to that used in the offline analysis and requires a minimum p_T of 100 GeV for anti- k_t , $R = 0.4$ jets. The jet trigger efficiencies are evaluated separately for each of the jet radii considered here. The p_T thresholds are set such that the triggers were fully efficient for each R value over the p_T range considered in this measurement, with the highest threshold trigger sampling the full luminosity. In addition to the jet triggers, a minimum-bias sample was constructed using three different triggers, each one corresponding to one of the following conditions: total E_T in the calorimeter less than 50 GeV at L1 and at least one track reconstructed at HLT; total E_T in the calorimeter between 50 and 600 GeV at L1; total E_T greater than 600 GeV at L1. More details about the triggering used in ATLAS heavy-ion collisions can be found in Refs. [37–39].

III. DATA AND MONTE CARLO SELECTION

The Pb+Pb data used in these measurements were collected in 2018, and the pp data used were collected in 2017, both at a per-nucleon-pair center-of-mass energy $\sqrt{s_{\text{NN}}} = 5.02$ TeV. Events were selected by the minimum-bias and jet triggers [37,40] described in Sec. II. Although only a small fraction of the Pb+Pb events (<0.5%) contain multiple collisions, these were suppressed utilizing the observed anticorrelation, expected from the nuclear geometry, between the total transverse energy deposited in both of the forward

TABLE I. The $\langle T_{AA} \rangle$ values and their uncertainties for the centrality selections used in this measurement, obtained from the TGLAUBERMC v3.2 modeling of the total transverse energy in the forward calorimeters, ΣE_T^{FCal} .

Centrality selection	$\langle T_{AA} \rangle \pm \delta \langle T_{AA} \rangle [\text{mb}^{-1}]$
0–10%	23.35 ± 0.20
10–20%	14.33 ± 0.17
20–40%	6.79 ± 0.16
40–60%	1.96 ± 0.09
60–80%	0.39 ± 0.03

calorimeters, ΣE_T^{FCal} , and the energy in both ZDCs, which is proportional to the number of observed spectator neutrons. Events with multiple collisions, called pileup, are not rejected in pp collisions.

The overlap area of the two colliding nuclei in Pb+Pb collisions is characterized by the event centrality, which is estimated from ΣE_T^{FCal} [41]. This measurement considers five centrality intervals as defined according to successive percentiles of the ΣE_T^{FCal} distribution obtained from minimum-bias collisions. The centrality intervals considered in this measurement are 0–10% (largest ΣE_T^{FCal} , most central collisions), 10–20%, 20–40%, 40–60%, and 60–80% (smallest ΣE_T^{FCal} , peripheral collisions). The values of the mean nuclear thickness function, $\langle T_{AA} \rangle$ [13], and their uncertainties [42] are determined using the TGLAUBERMC v3.2 package [43]. The $\langle T_{AA} \rangle$ values and their uncertainties are listed in Table I for each centrality interval considered in this measurement.

The analysis uses three Monte Carlo (MC) samples to evaluate the detector performance and correct for detector effects. The pp MC sample includes 3.2×10^7 PYTHIA 8 [44] pp dijet events generated at center-of-mass energy $\sqrt{s} = 5.02$ TeV with the A14 set of tuned parameters [45] and the NNPDF23LO parton distribution functions (PDFs) [46]. Pileup due to additional inelastic pp interactions is similarly generated using PYTHIA 8 with the same PDFs and utilizing the A3 set of tuned parameters [47], tuned for inclusive QCD processes, matching the number of extra collisions in the pp data. The MC sample for Pb+Pb collisions uses the 2018 detector conditions and contains 3.2×10^7 pp PYTHIA 8 events with the same tune and PDFs as used for the generation of the pp MC samples. The underlying event (UE) contribution to the detector signal is accounted for by overlaying the simulated pp events with dedicated minimum-bias Pb+Pb data events. The minimum-bias data events from Pb+Pb collisions are combined with the signal from the PYTHIA 8 simulation of hard scattering events at the digitization stage, and then reconstructed as a combined event. This procedure enables the “data overlay” sample to accurately reproduce the effects of the UE on the jet response. This sample is reweighted on an event-by-event basis to ensure the same centrality distribution as is measured in the triggered data samples. Finally, pp HERWIG7 [48,49] events using the UEEE5 tune [50] and the CTEQ6L1 PDFs [51] are used for flavor uncertainty studies

and comparisons with pp data. The detector response in all three MC samples is simulated utilizing GEANT4 [52,53].

IV. JET RECONSTRUCTION AND PERFORMANCE

The jet reconstruction procedures follow those used by ATLAS for previous jet measurements in Pb+Pb collisions [14,24]. Jets are reconstructed using the anti- k_t algorithm [32] implemented in the FastJet software package [54]. In both the pp and Pb+Pb collisions, jets with $R = 0.2, 0.3, 0.4, 0.5$, and 0.6 are formed by clustering calorimetric towers of spatial size $\Delta\eta \times \Delta\phi = 0.1 \times \pi/32$. In Pb+Pb collisions, a background subtraction procedure is applied in each event to estimate the UE average transverse energy density, $\rho(\eta, \phi)$, where the ϕ dependence is due to global azimuthal correlations in the particle production from the hydrodynamic flow [55]. The modulation accounts for the contribution to the UE of the second-, third-, and fourth-order azimuthal anisotropy harmonics characterized by values of flow coefficients v_n^{UE} [55]. An iterative procedure is used to remove the impact of jets on the estimated ρ and v_n^{UE} values. This background-subtraction method removes the average UE while any UE fluctuations are corrected for by the unfolding procedure described later. Jet R -, η -, and p_T -dependent correction factors derived in simulations are applied to the measured jet energy to correct for the calorimeter energy response [56,57]. An additional correction based on *in situ* studies of jets recoiling against photons and jets in other regions of the calorimeter is applied to account for differences between the data and MC [58]. This calibration is followed by a “cross-calibration” in which the jet energy scale (JES) of jets reconstructed by the procedure outlined in this section is related to the JES in 13 TeV pp collisions. The cross-calibration allows for the use of uncertainties obtained for the latter [57].

“Truth”-level jets are defined in the MC samples before detector simulation by applying the anti- k_t algorithm with $R = 0.2, 0.3, 0.4, 0.5$, and 0.6 to stable particles with a proper lifetime greater than 30 ps, but excluding muons and neutrinos, which do not leave significant energy deposits in the calorimeter. After the detector simulation the truth jets are matched to the nearest reconstructed jet in $\Delta R < 0.75R$. The performance of the jet reconstruction is characterized by the JES and jet energy resolution (JER), which correspond to the mean and variance, respectively, of the $p_T^{\text{reco}}/p_T^{\text{truth}}$ distribution, where p_T^{reco} is the reconstructed jet p_T and p_T^{truth} is the p_T of the matched truth-level jet. The JES and JER as a function of p_T^{truth} can be seen in Fig. 1 for $R = 0.2$ and $R = 0.6$ jets. The broadening of the JER with centrality is due to the UE fluctuations, which are larger in more central collisions and cause the jet p_T to smear. Additionally, a larger jet radius allows for a larger contribution of the UE fluctuations in Pb+Pb collisions, causing the larger R jets to have a larger JER. In pp collisions, the JER is smaller for a larger jet radius because there are less jet energy fluctuations in and out of the larger jet cone. The deviation of the JES from unity for high- p_T $R = 0.2$ jets is due to the different requirements used in the determination of the jet calibration compared with this analysis. JES and JER effects are corrected for by the unfolding procedure described below. The efficiency of reconstructing a jet with

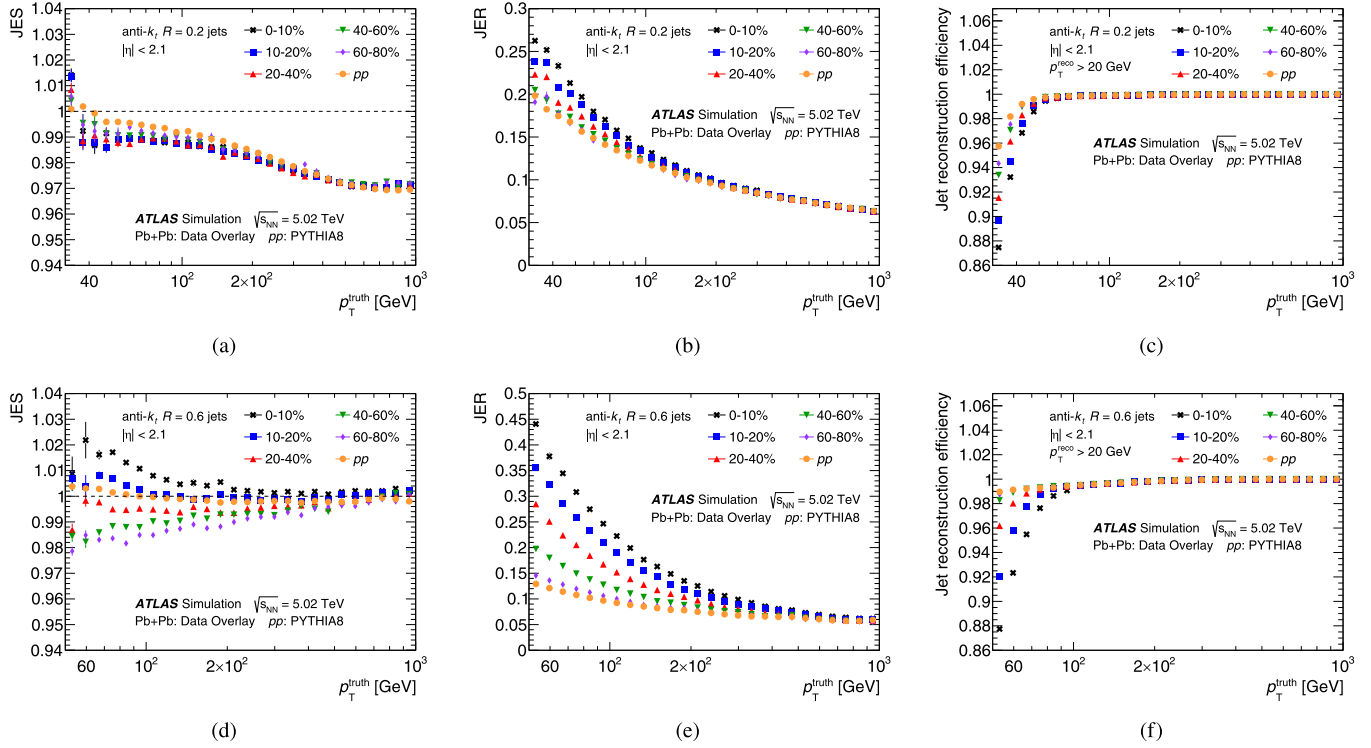


FIG. 1. The (a), (d) JES, (b), (e) JER, and (c), (f) jet reconstruction efficiency for (a)–(c) $R = 0.2$ and (d)–(f) $R = 0.6$ jets in pp collisions and the centrality selections in $\text{Pb}+\text{Pb}$ collisions used in this analysis.

$p_T > 20 \text{ GeV}$, as evaluated from the probability of a truth-jet matching to a reconstructed jet, can also be seen as a function of p_T^{truth} in Fig. 1. The lower p_T bounds in this figure are based on the p_T requirements used in the analysis, which are different for the various jet radii in order to minimize the effects from the UE.

V. DATA ANALYSIS

The analysis and dijet selection used here closely follow those in Ref. [28]. In each data event, the reconstructed leading dijet is constructed from the two highest- p_T^{reco} jets in the event with reconstructed leading $p_{T,1}^{\text{reco}} > 79 \text{ GeV}$, and reconstructed subleading $p_{T,2}^{\text{reco}} > 32 \text{ GeV}$ for $R = 0.2, 0.3$, and 0.4 jets, $p_{T,2}^{\text{reco}} > 41 \text{ GeV}$ for $R = 0.5$ jets, and $p_{T,2}^{\text{reco}} > 51 \text{ GeV}$ for $R = 0.6$ jets. The minimum $p_{T,1}^{\text{reco}}$ was based on the minimum p_T for which the trigger is fully efficient for the various jet radii. The minimum $p_{T,2}^{\text{reco}}$ was based on 0.32 of the minimum p_T for which the rate of jets created by UE fluctuations becomes negligible. For $R = 0.2, 0.3$, and 0.4 jets, the rate of jets created by UE fluctuations is negligible above approximately 100 GeV, so results are quoted for leading jet $p_{T,1} > 100 \text{ GeV}$. A minimum x_J of 0.32 implies $p_{T,2}^{\text{reco}} = 0.32 p_{T,1}^{\text{reco}}$, giving a corresponding minimum subleading jet $p_{T,1}^{\text{reco}} > 32 \text{ GeV}$. The rate of jets created by the UE fluctuations depends on the jet radius, so an analogous minimum $p_{T,2}^{\text{reco}}$ was selected for the $R = 0.5$ and 0.6 jets, and the results are quoted for leading jet $p_{T,1} > 158 \text{ GeV}$. The lower $p_{T,1}$ bins, from 79 to 100 (158) GeV for $R = 0.2, 0.3$, and 0.4 ($R = 0.5$ and 0.6) jets, serve as underflow bins in the

unfolding to account for the jet p_T migration due to the JER. Both jets are required to have $|y_T^{\text{reco}}| < 2.1$. These dijets are required to be back-to-back with $|\phi_1 - \phi_2| > 7\pi/8$. Leading dijets meeting these criteria represent approximately 62% of inclusive $R = 0.2$ jets with $100 < p_T^{\text{reco}} < 562 \text{ GeV}$, and approximately 72% of inclusive $R = 0.6$ jets with $158 < p_T^{\text{reco}} < 562 \text{ GeV}$. Events in which the leading dijets do not meet these criteria are discarded. For dijets matching the selection criteria, two-dimensional $(p_{T,1}^{\text{reco}}, p_{T,2}^{\text{reco}})$ distributions are constructed symmetrically across $p_{T,1}^{\text{reco}} = p_{T,2}^{\text{reco}}$. The distributions are symmetrized to account for the possibility of swapping the leading and subleading jet definition due to the finite JER.

The measured $(p_{T,1}^{\text{reco}}, p_{T,2}^{\text{reco}})$ distributions are a combination of the dijet signal and pairs of uncorrelated jets. Since the UE subtraction accounts for azimuthal correlations in the particle production due to hydrodynamic flow, the contribution from uncorrelated dijets is largely independent of the $|\phi_1 - \phi_2|$ of the jets; therefore, a $|\phi_1 - \phi_2|$ sideband method is used to remove these pairs as a function of $(p_{T,1}^{\text{reco}}, p_{T,2}^{\text{reco}})$. The symmetrized two-dimensional $(p_{T,1}^{\text{reco}}, p_{T,2}^{\text{reco}})$ distribution of background combinatoric dijets is determined using dijets with $1 < |\phi_1 - \phi_2| < 1.4$ which, after normalizing to the $|\phi_1 - \phi_2|$ window of the signal band, is subtracted from the dijet yields. This effect is strongest for 0–10% centrality $\text{Pb}+\text{Pb}$ events at low $p_{T,1}^{\text{reco}}$. In the most central collisions, combinatoric dijets constitute 2% of the $R = 0.2$ dijets with $p_{T,1}^{\text{reco}} > 100 \text{ GeV}$ and $p_{T,2}^{\text{reco}} > 32 \text{ GeV}$, and 1% of the $R = 0.6$ dijets with $p_{T,1}^{\text{reco}} > 158 \text{ GeV}$ and $p_{T,2}^{\text{reco}} > 51 \text{ GeV}$. The combinatoric dijet rate drops off rapidly with increasing $p_{T,1}^{\text{reco}}$ and more peripheral events. Because of how the leading dijet is

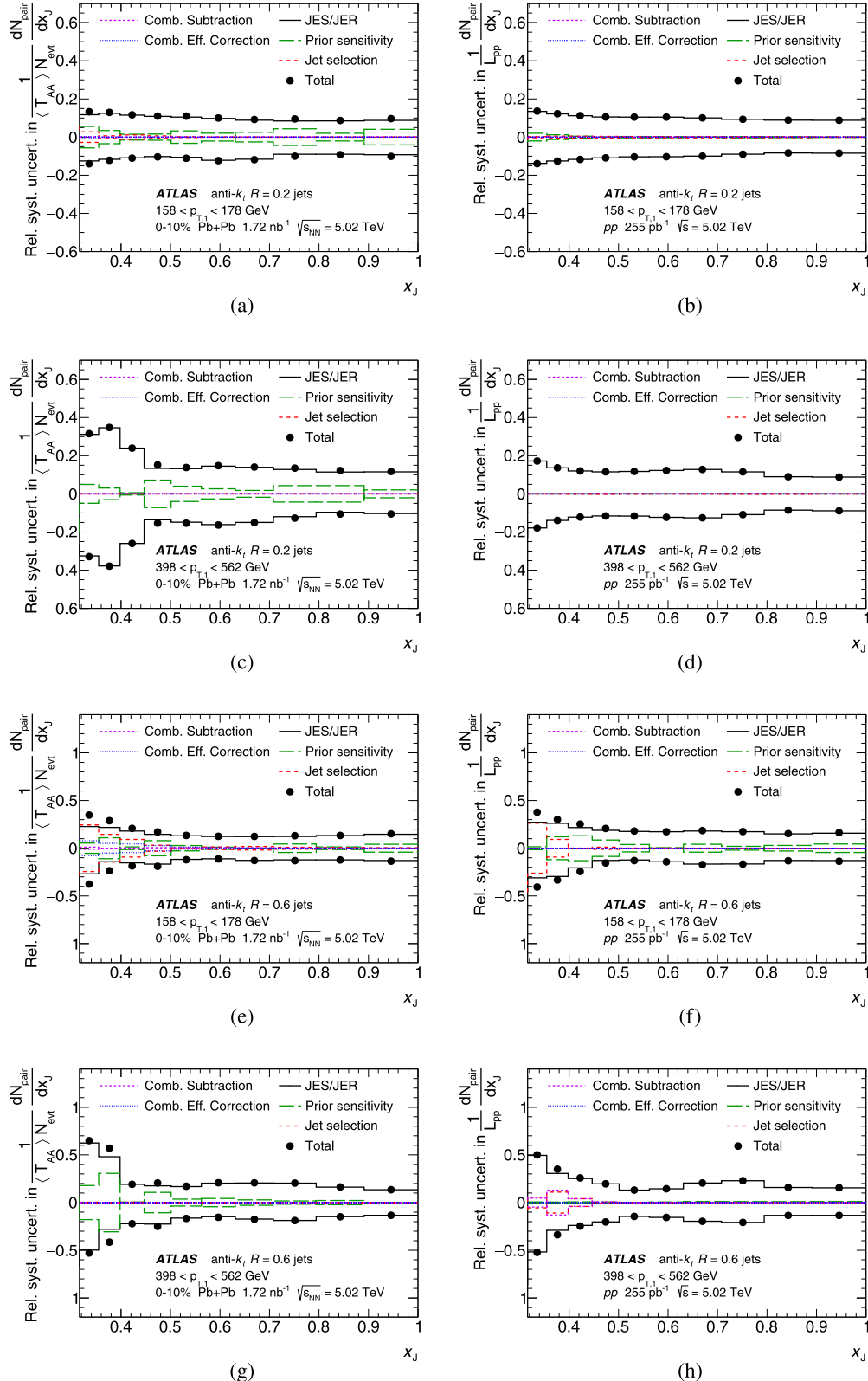


FIG. 2. Relative systematic uncertainties in the absolutely normalized x_J distributions in (a), (c), (e), (g) 0–10% central $\text{Pb}+\text{Pb}$ collisions and (b), (d), (f), (h) pp collisions for (a), (b), (c), (d) $R = 0.2$ and (e), (f), (g), (h) $R = 0.6$ jets for leading jets with (a), (b), (e), (f) $158 < p_{T,1} < 178 \text{ GeV}$ and (c), (d), (g), (h) $398 < p_{T,1} < 562 \text{ GeV}$. Jets are selected with $|y| < 2.1$ and $|\phi_1 - \phi_2| > 7\pi/8$. The normalization uncertainties (not shown) are $\delta\langle T_{AA} \rangle / \langle T_{AA} \rangle = 0.9\%$ in 0–10% $\text{Pb}+\text{Pb}$ collisions and $\delta L_{\text{pp}} / L_{\text{pp}} = 1\%$ in pp collisions.

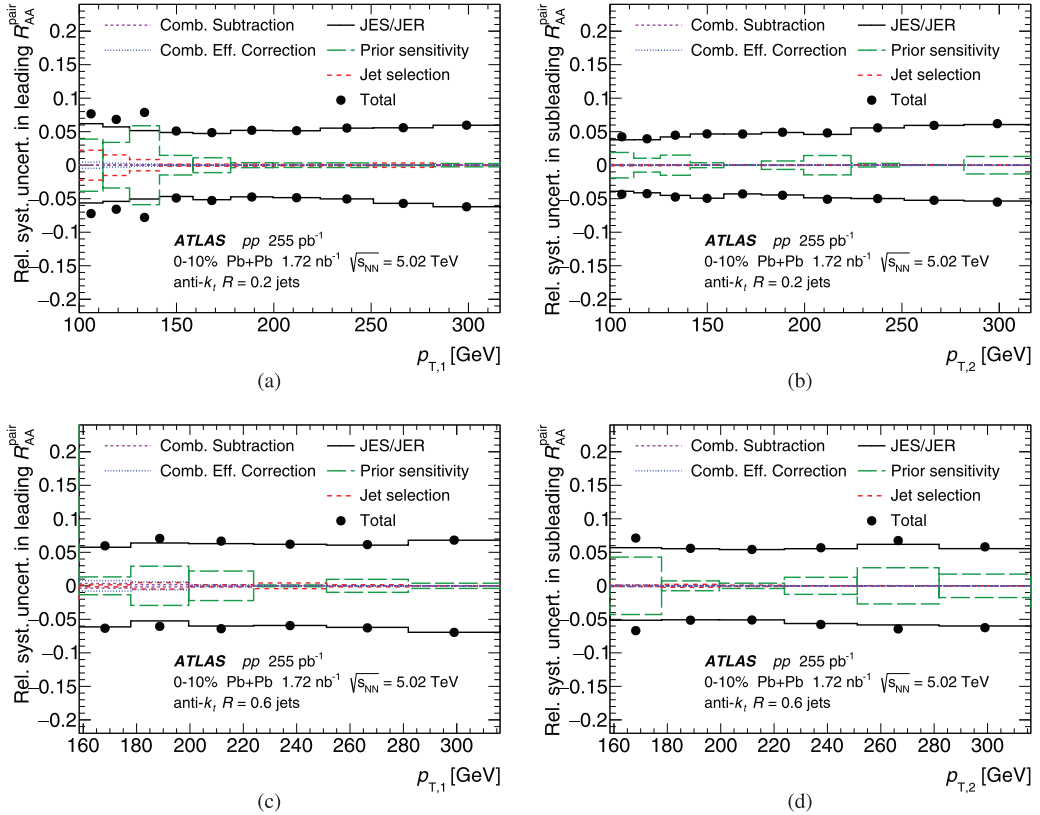


FIG. 3. Relative systematic uncertainties in the R_{AA}^{pair} for (a), (c) leading and (b), (d) subleading (a), (b) $R = 0.2$ and (c), (d) $R = 0.6$ jets. Jets are selected with $|y| < 2.1$ and $|\phi_1 - \phi_2| > 7\pi/8$. The normalization uncertainties (not shown) are $\delta \langle T_{AA} \rangle / \langle T_{AA} \rangle = 0.9\%$ in 0–10% Pb+Pb collisions and $\delta L_{pp} / L_{pp} = 1\%$ in pp collisions.

defined, the presence of residual combinatoric dijets in the sample results in an inefficiency for genuine jet pairs, where one of the jets might be replaced by an uncorrelated third jet. This effect is corrected for using the measured inclusive jet spectrum from minimum-bias events, reweighted to match the centrality distribution in the triggered data, to determine the efficiency loss as a function of the measured jet p_T , following the method discussed in Ref. [27]. This efficiency correction is the largest in the 0–10% centrality interval, being at most 3% for $R = 0.2$ jets and 7% for $R = 0.6$ jets.

To correct for the effects of the JES and JER, the measured $(p_{T,1}^{\text{reco}}, p_{T,2}^{\text{reco}})$ distributions are unfolded using the iterative Bayesian unfolding procedure [59] as implemented in the RooUnfold [60] software package. A two-dimensional unfolding is used to account for bin migration of both the leading and the subleading jet p_T and to account for possible swapping of the leading and subleading jet. Separate response matrices are generated for pp collisions and for each centrality selection in Pb+Pb collisions, for each R value used. The response matrix used in the unfolding contains the relationship between $(p_{T,1}^{\text{truth}}, p_{T,2}^{\text{truth}})$ and $(p_{T,1}^{\text{reco}}, p_{T,2}^{\text{reco}})$. It is populated by identifying the leading and subleading truth-level jets in the MC sample, which are matched to the corresponding reconstructed jets with $\Delta R < 0.75R$. To account for migration from lower jet p_T^{reco} , the response matrices are populated with truth-level jets down to $p_{T,1}^{\text{truth}}$ of 20 GeV and $p_{T,2}^{\text{truth}}$ of 10 GeV. As

with the reconstructed data, truth dijets are required to have $|\phi_1^{\text{truth}} - \phi_2^{\text{truth}}| > 7\pi/8$, with each jet having $|y^{\text{truth}}| < 2.1$. The two selected reconstructed jets from the MC simulations are required to meet the same selection criteria as applied to dijets measured in data. Truth dijets that do not match to a reconstructed dijet meeting the selection criteria are accounted for by using an efficiency correction in the unfolding.

Similarly to the construction of the data distributions, the response matrix is populated symmetrically in $p_{T,1}$ and $p_{T,2}$. The symmetrization is done in order to regularize the response matrix [27]. The unfolding requires an assumed initial distribution, referred to here as the prior, which is similar to the measured distributions. To generate the prior, the response matrices are reweighted along the $p_{T,1}^{\text{truth}}$ and $p_{T,2}^{\text{truth}}$ axes by the ratio of the two-dimensional reconstructed yields in data to those from simulation. The number of iterations used in the unfolding is tuned separately for each centrality in Pb+Pb collisions and for pp collisions, for each jet radius. The number of iterations in each case is selected to optimize the balance between the accuracy of the final unfolded yield, and the increased statistical uncertainty that results from a larger number of iterations. In both Pb+Pb and pp collisions, the number of iterations depends on the jet radius, being larger for larger jet radii. In Pb+Pb collisions, the number of iterations also depends on centrality, being larger for more central collisions. Seven iterations were used for the $R = 0.6$ jets in 0–10%

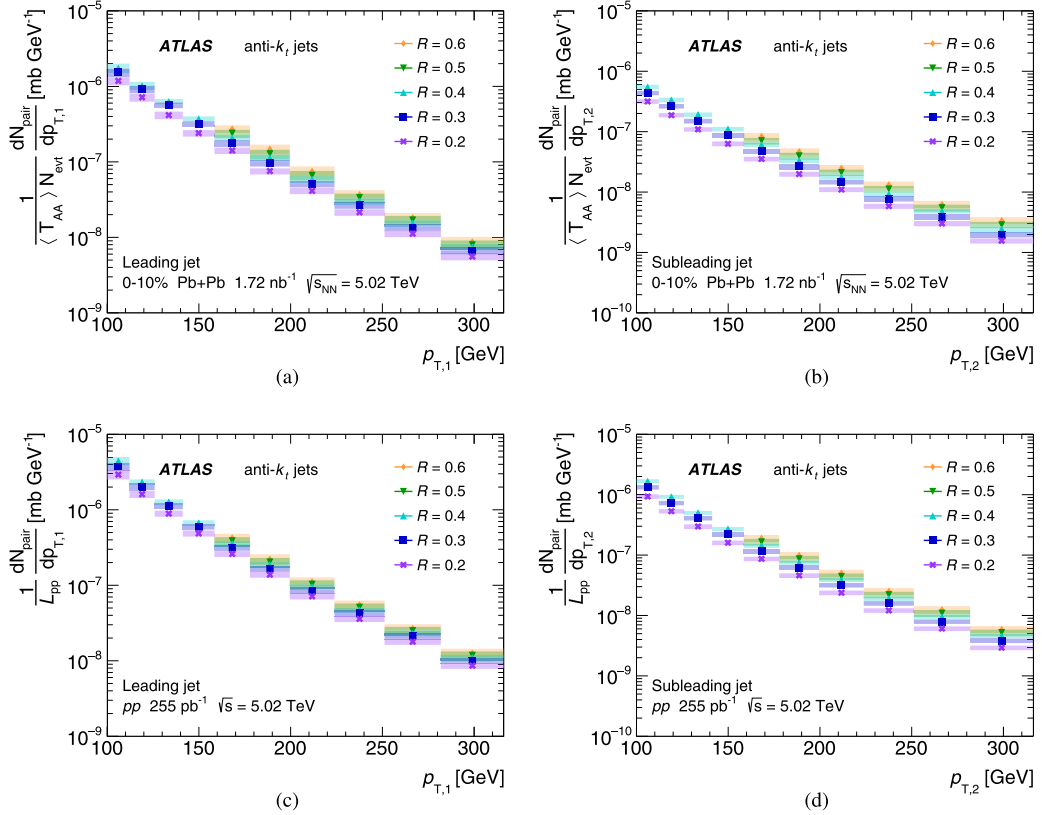


FIG. 4. The (a), (c) leading and (b), (d) subleading dijet yields in (a), (b) 0–10% central Pb+Pb collisions and the dijet cross sections in (c), (d) pp collisions as a function of p_T for the various jet radii. Jets are selected with $|y| < 2.1$ and $|\phi_1 - \phi_2| > 7\pi/8$. The normalization uncertainties (not shown) are $\delta\langle T_{AA} \rangle / \langle T_{AA} \rangle = 0.9\%$ in 0–10% Pb+Pb collisions and $\delta L_{pp} / L_{pp} = 1\%$ in pp collisions. The boxes correspond to systematic uncertainties and the bars to statistical uncertainties.

central Pb+Pb collisions, while two iterations were used for the $R = 0.2$ jets in 60–80% central Pb+Pb collisions. In pp collisions, seven iterations were used for the $R = 0.6$ jets and three iterations were used for the $R = 0.2$ jets.

To evaluate the statistical uncertainties of the data and the MC simulations, 100 bootstrap [61] variations following a Poisson distribution were used. The nominal data was unfolded with each of the response matrix variations to obtain the statistical uncertainties of the MC sample. Similarly, each variation of the data was unfolded with the nominal response matrix to obtain the statistical uncertainties of the data. The statistical uncertainties were obtained from the standard deviation of both the data and MC variations of the unfolded distributions. The data and MC components were added in quadrature to obtain the total statistical uncertainty.

To extract the measurements of the dijet momentum balance observable, x_J , the unfolded two-dimensional ($p_{T,1}, p_{T,2}$) distributions are first reflected about $p_{T,1} = p_{T,2}$ to restore the leading and subleading hierarchy. Then, following the procedure discussed in Refs. [27, 28, 62], the two-dimensional distributions are projected into bins of x_J for different $p_{T,1}$ slices. After projecting the resulting distributions over selections of $p_{T,1}$, the absolutely normalized x_J distributions are extracted by normalizing the x_J distributions either by the integrated luminosity in pp collisions or the number of events

and the $\langle T_{AA} \rangle$ in Pb+Pb collisions, as described in Eqs. (6) and (7).

VI. SYSTEMATIC UNCERTAINTIES

Systematic uncertainties for this measurement are attributed to three categories of sources arising from: the analysis and unfolding procedure, the uncertainties in the JES and JER, and the global normalization. For each uncertainty component in the first two categories, the entire analysis procedure is repeated accounting for the change in the analysis procedure or the response matrix and the result is compared with the nominal one. The third category applies only to the absolutely normalized x_J distributions, J_{AA} distributions, and $R_{AA}^{\text{pair}}(p_{T,1})$ and $R_{AA}^{\text{pair}}(p_{T,2})$ distributions; it contains the uncertainty in the determination of the mean nuclear thickness function $\langle T_{AA} \rangle$, and the pp luminosity. The $\langle T_{AA} \rangle$ uncertainties are shown in Table I, while the relative luminosity uncertainty in pp collisions is $\delta L_{pp} / L_{pp} = 1\%$ [33]. These uncertainties are independent of the jet p_T and are noted on the figures.

The systematic uncertainty in the JES has five parts. Four parts are identical to those in Ref. [28], which correspond to the *in situ* studies, the cross-calibration, the flavor uncertainties, and the modification of parton showers due to quenching. The modifications to the parton shower can impact

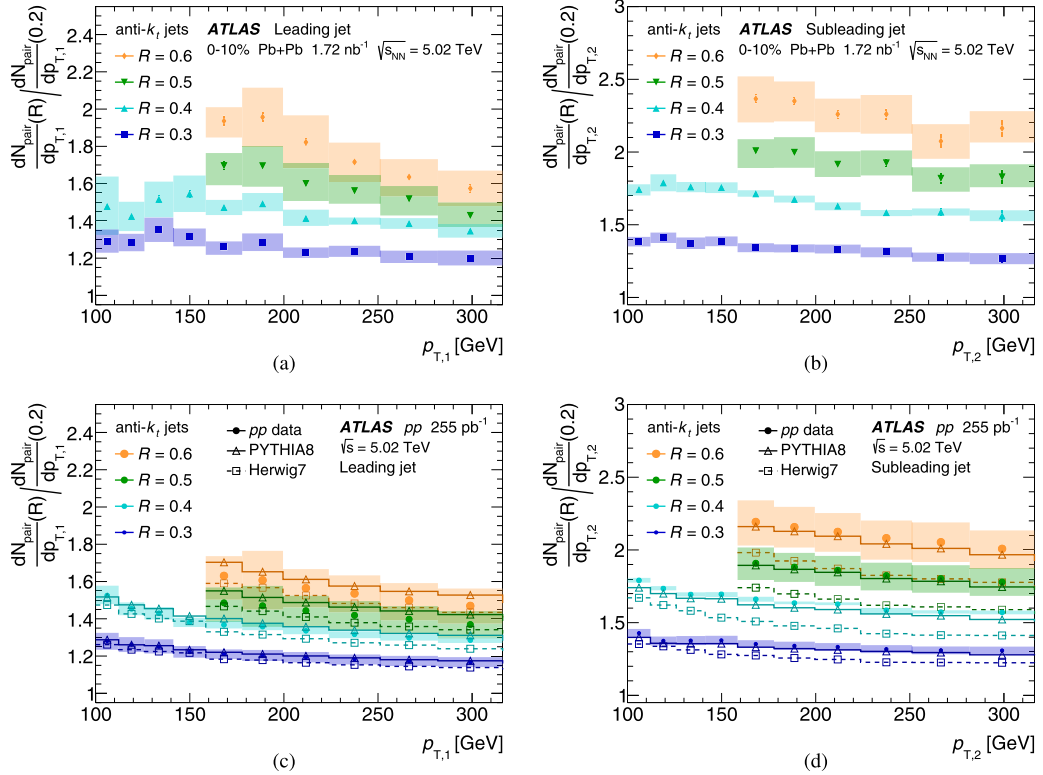


FIG. 5. The (a), (c) leading and (b), (d) subleading dijet cross-section ratios for R jets with respect to $R = 0.2$ jets as a function of p_T for the various jet radii in (a), (b) 0–10% central Pb+Pb and (c), (d) pp collisions. The pp data are compared with PYTHIA 8 and HERWIG7 simulations. Jets are selected with $|y| < 2.1$ and $|\phi_1 - \phi_2| > 7\pi/8$. The boxes correspond to systematic uncertainties and the bars to statistical uncertainties.

the detector response to jets in Pb+Pb collisions resulting in a small disagreement in the JES between data and simulations. The extent of this disagreement, and corresponding uncertainty contribution is evaluated by the method used in Ref. [57] for 2015 and 2011 data, which compares the jet p_T measured in the calorimeter with the sum of the transverse momenta of charged particles within the jet, in both the data

and MC samples. This uncertainty is determined as a function of the event centrality and is found to be independent of the jet p_T and η . The selected charged-particle tracks have $p_T > 4$ GeV in order to exclude particles from the UE. The sum of the charged-particle transverse momenta provides a data-driven estimate of the centrality dependence of the JES arising from the observed centrality-dependent modification

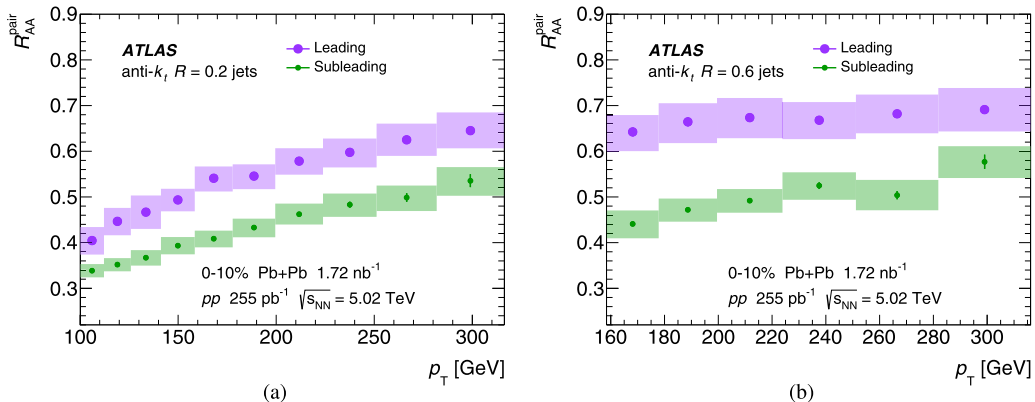


FIG. 6. The leading and subleading jet R_{AA}^{pair} distributions in dijets as a function of jet p_T for (a) $R = 0.2$ and (b) $R = 0.6$ jets in 0–10% Pb+Pb collisions. Jets are selected with $|y| < 2.1$ and $|\phi_1 - \phi_2| > 7\pi/8$. The normalization uncertainties (not shown) are $\delta\langle T_{AA}\rangle/\langle T_{AA}\rangle = 0.9\%$ in 0–10% Pb+Pb collisions and $\delta L_{pp}/L_{pp} = 1\%$ in pp collisions. The boxes correspond to systematic uncertainties and the bars to statistical uncertainties.

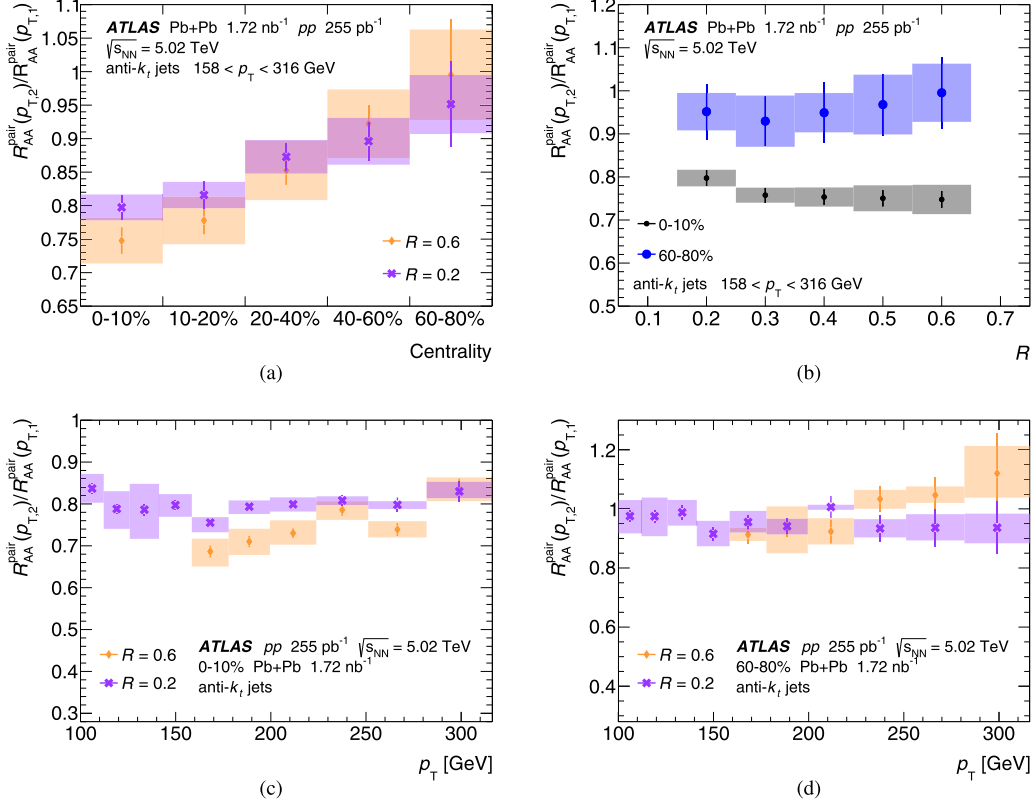


FIG. 7. The double ratio $R_{AA}^{\text{pair}}(p_{T,2})/R_{AA}^{\text{pair}}(p_{T,1})$ of the subleading to leading jet R_{AA}^{pair} distributions in dijets as a function of (a) centrality and (b) jet radius for $158 < p_T < 316 \text{ GeV}$, and as a function of jet p_T for (c) 0–10% and (d) 60–80% central Pb+Pb collisions. Jets are selected with $|y| < 2.1$ and $|\phi_1 - \phi_2| > 7\pi/8$. The boxes correspond to systematic uncertainties and the bars to statistical uncertainties.

of the jet fragmentation due to jet quenching in Pb+Pb collisions [63]. The size of this centrality-dependent uncertainty in the JES reaches 1.2% in the most central collisions and its value is applied independently of x_J . The systematic uncertainties from the JES discussed above are derived for $R = 0.4$ jets.

The fifth component accounts for the potential difference in uncertainties between $R = 0.4$ and the other jet radii. It does not depend on the collision centrality for $R = 0.2$ and $R = 0.3$ jets, but contains a centrality dependent contribution for $R = 0.5$ and $R = 0.6$ jets to account for data and MC differences of the jet response due to the larger area. The centrality-independent component is assessed by comparing the p_T for matched $R = 0.2$, $R = 0.3$, $R = 0.5$, and $R = 0.6$ jets with $R = 0.4$ jets measured in the data and the MC samples. For each individual component, the JES in the MC simulation is modified as a function of p_T and η by one standard deviation, and the response matrix is recomputed.

The uncertainty due to the JER is evaluated by repeating the unfolding procedure with modified response matrices, where an additional contribution is added to the resolution of the reconstructed p_T in the MC sample using a Gaussian smearing procedure. The smearing factor is evaluated using an *in situ* technique in 13 TeV pp data that involves studies of dijet p_T balance [64]. Furthermore, an uncertainty is included to account for differences between the tower-based jet reconstruction and the jet reconstruction used in analyses of 13 TeV

pp data, as well as differences in the calibration procedures. Similarly to the JES, an additional uncertainty is assigned to the JER to account for differences between the $R = 0.4$ jets and the other jet radii. The changes in the response are propagated through the unfolding and the resulting uncertainty is symmetrized.

Two sources of systematic uncertainty are included to account for uncertainties in the removal of the combinatoric background. The first contribution stems from the combinatoric subtraction method, and is determined by extracting the two-dimensional $(p_{T,1}, p_{T,2})$ distribution of combinatoric jets from an alternative sideband of $1.1 < |\phi_1 - \phi_2| < 1.5$ as was done in Refs. [27,28]. The second contribution stems from the sensitivity of the analysis to the efficiency correction for combinatoric jets, and is evaluated by repeating the analysis without the inclusion of this efficiency correction. The deviation from the nominal result is symmetrized and taken as the uncertainty contribution. Both these contributions are found to be negligible compared with the other sources of systematic uncertainties.

Additional sources of systematic uncertainty that account for the unfolding procedure are considered. The sensitivity to the Bayesian prior is evaluated by modifying the weights applied when producing the response matrix in a centrality-dependent manner in order to enclose the data $(p_{T,1}^{\text{reco}}, p_{T,2}^{\text{reco}})$ distributions between the corresponding MC distributions based on the nominal and alternative priors. There is a

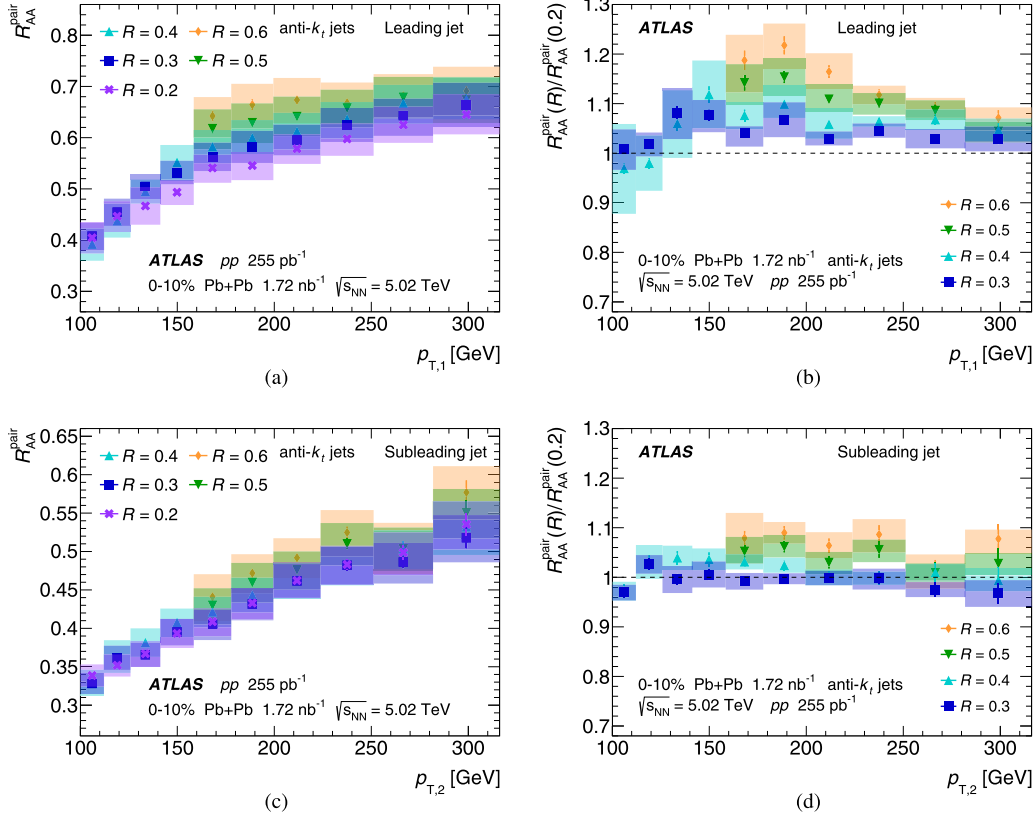


FIG. 8. The (a), (b) leading and (c), (d) subleading jet (a), (c) R_{AA}^{pair} distributions in dijets and the corresponding (b), (d) $R_{AA}^{\text{pair}}(R)/R_{AA}^{\text{pair}}(0.2)$ ratios as a function of jet p_T in 0–10% central Pb+Pb collisions. Jets are selected with $|y| < 2.1$ and $|\phi_1 - \phi_2| > 7\pi/8$. The normalization uncertainties (not shown) are $\delta\langle T_{AA} \rangle / \langle T_{AA} \rangle = 0.9\%$ in 0–10% Pb+Pb collisions and $\delta L_{pp} / L_{pp} = 1\%$ in pp collisions. The boxes correspond to systematic uncertainties and the bars to statistical uncertainties.

sensitivity to the minimum p_T^{jet} in the analysis at small x_J and small $p_{T,1}$ due to the efficiency correction made as part of the unfolding. The sensitivity of the result to this effect is evaluated by varying the minimum reconstructed p_T^{jet} , motivated by the magnitude of the JER, from 32 to 39 GeV for $R = 0.2, 0.3$, and 0.4 jets, from 41 to 51 GeV for $R = 0.5$

jets, and from 51 to 63 GeV for $R = 0.6$ jets, for both the data and simulation. This results in a significant contribution to the systematic uncertainties at low x_J in low $p_{T,1}$ bins. For each of these contributions the deviation of the unfolded result from the nominal is symmetrized and taken as a contribution to the systematic uncertainties.

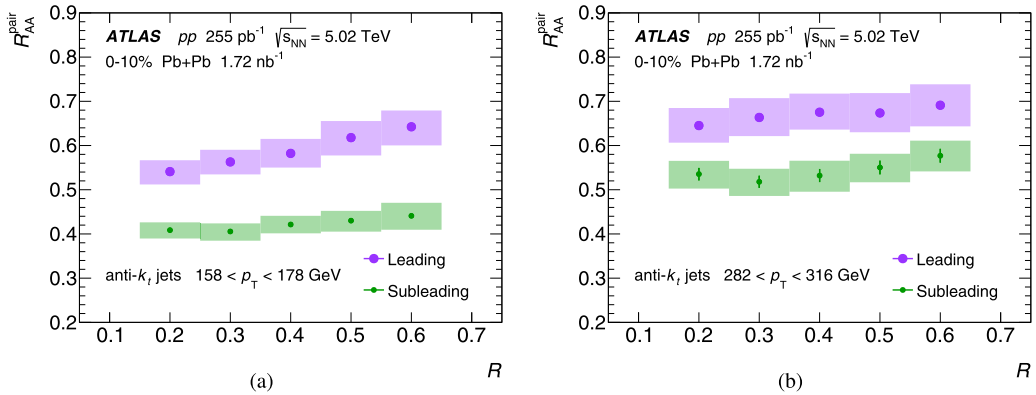


FIG. 9. The leading and subleading jet R_{AA}^{pair} distributions in dijets as a function of jet radius in 0–10% central Pb+Pb collisions, for (a) $158 < p_T < 178 \text{ GeV}$ and (b) $282 < p_T < 316 \text{ GeV}$. Jets are selected with $|y| < 2.1$ and $|\phi_1 - \phi_2| > 7\pi/8$. The normalization uncertainties (not shown) are $\delta\langle T_{AA} \rangle / \langle T_{AA} \rangle = 0.9\%$ in 0–10% Pb+Pb collisions and $\delta L_{pp} / L_{pp} = 1\%$ in pp collisions. The boxes correspond to systematic uncertainties and the bars to statistical uncertainties.

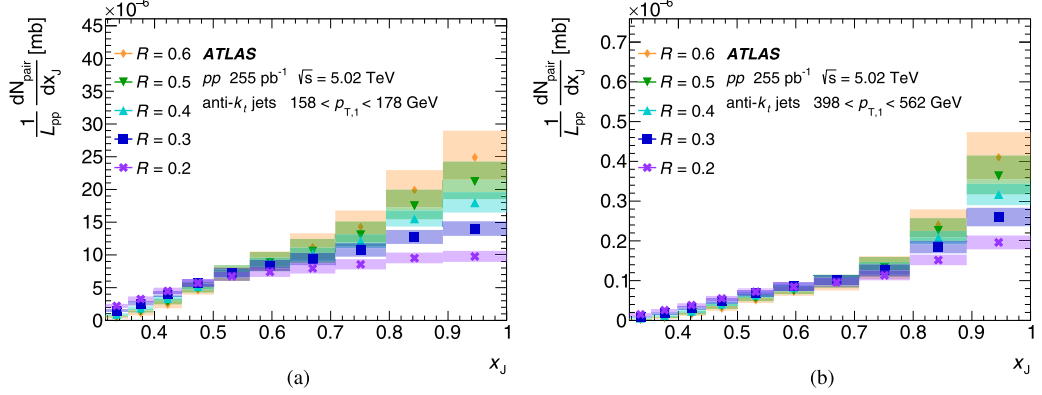


FIG. 10. The absolutely normalized x_J distributions in pp collisions for leading jets with (a) $158 < p_{T,1} < 178$ GeV and (b) $398 < p_{T,1} < 562$ GeV. Jets are selected with $|y| < 2.1$ and $|\phi_1 - \phi_2| > 7\pi/8$. The normalization uncertainty (not shown) is $\delta L_{pp}/L_{pp} = 1\%$. The boxes correspond to systematic uncertainties and the bars to statistical uncertainties.

The systematic uncertainties in the absolutely normalized x_J distributions can be seen in Fig. 2, for 0–10% central $Pb+Pb$ and pp collisions, and for $R = 0.2$ and $R = 0.6$ jets. In central $Pb+Pb$ collisions for $R = 0.2$ jets, the total uncertainties are driven by the JES and JER uncertainties; for $R = 0.6$ jets in these collisions, the total systematic uncertainties are driven by the unfolding’s sensitivity to the choice of prior and its closure. In pp collisions, the total uncertainties are largely driven by the JES and JER uncertainties for both the

$R = 0.2$ and $R = 0.6$ jets. The relative uncertainties are largest at low x_J in both collision systems; however, the yield in these x_J regions is small. Similar trends were obtained for the systematic uncertainties of $R = 0.3$, $R = 0.4$, and $R = 0.5$ jets, with similar values of the relative uncertainties.

The systematic uncertainty contributions are similarly propagated to the calculation of R_{AA}^{pair} and J_{AA} . The centrality-independent components of the JES and JER, and the centrality-independent part of the jet radius dependent

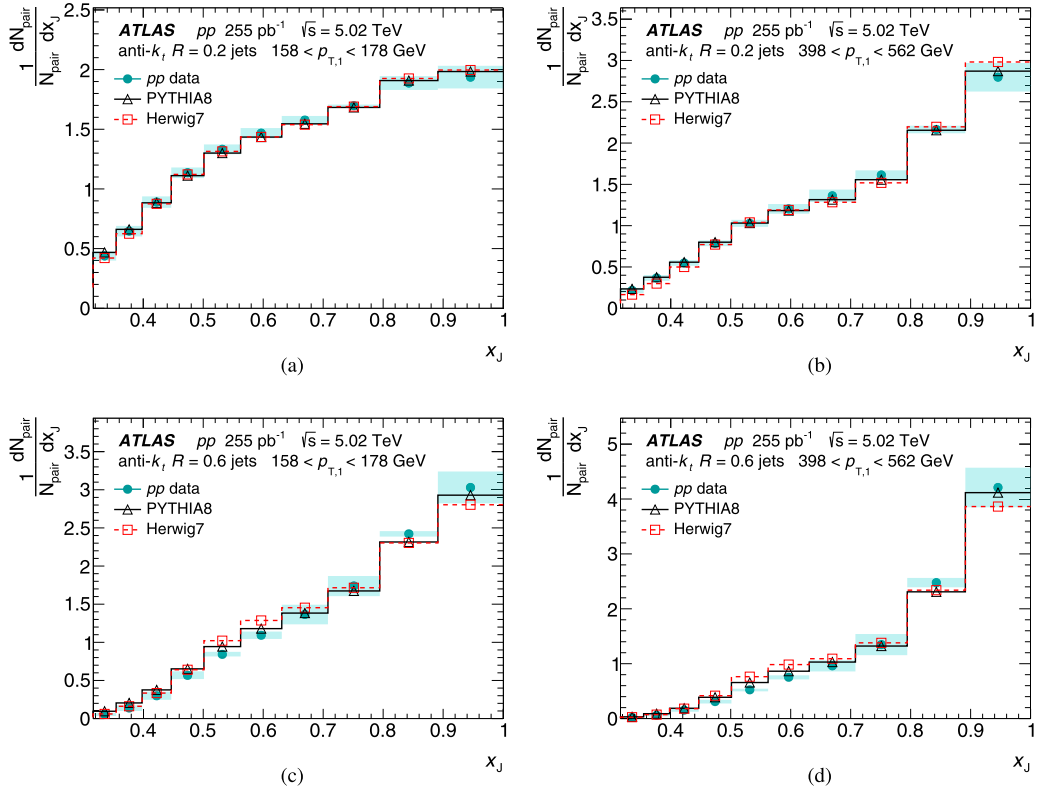


FIG. 11. The dijet-yield-normalized x_J distributions in pp collisions, and in PYTHIA 8 and HERWIG7 simulations, for (a), (b) $R = 0.2$ and (c), (d) $R = 0.6$ jets with (a), (c) $158 < p_{T,1} < 178$ GeV and (b), (d) $398 < p_{T,1} < 562$ GeV. Jets are selected with $|y| < 2.1$ and $|\phi_1 - \phi_2| > 7\pi/8$. The boxes correspond to systematic uncertainties and the bars to statistical uncertainties.

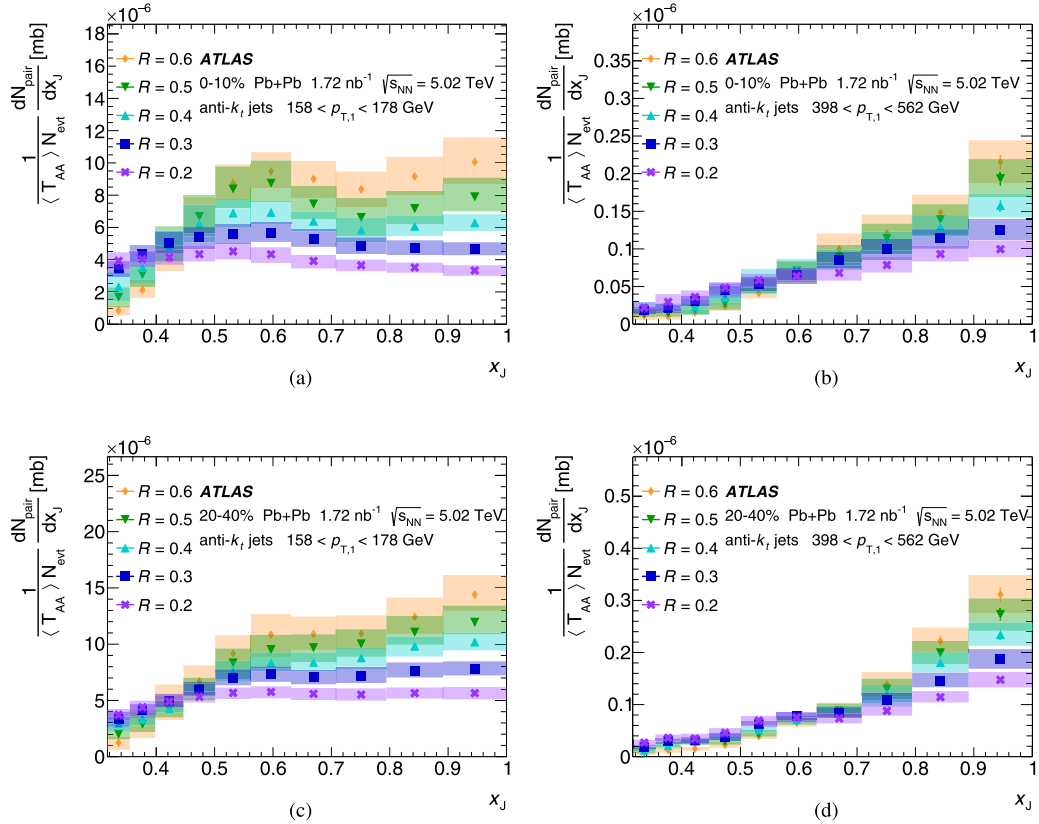


FIG. 12. The absolutely normalized x_J distributions in (a), (b) 0–10% and (c), (d) 20–40% central Pb+Pb collisions, for leading jets with (a), (c) $158 < p_{T,1} < 178$ GeV and (b), (d) $398 < p_{T,1} < 562$ GeV. Jets are selected with $|y| < 2.1$ and $|\phi_1 - \phi_2| > 7\pi/8$. The normalization uncertainties (not shown) are $\delta \langle T_{AA} \rangle / \langle T_{AA} \rangle = 0.9\%$ and 2% for Pb+Pb centrality selections 0–10% and 20–40%, respectively. The boxes correspond to systematic uncertainties and the bars to statistical uncertainties.

uncertainty are treated as correlated between Pb+Pb and pp collisions. The rest of the contributions to the systematic uncertainty are treated as uncorrelated between Pb+Pb and pp . The resulting uncertainties in $R_{AA}^{\text{pair}}(p_{T,1})$ and $R_{AA}^{\text{pair}}(p_{T,2})$ are shown for 0–10% central Pb+Pb collisions in Fig. 3 for $R = 0.2$ and $R = 0.6$ jets; these uncertainties are dominated by the JES and JER. Similar trends were obtained for the systematic uncertainties of $R = 0.3$, $R = 0.4$, and $R = 0.5$ jets, with similar values of the relative uncertainties. In the ratio $R_{AA}^{\text{pair}}(p_{T,2})/R_{AA}^{\text{pair}}(p_{T,1})$ each source of systematic uncertainty is treated as fully correlated between $R_{AA}^{\text{pair}}(p_{T,2})$ and $R_{AA}^{\text{pair}}(p_{T,1})$, including the global systematic uncertainties. The ratios allow the cancellation of systematic uncertainties and improve the precision of the measurements.

VII. RESULTS

A. R_{AA}^{pair} distributions

The leading and subleading dijet yields in 0–10% central Pb+Pb collisions and the dijet cross sections in pp collisions are shown in Fig. 4 for the various jet radii. These distributions correspond to the numerators and denominators in Eqs. (4) and (5). Figure 5 shows the dijet cross-section ratios of $R = 0.3, 0.4, 0.5, 0.6$ jets with respect to $R = 0.2$ jets in

central Pb+Pb and pp collisions. The dijet yields increase with increasing jet radius at a given jet p_T , for both the leading and subleading jets in both collision systems. Additionally, the dijet cross-section ratios in pp data, for R jets with respect to $R = 0.2$ jets, are compared with PYTHIA 8 and HERWIG7 simulations in Fig. 5. Generally the PYTHIA 8 results are closer to the data than the HERWIG7 results. HERWIG7 consistently underpredicts the cross-section ratios.

The R_{AA}^{pair} distributions are shown in Fig. 6 for $R = 0.2$ and $R = 0.6$ jets. For both jet radii, the leading jet $R_{AA}^{\text{pair}}(p_{T,1})$ is larger than the subleading jet $R_{AA}^{\text{pair}}(p_{T,2})$ for all p_T considered here. It is also observed that $R_{AA}^{\text{pair}}(p_{T,1})$ and $R_{AA}^{\text{pair}}(p_{T,2})$ generally increase with increasing p_T , except for the leading $R_{AA}^{\text{pair}}(p_{T,1})$ of the $R = 0.6$ jets, which is flatter as a function of p_T . This behavior had also been previously observed with $R = 0.4$ jets in Ref. [28].

To understand the differences between the R_{AA}^{pair} of leading and subleading jets, the $R_{AA}^{\text{pair}}(p_{T,2})/R_{AA}^{\text{pair}}(p_{T,1})$ ratio is considered. Figure 7 shows $R_{AA}^{\text{pair}}(p_{T,2})/R_{AA}^{\text{pair}}(p_{T,1})$ as a function of centrality, jet radius, and p_T for jets with $158 < p_T < 316$ GeV. The overall trend as a function of centrality is as expected; for all jet radii, the most central collisions show the most suppression of the subleading jet relative to the leading jet in the dijet, and the most peripheral collisions show the

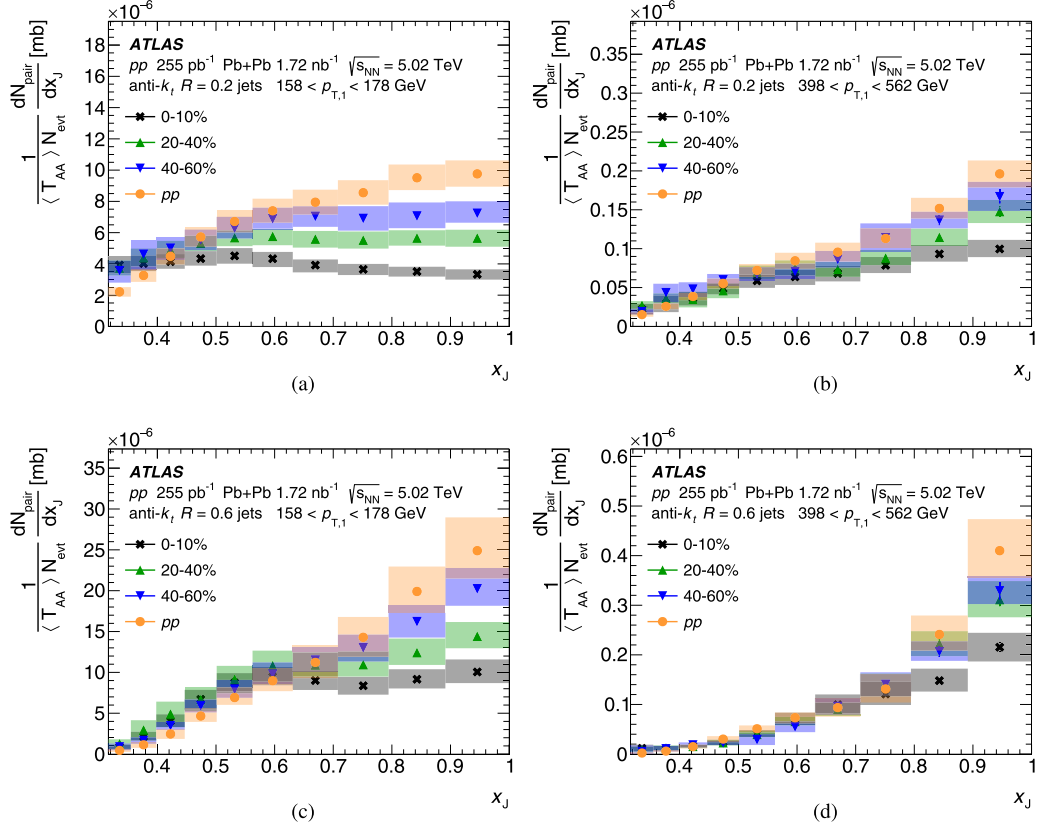


FIG. 13. The absolutely normalized x_J distributions for (a), (b) $R = 0.2$ and (c), (d) $R = 0.6$ jets for three centrality selections in Pb+Pb collisions and pp collisions. Leading jets with (a), (c) $158 < p_{T,1} < 178$ GeV and (b), (d) $398 < p_{T,1} < 562$ GeV are shown. Jets are selected with $|y| < 2.1$ and $|\phi_1 - \phi_2| > 7\pi/8$. The normalization uncertainties (not shown) are $\delta(T_{AA})/(T_{AA}) = 0.9\%$, 2% , and 5% in $0-10\%$, $20-40\%$, and $40-60\%$ Pb+Pb collisions, respectively, and $\delta L_{pp}/L_{pp} = 1\%$ in pp collisions. The boxes correspond to systematic uncertainties and the bars to statistical uncertainties.

least. This can be explained in terms of a path length dependent jet energy loss, which causes the subleading jets to experience an additional amount of quenching by traversing a longer distance within the QGP medium compared with the leading jets. The R dependence of this ratio is shown for both the most central and most peripheral Pb+Pb collisions; no significant R dependence is observed for either. For central Pb+Pb collisions the value of this ratio is approximately 0.7–0.8, whereas for peripheral collisions the value is higher, it is approximately 0.9–1.1. Additionally, the $R_{AA}^{\text{pair}}(p_{T,2})/R_{AA}^{\text{pair}}(p_{T,1})$ ratio shows no significant dependence on p_T for smaller jet radii while for larger jet radii the ratio slightly increases with increasing p_T , for both central and peripheral collisions.

Discussion of the R_{AA}^{pair} distributions

To evaluate the R dependence of the R_{AA}^{pair} distributions, the leading and subleading jet R_{AA} , along with the corresponding $R_{AA}^{\text{pair}}(R)/R_{AA}^{\text{pair}}(0.2)$ ratios, are shown in Fig. 8 for the various jet radii for the 0–10% centrality selection. Some R dependence is observed for the leading jets, with $R_{AA}^{\text{pair}}(p_{T,1})$ increasing with the jet radius. In the most central collisions at a p_T of approximately 200 GeV, the $R_{AA}^{\text{pair}}(p_{T,1})$ of $R = 0.2$ jets

is approximately 0.55, whereas for $R = 0.6$ it is closer to 0.65. This R dependence is consistent with larger R jets being less suppressed than smaller R jets. A similar R dependence was observed in Ref. [20]. An R dependence is also observed for subleading jets, but the $R_{AA}^{\text{pair}}(p_{T,2})$ values and the deviations from unity in the $R_{AA}^{\text{pair}}(R)/R_{AA}^{\text{pair}}(0.2)$ ratio is smaller than for the leading jets. Since the $R_{AA}^{\text{pair}}(p_{T,2})/R_{AA}^{\text{pair}}(p_{T,1})$ ratio shows no significant dependence on R or p_T (as seen in Fig. 7), the $R_{AA}^{\text{pair}}(p_{T,2})$ of subleading jets can be seen, approximately, as a scaled down version of the $R_{AA}^{\text{pair}}(p_{T,1})$ of leading jets, by a factor only dependent on centrality.

Additionally, the R_{AA}^{pair} distribution as a function of the jet radius is shown in Fig. 9 for two p_T selections in 0–10% central collisions, $158 < p_T < 178$ GeV and $282 < p_T < 316$ GeV. Some R dependence of R_{AA}^{pair} is observed, with R_{AA}^{pair} increasing with the jet radius, a dependence that is stronger at lower p_T .

B. x_J distributions

The absolutely normalized x_J distributions in pp collisions, as defined in Eq. (6), are shown in Fig. 10, for leading jets with $158 < p_{T,1} < 178$ GeV and $398 < p_{T,1} < 562$ GeV for

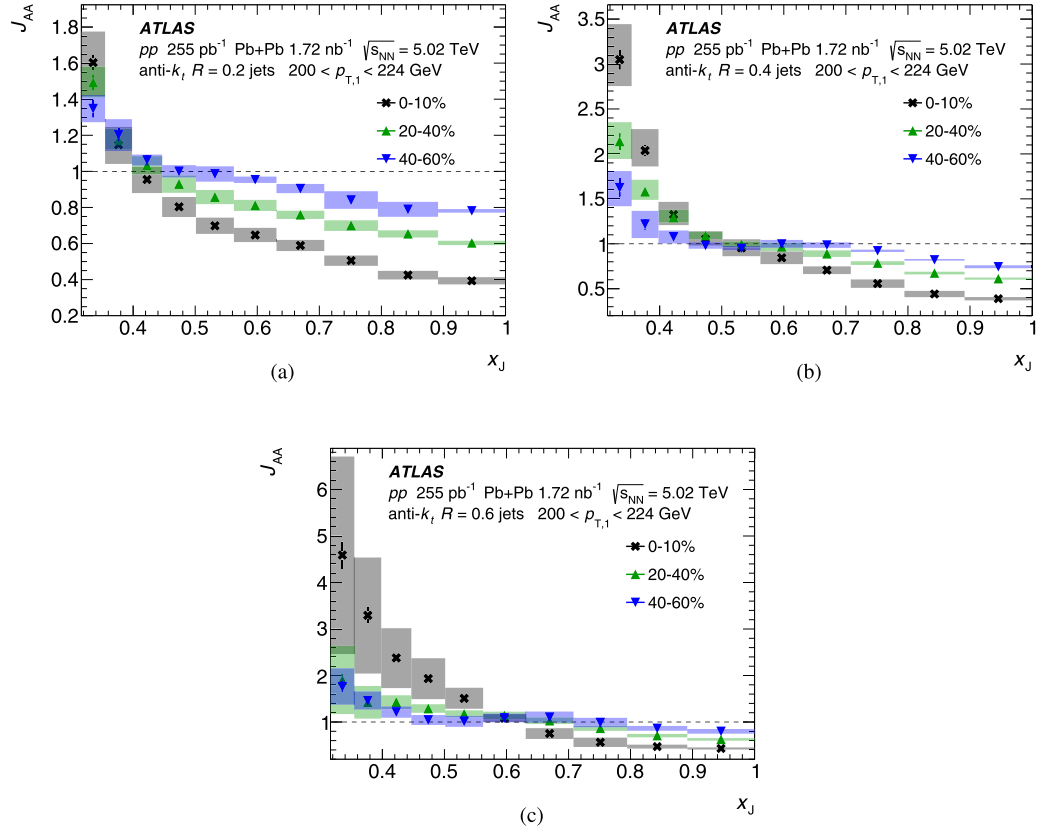


FIG. 14. The J_{AA} distributions for (a) $R = 0.2$, (b) $R = 0.4$, and (c) $R = 0.6$ jets for three centrality selections in Pb+Pb collisions and pp collisions. Leading jets with $200 < p_{T,1} < 224$ GeV are shown. Jets are selected with $|y| < 2.1$ and $|\phi_1 - \phi_2| > 7\pi/8$. The normalization uncertainties (not shown) are $\delta\langle T_{AA}\rangle/\langle T_{AA}\rangle = 0.9\%$, 2% , and 5% in $0-10\%$, $20-40\%$, and $40-60\%$ Pb+Pb collisions, respectively, and $\delta L_{pp}/L_{pp} = 1\%$ in pp collisions. The boxes correspond to systematic uncertainties and the bars to statistical uncertainties.

all jet radii considered here. The shapes of the distributions are similar for the two $p_{T,1}$ selections shown. In both cases, the distributions are peaked toward balanced dijets as expected. The distributions are more sharply peaked at $x_J \approx 1$ for larger radius jets. This is expected if the larger radius jets cluster together radiation that could be reconstructed as separate jets for the smaller radii. For higher $p_{T,1}$, the distributions for the various jet radii are closer together than for lower $p_{T,1}$, presumably because higher p_T jets are more collimated.

A comparison of the pp data to PYTHIA 8 and HERWIG7 simulations is shown in Fig. 11. Here the dijet-yield-normalized x_J distributions are plotted for $R = 0.2$ and $R = 0.6$ jets with $158 < p_{T,1} < 178$ GeV and $398 < p_{T,1} < 562$ GeV. The dijet-yield-normalized x_J distributions are considered in order to take out any overall cross-section difference between the models and data. The pp data are well described by the simulations for the various jet radii.

Discussion of the x_J distributions

Figure 12 shows the R dependence of the absolutely normalized x_J distributions in Pb+Pb collisions, as defined in Eq. (7), for the centrality selections $0-10\%$ and $20-40\%$, and the same $p_{T,1}$ selections as shown for pp collisions. The x_J distributions in Pb+Pb collisions are broadened compared

with those in pp collisions in Fig. 10. The magnitude of the modification is larger for lower $p_{T,1}$ values and for more central collisions. For the $158 < p_{T,1} < 178$ GeV selection in mid-central collisions, the peak at balanced dijets remains compared with pp collisions, but becomes weaker as the jet radius decreases. For this $p_{T,1}$ selection in $0-10\%$ central collisions, the distributions are nearly flat for $x_J > 0.5$. For the $398 < p_{T,1} < 562$ GeV selection, the x_J distributions in both central and mid-central Pb+Pb collisions remain peaked at $x_J \approx 1$ for the jet radii considered here.

To look more closely at the centrality dependent modification from the distributions in pp collisions, Fig. 13 shows the overlaid x_J distributions for $0-10\%$, $20-40\%$, and $40-60\%$ central Pb+Pb collisions. Two $p_{T,1}$ selections, $158 < p_{T,1} < 178$ GeV and $398 < p_{T,1} < 562$ GeV, for $R = 0.2$ and $R = 0.6$ jets are shown. As expected, x_J distributions in the most central Pb+Pb collisions are the most modified compared with those in pp collisions, with the rate of balanced dijets being strongly suppressed.

C. J_{AA} distributions

The ratio of the dijet yields in Pb+Pb collisions to pp collisions, J_{AA} , is defined in Eq. (9). The J_{AA} distributions for $0-10\%$, $20-40\%$, and $40-60\%$, are shown in Fig. 14 for

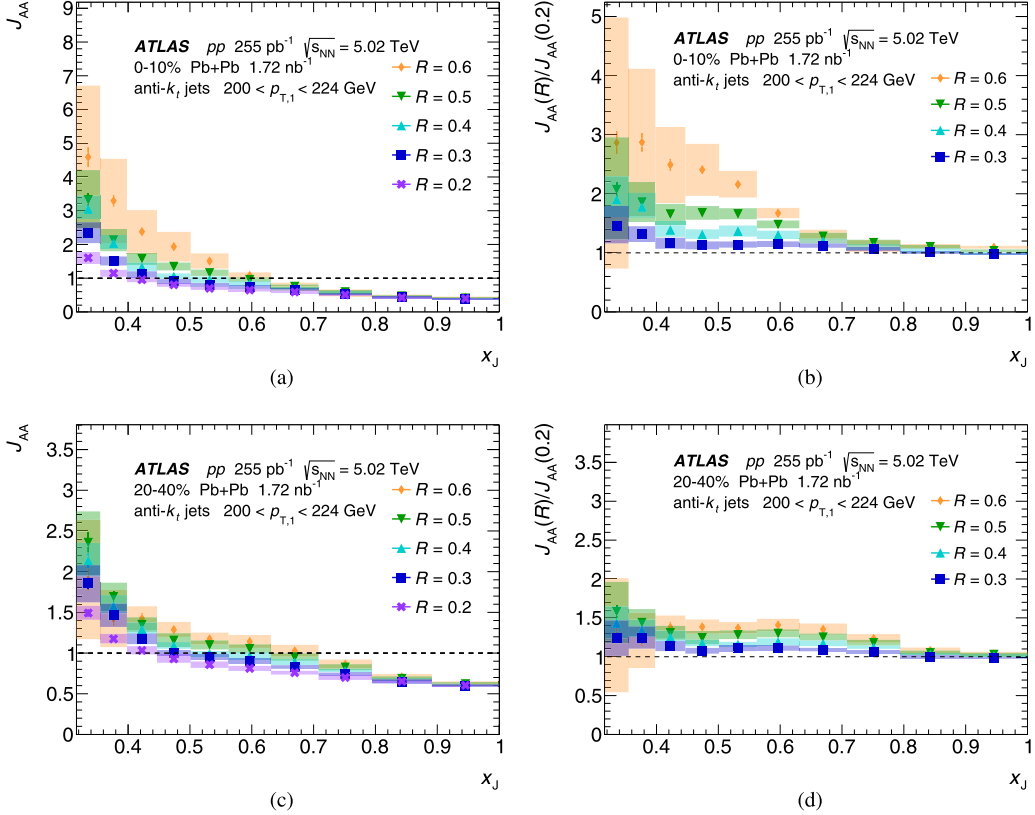


FIG. 15. The (a), (c) J_{AA} distributions and its corresponding (b), (d) $J_{AA}(R)/J_{AA}(0.2)$ ratios in (a), (b) 0–10% and (c), (d) 20–40% central Pb+Pb collisions, for $200 < p_{T,1} < 224$ GeV. Jets are selected with $|y| < 2.1$ and $|\phi_1 - \phi_2| > 7\pi/8$. The normalization uncertainties in J_{AA} (not shown) are $\delta(T_{AA})/\langle T_{AA} \rangle = 0.9\%$ and 2% in 0–10% and 20–40% Pb+Pb collisions, respectively, and $\delta L_{pp}/L_{pp} = 1\%$ in pp collisions. The boxes correspond to systematic uncertainties and the bars to statistical uncertainties.

$R = 0.2$, $R = 0.4$, and $R = 0.6$ jets. The p_T selection of $200 < p_{T,1} < 224$ GeV was chosen because it is representative of the overall trends in the results. For the various centralities, there is a suppression in the number of balanced (high x_J) dijets and an enhancement in the number of imbalanced (low x_J) dijets, with the modifications being larger towards more central collisions. While the enhancement at low x_J can be large in terms of J_{AA} , it is worth recalling that the corresponding absolute dijet yields are small at low x_J , especially for the larger R jets, as was previously seen in Fig. 12. The larger uncertainties in J_{AA} for the $R = 0.6$ jets, especially in the most central collisions, are driven by the sensitivity to the unfolding prior weights as well as the JES and JER, which affect the bins at low x_J and low p_T where the dijet yields are small.

Discussion of the J_{AA} distributions

The J_{AA} distributions are overlaid for the various jet radii in Fig. 15, along with their corresponding $J_{AA}(R)/J_{AA}(0.2)$ ratios. In the most central collisions, 0–10%, a larger J_{AA} is observed for larger jet radius, a trend more noticeable towards lower x_J . In 20–40% central collisions, the same quantitative trend is observed but the magnitude of the deviation from unity is smaller. Similarly, in terms of the $J_{AA}(R)/J_{AA}(0.2)$ ratios, at low x_J there is a spread of the central values of J_{AA}

for the various jet radii and the uncertainties are larger. The large uncertainties in the J_{AA} of the larger jets at low x_J values were previously noted in the discussion of Fig. 14 and affect the $J_{AA}(R)/J_{AA}(0.2)$ ratios as well. At high x_J , the J_{AA} values show an R dependence of smaller magnitude.

To evaluate the R dependence of these distributions, the J_{AA} is plotted as a function of the jet radius in Fig. 16, for several $p_{T,1}$ selections at x_J values of $0.89 < x_J < 1.0$ and $0.50 < x_J < 0.56$ in the most central collisions. The corresponding $J_{AA}(R)/J_{AA}(0.2)$ ratios are shown in Fig. 17. For nearly balanced dijets ($0.89 < x_J < 1.0$), a small R dependence to J_{AA} is observed [more noticeable in the $J_{AA}(R)/J_{AA}(0.2)$ ratios], with J_{AA} increasing with the jet radius, and dependent on $p_{T,1}$. As the dijets become more imbalanced ($0.50 < x_J < 0.56$), this R dependence becomes stronger. For both balanced and imbalanced dijets, the R dependence is observed to be larger for lower $p_{T,1}$ values. This R -dependent behavior can be explained by considering that the subleading jets, which have lost energy and thus caused the dijets to become imbalanced, recover some of the lost energy as the jet radius increases. Another contribution comes from the medium response, which can add energy to the jets.

To assess the p_T dependence of the $J_{AA}(R)/J_{AA}(0.2)$ ratios, Fig. 18 shows the $J_{AA}(R)/J_{AA}(0.2)$ ratios as a function of $p_{T,1}$, for $R = 0.4$ and $R = 0.6$ jets, and two x_J selections,

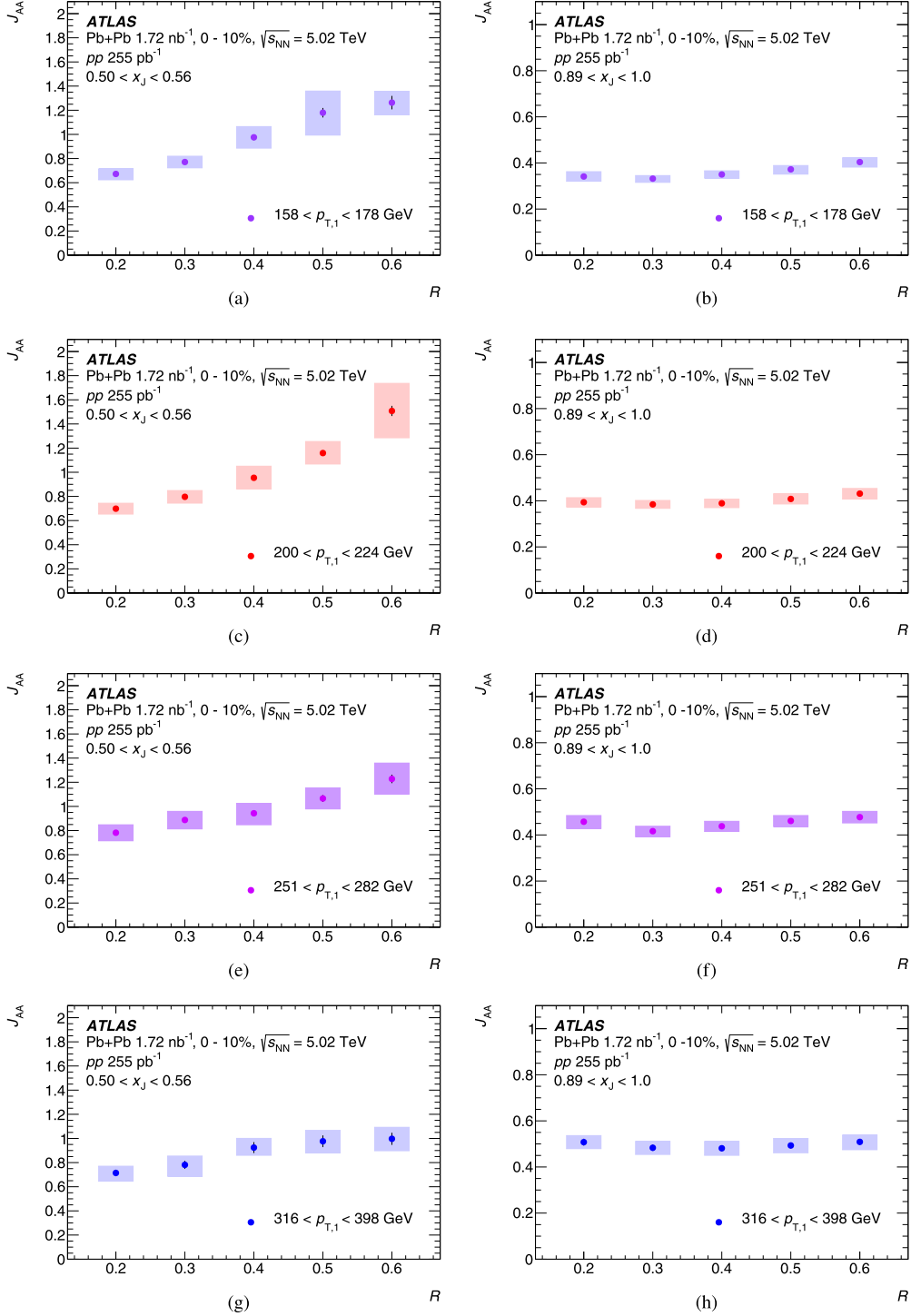


FIG. 16. The J_{AA} values as a function of R for jets with (a), (b) $158 < p_{T,1} < 178 \text{ GeV}$, (c), (d) $200 < p_{T,1} < 224 \text{ GeV}$, (e), (f) $251 < p_{T,1} < 282 \text{ GeV}$, and (g), (h) $316 < p_{T,1} < 398 \text{ GeV}$ in 0–10% central Pb+Pb collisions, for (a), (c), (e), (g) $0.50 < x_J < 0.56$ and (b), (d), (f), (h) $0.89 < x_J < 1.0$. Jets are selected with $|y| < 2.1$ and $|\phi_1 - \phi_2| > 7\pi/8$. The normalization uncertainties (not shown) are $\delta\langle T_{AA}\rangle/\langle T_{AA}\rangle = 0.9\%$ and 2% in 0–10% and 20–40% Pb+Pb collisions, respectively, and $\delta L_{pp}/L_{pp} = 1\%$ in pp collisions. The boxes correspond to systematic uncertainties and the bars to statistical uncertainties.

$0.50 < x_J < 0.56$ and $0.89 < x_J < 1.0$. The $J_{AA}(R)/J_{AA}(0.2)$ ratios come closer to unity with increasing $p_{T,1}$, with the modification being larger for larger R jets. The deviations from unity are much smaller for balanced dijets than for imbalanced dijets.

D. Comparison with theory

Results are compared with the linear Boltzmann transport (LBT) [65] and JETSCAPE [66] models. Both of these models use PYTHIA 8 pp as the baseline for the hard processes,

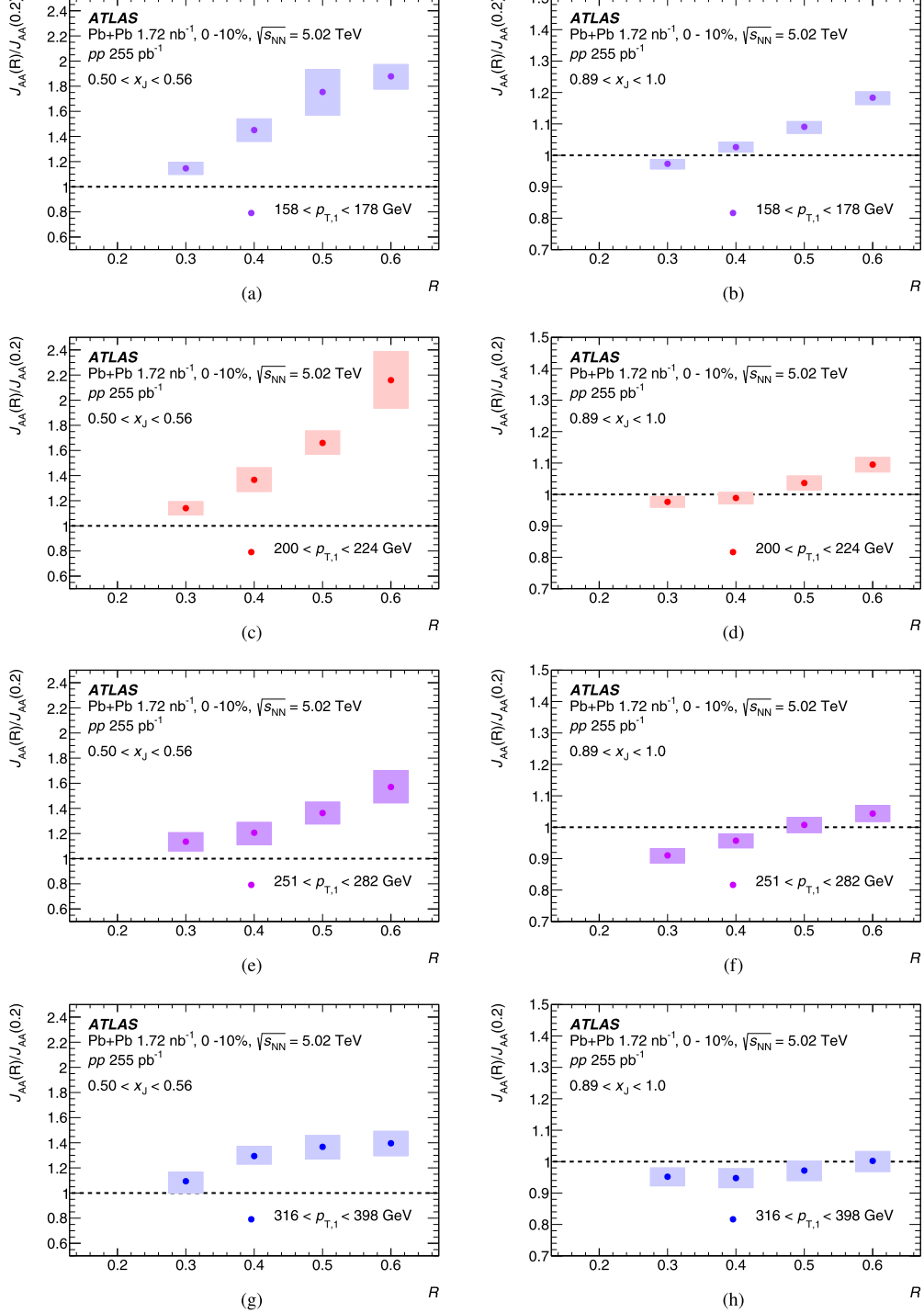


FIG. 17. The $J_{AA}(R)/J_{AA}(0.2)$ ratios as a function of R for jets with (a), (b) $158 < p_{T,1} < 178$ GeV, (c), (d) $200 < p_{T,1} < 224$ GeV, (e), (f) $251 < p_{T,1} < 282$ GeV, (g), (h) $316 < p_{T,1} < 398$ GeV in 0–10% central Pb+Pb collisions, for (a), (c), (e), (g) $0.50 < x_J < 0.56$ and (b), (d), (f), (h) $0.89 < x_J < 1.0$. Jets are selected with $|y| < 2.1$ and $|\phi_1 - \phi_2| > 7\pi/8$. The boxes correspond to systematic uncertainties and the bars to statistical uncertainties.

but with a different evolution of the parton showers. The LBT model uses Boltzmann transport equations to describe the propagation of jet and medium partons as they traverse a QGP, including elastic and inelastic perturbative QCD

processes. The JETSCAPE model combines [67], in tune v3.5 AA22, the LBT model at low parton virtuality with a MATTER [68] medium-modified parton shower at high parton virtuality.

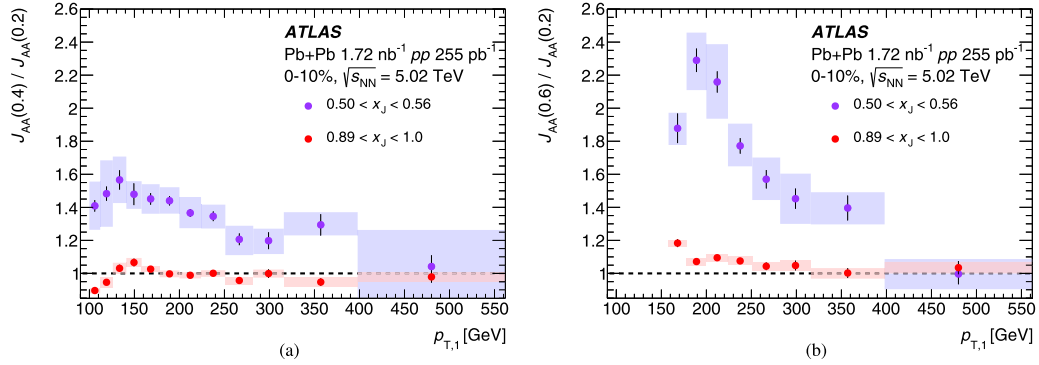


FIG. 18. The $J_{AA}(R)/J_{AA}(0.2)$ ratios as a function of $p_{T,1}$ for (a) $R = 0.4$ and (b) $R = 0.6$ jets in 0–10% central Pb+Pb collisions, for $0.50 < x_J < 0.56$ and $0.89 < x_J < 1.0$. Jets are selected with $|y| < 2.1$ and $|\phi_1 - \phi_2| > 7\pi/8$. The boxes correspond to systematic uncertainties and the bars to statistical uncertainties.

Figure 19 shows the R_{AA}^{pair} distributions of the leading and subleading jets in dijets compared with the LBT and JETSCAPE models, for $R = 0.2$ and $R = 0.6$ jets in 0–10% central collisions. For both the large and small- R jets, the models predict that the subleading jets are more suppressed than the leading jets in dijets in terms of the R_{AA}^{pair} . However, they have varying degrees of success in describing the measured R_{AA}^{pair} values. For $R = 0.2$ jets, the LBT model underestimates the data for both the leading and subleading jets; the JETSCAPE model describes the leading jet R_{AA}^{pair} distribution well, but overestimates the subleading jet distribution. For $R = 0.6$ jets, the LBT model fully describes the leading jet R_{AA}^{pair} distribution, but overestimates the subleading jet distribution; the JETSCAPE model describes the subleading jet R_{AA}^{pair} distribution, but underestimates the leading jet distribution.

The $R_{AA}^{\text{pair}}(R = 0.6)/R_{AA}^{\text{pair}}(R = 0.2)$ ratio is shown in Fig. 20 for both the leading and subleading jets in 0–10% central collisions. For both the leading and subleading jet R_{AA}^{pair} , the data lies between the models for the full p_T range, with the LBT model above the data and the JETSCAPE model

below the data. Additionally, the data show larger values of the $R_{AA}^{\text{pair}}(R = 0.6)/R_{AA}^{\text{pair}}(R = 0.2)$ ratio for the leading jets than for the subleading jets. The JETSCAPE model predicts this order while the LBT model predicts the opposite order.

Figure 21 shows the absolutely normalized x_J distributions in data compared with the JETSCAPE model for the various jet radii in pp and 0–10% central Pb+Pb collisions. At high x_J values ($x_J > 0.65$), the model describes the pp data well, while at lower x_J values it overestimates the data. In the case of the Pb+Pb data, the model describes the data at high x_J values. For $0.45 < x_J < 0.65$, the model underestimates the Pb+Pb data. For lower x_J values, the model overestimates the Pb+Pb data.

VIII. CONCLUSION

This paper presents a measurement of the dependence of the dijet momentum balance on the jet radius, in Pb+Pb and pp collisions at $\sqrt{s_{NN}} = 5.02 \text{ TeV}$. Dijets were studied for jet radii $R = 0.2, 0.3, 0.4, 0.5$, and 0.6 by measuring the

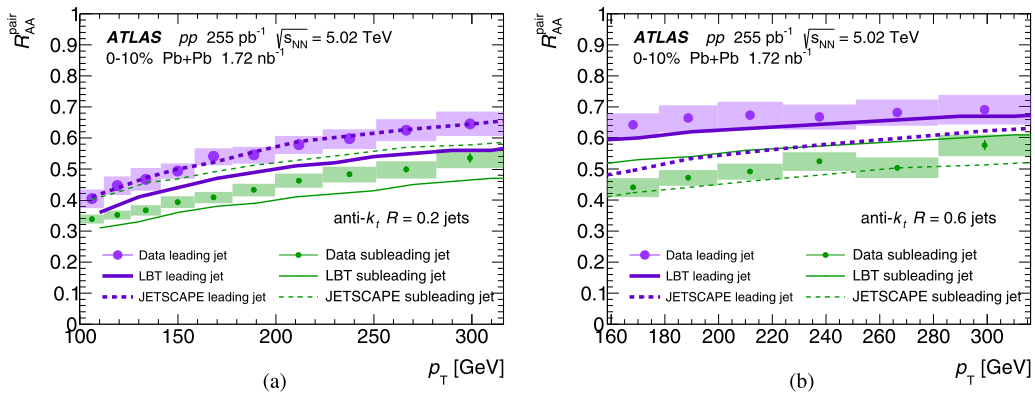


FIG. 19. The leading and subleading jet R_{AA}^{pair} distributions in dijets in data, compared with the LBT and JETSCAPE (LBT + MATTER) models. (a) $R = 0.2$ and (b) $R = 0.6$ jets are shown for 0–10% central collisions. Jets are selected with $|y| < 2.1$ and $|\phi_1 - \phi_2| > 7\pi/8$. The normalization uncertainties in the data (not shown) are $\delta \langle T_{AA} \rangle / \langle T_{AA} \rangle = 0.9\%$ in 0–10% Pb+Pb collisions and $\delta L_{pp} / L_{pp} = 1\%$ in pp collisions. The boxes correspond to systematic uncertainties and the bars to statistical uncertainties.

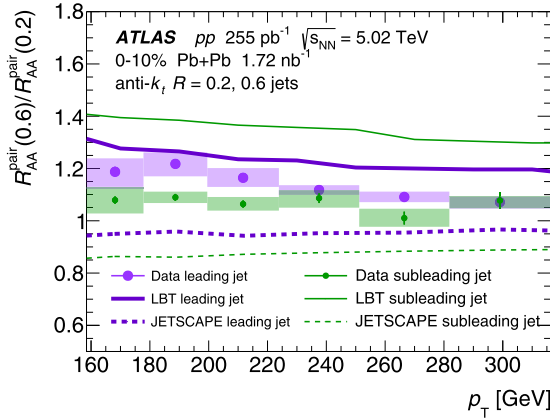


FIG. 20. The leading and subleading jet $R_{AA}^{\text{pair}}(R = 0.6)/R_{AA}^{\text{pair}}(R = 0.2)$ in dijets in data compared with the LBT and JETSCAPE (LBT + MATTER) models for 0–10% central collisions. Jets are selected with $|y| < 2.1$ and $|\phi_1 - \phi_2| > 7\pi/8$. The boxes correspond to systematic uncertainties and the bars to statistical uncertainties.

absolutely normalized x_J , J_{AA} , and R_{AA}^{pair} distributions. The measurement covers a broad transverse momentum range, with leading jet $p_{T,1}$ ranging from 100 to 562 GeV for $R = 0.2, 0.3$, and 0.4 jets and from 158 to 562 GeV for $R = 0.5$ and 0.6 jets.

The R_{AA}^{pair} results show that subleading jets in dijets are more suppressed than leading jets, for the various jet radii considered. Significant jet radius dependence of the R_{AA}^{pair} is observed, with jet suppression decreasing (R_{AA}^{pair} increasing) with increasing jet radius. This jet radius dependence is observed in both the leading jet $R_{AA}^{\text{pair}}(p_{T,1})$ and subleading jet $R_{AA}^{\text{pair}}(p_{T,2})$, although not in the $R_{AA}^{\text{pair}}(p_{T,2})/R_{AA}^{\text{pair}}(p_{T,1})$ ratio, which is dependent on centrality only.

The results show that larger jet radii give x_J distributions peaked at higher x_J values, whereas smaller jet radii give flatter distributions. This is true in both the Pb+Pb and pp collisions, but the Pb+Pb collisions lead to broader and more

modified distributions compared with pp , with the modifications being larger for more central collisions.

The J_{AA} results for more imbalanced dijets, primarily at low leading jet transverse momentum, show that jet suppression decreases (J_{AA} increases) with increasing jet radius. For more balanced dijets, the suppression is also present and dependent on the jet radius, but smaller in magnitude than for imbalanced dijets.

These results present a comprehensive look at the modification of dijet rates in Pb+Pb collisions compared with pp collisions. These results are complementary to existing measurements of the jet radius dependence of jet suppression, and will provide important new constraints to theoretical models of jet energy loss.

ACKNOWLEDGMENTS

We thank CERN for the very successful operation of the LHC and its injectors, as well as the support staff at CERN and at our institutions worldwide without whom ATLAS could not be operated efficiently.

The crucial computing support from all WLCG partners is acknowledged gratefully, in particular from CERN, the ATLAS Tier-1 facilities at TRIUMF/SFU (Canada), NDGF (Denmark, Norway, Sweden), CC-IN2P3 (France), KIT/GridKA (Germany), INFN-CNAF (Italy), NL-T1 (Netherlands), PIC (Spain), RAL (UK) and BNL (USA), the Tier-2 facilities worldwide and large non-WLCG resource providers. Major contributors of computing resources are listed in Ref. [69].

We gratefully acknowledge the support of ANPCyT, Argentina; YerPhi, Armenia; ARC, Australia; BMWFW and FWF, Austria; ANAS, Azerbaijan; CNPq and FAPESP, Brazil; NSERC, NRC and CFI, Canada; CERN; ANID, Chile; CAS, MOST and NSFC, China; Minciencias, Colombia; MEYS CR, Czech Republic; DNRF and DNSRC, Denmark; IN2P3-CNRS and CEA-DRF/IRFU, France; SRNSFG, Georgia; BMBF, HGF and MPG, Germany; GSRI, Greece; RGC and Hong Kong SAR, China; ISF and Benoziyo Center, Israel; INFN, Italy; MEXT and JSPS, Japan; CNRST,

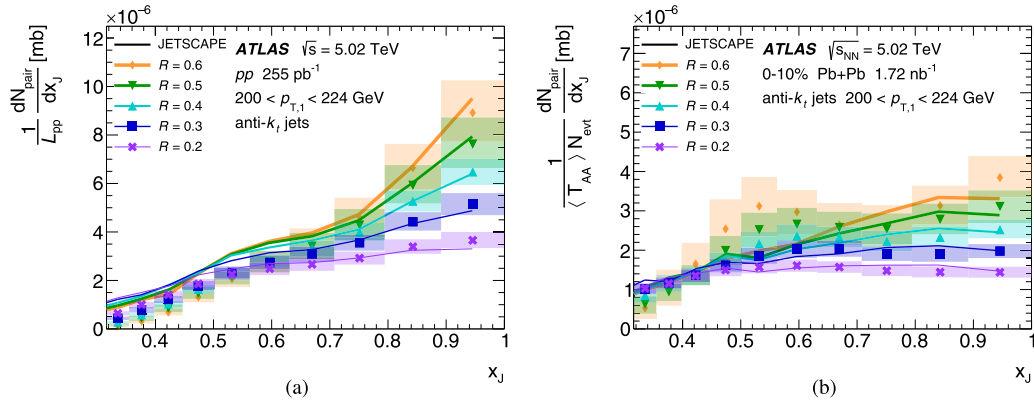


FIG. 21. The x_J distributions in data compared with the JETSCAPE (LBT + MATTER) model, for $R = 0.2, 0.3, 0.4, 0.5$, and 0.6 jets in (a) pp and (b) 0–10% central Pb+Pb collisions, for $200 < p_{T,1} < 224$ GeV. Jets are selected with $|y| < 2.1$ and $|\phi_1 - \phi_2| > 7\pi/8$. The normalization uncertainties in the data (not shown) are $\delta\langle T_{AA}\rangle/\langle T_{AA}\rangle = 0.9\%$ in 0–10% Pb+Pb collisions and $\delta L_{pp}/L_{pp} = 1\%$ in pp collisions. The boxes correspond to systematic uncertainties and the bars to statistical uncertainties.

Morocco; NWO, Netherlands; RCN, Norway; MNiSW, Poland; FCT, Portugal; MNE/IFA, Romania; MSTDI, Serbia; MSSR, Slovakia; ARIS and MVZI, Slovenia; DSi/NRF, South Africa; MICIU/AEI, Spain; SRC and Wallenberg Foundation, Sweden; SERI, SNSF and Cantons of Bern and Geneva, Switzerland; NSTC, Taipei; TENMAK, Türkiye; STFC/UKRI, United Kingdom; DOE and NSF, USA.

Individual groups and members have received support from BCKDF, CANARIE, CRC and DRAC, Canada; CERN-CZ, FORTE and PRIMUS, Czech Republic; COST, ERC, ERDF, Horizon 2020, ICSC-NextGenerationEU and Marie Skłodowska-Curie Actions, European Union; Investissements d'Avenir Labex, Investissements d'Avenir Idex and ANR, France; DFG and AvH Foundation, Germany; Herakleitos, Thales and Aristeia programmes co-financed by EU-ESF and the Greek NSRF, Greece; BSF-NSF and MINERVA, Israel; NCN and NAWA, Poland; La Caixa Banking Foundation, CERCA Programme Generalitat de Catalunya and PROMETEO and GenT Programmes Generalitat Valenciana, Spain; Göran Gustafssons Stiftelse, Sweden; The Royal Society and Leverhulme Trust, United Kingdom.

In addition, individual members wish to acknowledge support from Armenia: Yerevan Physics Institute (FAPERJ); CERN: European Organization for Nuclear Research (CERN PJAS); Chile: Agencia Nacional de Investigación y Desarrollo (FONDECYT 1230812, FONDECYT 1230987, FONDECYT 1240864); China: Chinese Ministry of Science and Technology (MOST-2023YFA1605700), National Natural Science Foundation of China (NSFC- 12175119, NSFC 12275265, NSFC-12075060); Czech Republic: Czech Science Foundation (GACR - 24-11373S), Ministry of Education Youth and Sports (FORTE CZ.02.01.01/00/22_008/0004632), PRIMUS Research Programme (PRIMUS/21/SCI/017); EU: H2020 European Research Council (ERC - 101002463); European Union: European Research Council (ERC-948254, ERC 101089007), Horizon 2020 Framework Programme (MUCCA- CHIST-ERA-19-XAI-00), European Union, Future Artificial Intelligence Research (FAIR-NextGenerationEU PE00000013), Italian Center for High Performance Computing, Big Data and Quantum Computing

(ICSC, NextGenerationEU); France: Agence Nationale de la Recherche (ANR-20-CE31-0013, ANR-21-CE31-0013, ANR-21-CE31-0022, ANR-22-EDIR-0002), Investissements d'Avenir Labex (ANR-11-LABX-0012); Germany: Baden-Württemberg Stiftung (BW Stiftung-Postdoc Eliteprogramme), Deutsche Forschungsgemeinschaft (DFG - 469666862, DFG - CR 312/5-2); Italy: Istituto Nazionale di Fisica Nucleare (ICSC, NextGenerationEU), Ministero dell'Università e della Ricerca (PRIN-20223N7F8K-PNRR M4.C2.1.1); Japan: Japan Society for the Promotion of Science (JSPS KAKENHI JP22H01227, JSPS KAKENHI JP22H04944, JSPS KAKENHI JP22KK0227, JSPS KAKENHI JP23KK0245); Netherlands: Netherlands Organisation for Scientific Research (NWO Veni 2020-VI.Veni.202.179); Norway: Research Council of Norway (RCN-314472); Poland: Ministry of Science and Higher Education (IDUB AGH, POB8, D4 no 9722), Polish National Agency for Academic Exchange (PPN/PPO/2020/1/00002/U/00001), Polish National Science Centre (NCN 2021/42/E/ST2/00350, NCN OPUS nr 2022/47/B/ST2/03059, NCN UMO-2019/34/E/ST2/00393, UMO-2020/37/B/ST2/01043, UMO-2021/40/C/ST2/00187, UMO-2022/47/O/ST2/00148, UMO-2023/49/B/ST2/04085); Slovenia: Slovenian Research Agency (ARIS Grant No. J1-3010); Spain: Generalitat Valenciana (Artemisa, FEDER, IDIFEDER/2018/048), Ministry of Science and Innovation (MCIN & NextGenEU PCI2022-135018-2, MCIN & FEDER PID2021-125273NB, RYC2019-028510-I, RYC2020-030254-I, RYC2021-031273-I, RYC2022-038164-I), PROMETEO and GenT Programmes Generalitat Valenciana (CIDEgent/2019/027); Sweden: Swedish Research Council (Swedish Research Council 2023-04654, VR 2018-00482, VR 2022-03845, VR 2022-04683, VR 2023-03403, VR Grant No. 2021-03651), Knut and Alice Wallenberg Foundation (KAW 2018.0157, KAW 2018.0458, KAW 2019.0447, KAW 2022.0358); Switzerland: Swiss National Science Foundation (SNSF-PCEFP2_194658); United Kingdom: Leverhulme Trust (Leverhulme Trust RPG-2020-004), Royal Society (NIF-R1-231091); USA: U.S. Department of Energy (ECA DE-AC02-76SF00515), Neubauer Family Foundation.

-
- [1] L. Evans and P. Bryant, LHC Machine, *J. Instrum.* **3**, S08001 (2008).
 - [2] B. Müller, J. Schukraft, and B. Wyslouch, First results from Pb+Pb collisions at the LHC, *Annu. Rev. Nucl. Part. Sci.* **62**, 361 (2012).
 - [3] G. Roland, K. Safarik, and P. Steinberg, Heavy-ion collisions at the LHC, *Prog. Part. Nucl. Phys.* **77**, 70 (2014).
 - [4] I. Arsene *et al.*, Quark gluon plasma and color glass condensate at RHIC? The perspective from the BRAHMS experiment, *Nucl. Phys. A* **757**, 1 (2005).
 - [5] B. B. Back *et al.*, The PHOBOS perspective on discoveries at RHIC, *Nucl. Phys. A* **757**, 28 (2005).
 - [6] J. Adams *et al.*, Experimental and theoretical challenges in the search for the quark gluon plasma: The STAR Collaboration's critical assessment of the evidence from RHIC collisions, *Nucl. Phys. A* **757**, 102 (2005).
 - [7] K. Adcox *et al.*, Formation of dense partonic matter in relativistic nucleus-nucleus collisions at RHIC: Experimental evaluation by the PHENIX collaboration, *Nucl. Phys. A* **757**, 184 (2005).
 - [8] A. Adare *et al.*, An upgrade proposal from the PHENIX collaboration, [arXiv:1501.06197](https://arxiv.org/abs/1501.06197).
 - [9] W. Busza, K. Rajagopal, and W. van der Schee, Heavy ion collisions: The big picture, and the big questions, *Annu. Rev. Nucl. Part. Sci.* **68**, 339 (2018).
 - [10] M. Connors, C. Nattrass, R. Reed, and S. Salur, Jet measurements in heavy ion physics, *Rev. Mod. Phys.* **90**, 025005 (2018).

- [11] L. Cunqueiro and A. M. Sickles, Studying the QGP with jets at the LHC and RHIC, *Prog. Part. Nucl. Phys.* **124**, 103940 (2022).
- [12] I. Vitev, S. Wicks, and B.-W. Zhang, A theory of jet shapes and cross sections: from hadrons to nuclei, *J. High Energy Phys.* **11** (2008) 093.
- [13] M. L. Miller, K. Reygers, S. J. Sanders, and P. Steinberg, Glauber modeling in high energy nuclear collisions, *Annu. Rev. Nucl. Part. Sci.* **57**, 205 (2007).
- [14] ATLAS Collaboration, Measurement of the nuclear modification factor for inclusive jets in Pb+Pb collisions at $\sqrt{s_{NN}} = 5.02$ TeV with the ATLAS detector, *Phys. Lett. B* **790**, 108 (2019).
- [15] CMS Collaboration, First measurement of large area jet transverse momentum spectra in heavy-ion collisions, *J. High Energy Phys.* **05** (2021) 284.
- [16] ALICE Collaboration, Measurements of inclusive jet spectra in pp and central Pb-Pb collisions at $\sqrt{s_{NN}} = 5.02$ TeV, *Phys. Rev. C* **101**, 034911 (2020).
- [17] ATLAS Collaboration, Measurement of suppression of large-radius jets and its dependence on substructure in Pb+Pb collisions at $\sqrt{s_{NN}} = 5.02$ TeV with the ATLAS detector, *Phys. Rev. Lett.* **131**, 172301 (2023).
- [18] D. Pablos, Jet suppression from a small to intermediate to large radius, *Phys. Rev. Lett.* **124**, 052301 (2020).
- [19] Y. Mehtar-Tani, D. Pablos, and K. Tywoniuk, Jet suppression and azimuthal anisotropy from RHIC to LHC, [arXiv:2402.07869](https://arxiv.org/abs/2402.07869).
- [20] ATLAS Collaboration, Measurement of the jet radius and transverse momentum dependence of inclusive jet suppression in lead-lead collisions at $\sqrt{s_{NN}} = 2.76$ TeV with the ATLAS detector, *Phys. Lett. B* **719**, 220 (2013).
- [21] ALICE Collaboration, Measurement of the radius dependence of charged-particle jet suppression in Pb-Pb collisions at $\sqrt{s_{NN}} = 5.02$ TeV, *Phys. Lett. B* **849**, 138412 (2024).
- [22] S. Cao and X.-N. Wang, Jet quenching and medium response in high-energy heavy-ion collisions: a review, *Rep. Prog. Phys.* **84**, 024301 (2021).
- [23] G.-Y. Qin and B. Müller, Explanation of dijet asymmetry in Pb-Pb collisions at the large hadron collider, *Phys. Rev. Lett.* **106**, 162302 (2011).
- [24] ATLAS Collaboration, Measurements of azimuthal anisotropies of jet production in Pb+Pb collisions at $\sqrt{s_{NN}} = 5.02$ TeV with the ATLAS detector, *Phys. Rev. C* **105**, 064903 (2022).
- [25] J. G. Milhano and K. C. Zapp, Origins of the di-jet asymmetry in heavy-ion collisions, *Eur. Phys. J. C* **76**, 288 (2016).
- [26] CMS Collaboration, In-medium modification of dijets in PbPb collisions at $\sqrt{s_{NN}} = 5.02$ TeV, *J. High Energy Phys.* **05** (2021) 116.
- [27] ATLAS Collaboration, Measurement of jet p_T correlations in Pb+Pb and pp collisions at $\sqrt{s_{NN}} = 2.76$ TeV with the ATLAS detector, *Phys. Lett. B* **774**, 379 (2017).
- [28] ATLAS Collaboration, Measurements of the suppression and correlations of dijets in Pb+Pb collisions at $\sqrt{s_{NN}} = 5.02$ TeV, *Phys. Rev. C* **107**, 054908 (2023).
- [29] ATLAS Collaboration, Observation of a centrality-dependent dijet asymmetry in lead-lead collisions at $\sqrt{s_{NN}} = 2.76$ TeV with the ATLAS detector at the LHC, *Phys. Rev. Lett.* **105**, 252303 (2010).
- [30] CMS Collaboration, Observation and studies of jet quenching in PbPb collisions at $\sqrt{s_{NN}} = 2.76$ TeV, *Phys. Rev. C* **84**, 024906 (2011).
- [31] ATLAS Collaboration, The ATLAS experiment at the CERN large hadron collider, *JINST* **3**, S08003 (2008).
- [32] M. Cacciari, G. P. Salam, and G. Soyez, The anti- k_t jet clustering algorithm, *J. High Energy Phys.* **04** (2008) 063.
- [33] ATLAS Collaboration, Luminosity determination in pp collisions at $\sqrt{s} = 13$ TeV using the ATLAS detector at the LHC, *Eur. Phys. J. C* **83**, 982 (2023).
- [34] ATLAS Collaboration, ATLAS insertable B-layer technical design report, ATLAS-TDR-19; CERN-LHCC-2010-013, 2010, <https://cds.cern.ch/record/1291633>, Addendum: ATLAS-TDR-19-ADD-1; CERN-LHCC-2012-009, 2012, <https://cds.cern.ch/record/1451888>.
- [35] B. Abbott *et al.*, Production and integration of the ATLAS insertable B-layer, *J. Instrum.* **13**, T05008 (2018).
- [36] ATLAS Collaboration, Software and computing for Run 3 of the ATLAS experiment at the LHC, [arXiv:2404.06335](https://arxiv.org/abs/2404.06335).
- [37] ATLAS Collaboration, Operation of the ATLAS trigger system in Run 2, *J. Instrum.* **15**, P10004 (2020).
- [38] ATLAS Collaboration, Trigger menu in 2017, ATL-DAQ-PUB-2018-002, 2018, <https://cds.cern.ch/record/2625986>.
- [39] ATLAS Collaboration, Trigger menu in 2018, ATL-DAQ-PUB-2019-001, 2019, <https://cds.cern.ch/record/2693402>.
- [40] ATLAS Collaboration, Performance of the ATLAS trigger system in 2015, *Eur. Phys. J. C* **77**, 317 (2017).
- [41] ATLAS Collaboration, Measurement of longitudinal flow decorrelations in Pb+Pb collisions at $\sqrt{s_{NN}} = 2.76$ and 5.02 TeV with the ATLAS detector, *Eur. Phys. J. C* **78**, 142 (2018).
- [42] ATLAS Collaboration, Measurement of W^\pm boson production in Pb+Pb collisions at $\sqrt{s_{NN}} = 5.02$ TeV with the ATLAS detector, *Eur. Phys. J. C* **79**, 935 (2019).
- [43] C. Loizides, J. Kamin, and D. d'Enterria, Improved Monte Carlo Glauber predictions at present and future nuclear colliders, *Phys. Rev. C* **97**, 054910 (2018); **99**, 019901(E) (2019).
- [44] T. Sjöstrand *et al.*, An introduction to PYTHIA 8.2, *Comput. Phys. Commun.* **191**, 159 (2015).
- [45] ATLAS Collaboration, ATLAS Pythia 8 tunes to 7 TeV data, ATL-PHYS-PUB-2014-021, 2014, <https://cds.cern.ch/record/1966419>.
- [46] NNPDF Collaboration, Parton distributions with LHC data, *Nucl. Phys. B* **867**, 244 (2013).
- [47] ATLAS Collaboration, The Pythia 8 A3 tune description of ATLAS minimum bias and inelastic measurements incorporating the Donnachie-Landshoff diffractive model, ATL-PHYS-PUB-2016-017, 2016, <https://cds.cern.ch/record/2206965>.
- [48] M. Bähr *et al.*, Herwig++ physics and manual, *Eur. Phys. J. C* **58**, 639 (2008).
- [49] J. Bellm *et al.*, Herwig 7.0/Herwig++ 3.0 release note, *Eur. Phys. J. C* **76**, 196 (2016).
- [50] S. Gieseke, C. Röhr, and A. Sióderek, Colour reconnections in Herwig++, *Eur. Phys. J. C* **72**, 2225 (2012).
- [51] J. Pumplin *et al.*, New generation of parton distributions with uncertainties from Global QCD analysis, *J. High Energy Phys.* **07** (2002) 012.
- [52] S. Agostinelli *et al.*, GEANT4—a simulation toolkit, *Nucl. Instrum. Methods Phys. Res., Sect. A* **506**, 250 (2003).
- [53] ATLAS Collaboration, The ATLAS simulation infrastructure, *Eur. Phys. J. C* **70**, 823 (2010).
- [54] M. Cacciari, G. P. Salam, and G. Soyez, FastJet user manual, *Eur. Phys. J. C* **72**, 1896 (2012).

- [55] ATLAS Collaboration, Measurement of the azimuthal anisotropy of charged particles produced in $\sqrt{s_{NN}} = 5.02\text{TeV}$ Pb+Pb collisions with the ATLAS detector, *Eur. Phys. J. C* **78**, 997 (2018).
- [56] ATLAS Collaboration, Jet energy measurement and its systematic uncertainty in proton-proton collisions at $\sqrt{s} = 7\text{ TeV}$ with the ATLAS detector, *Eur. Phys. J. C* **75**, 17 (2015).
- [57] ATLAS Collaboration, Jet energy scale and its uncertainty for jets reconstructed using the ATLAS heavy ion jet algorithm, ATLAS-CONF-2015-016, 2015, <https://cds.cern.ch/record/2008677>.
- [58] ATLAS Collaboration, Measurement of photon-jet transverse momentum correlations in 5.02 TeV Pb+Pb and pp collisions with ATLAS, *Phys. Lett. B* **789**, 167 (2019).
- [59] G. D'Agostini, A Multidimensional unfolding method based on Bayes' theorem, *Nucl. Instrum. Methods Phys. Res. Sect. A* **362**, 487 (1995).
- [60] T. Adye, Unfolding algorithms and tests using RooUnfold, [arXiv:1105.1160](https://arxiv.org/abs/1105.1160).
- [61] ATLAS Collaboration, Evaluating statistical uncertainties and correlations using the bootstrap method, ATL-PHYS-PUB-2021-011, 2021, <https://cds.cern.ch/record/2759945>.
- [62] ATLAS Collaboration, Measurements of the suppression and correlations of dijets in Xe+Xe collisions at $\sqrt{s_{NN}} = 5.44\text{ TeV}$, *Phys. Rev. C* **108**, 024906 (2023).
- [63] ATLAS Collaboration, Measurement of jet fragmentation in Pb+Pb and pp collisions at $\sqrt{s_{NN}} = 5.02\text{ TeV}$ with the ATLAS detector, *Phys. Rev. C* **98**, 024908 (2018).
- [64] ATLAS Collaboration, Jet energy scale and resolution measured in proton–proton collisions at $\sqrt{s} = 13\text{ TeV}$ with the ATLAS detector, *Eur. Phys. J. C* **81**, 689 (2021).
- [65] Y. He, S. Cao, W. Chen, T. Luo, L. G. Pang, and X. N. Wang, Interplaying mechanisms behind single inclusive jet suppression in heavy-ion collisions, *Phys. Rev. C* **99**, 054911 (2019).
- [66] J. H. Putschke *et al.*, The JETSCAPE framework, [arXiv:1903.07706](https://arxiv.org/abs/1903.07706).
- [67] JETSCAPE Collaboration, Multistage Monte Carlo simulation of jet modification in a static medium, *Phys. Rev. C* **96**, 024909 (2017).
- [68] S. Cao and A. Majumder, Nuclear modification of leading hadrons and jets within a virtuality ordered parton shower, *Phys. Rev. C* **101**, 024903 (2020).
- [69] ATLAS Collaboration, ATLAS Computing Acknowledgements, ATL-SOFT-PUB-2023-001 (2023), <https://cds.cern.ch/record/2869272>.

- G. Aad¹⁰⁴ E. Aakvaag¹⁷ B. Abbott¹²³ S. Abdelhameed^{119a} K. Abeling⁵⁶ N. J. Abicht⁵⁰ S. H. Abidi³⁰
 M. Aboelela⁴⁵ A. Aboulhorma^{36e} H. Abramowicz¹⁵⁵ H. Abreu¹⁵⁴ Y. Abulaiti¹²⁰ B. S. Acharya^{70a,70b,a}
 A. Ackermann^{64a} C. Adam Bourdarios⁴ L. Adamczyk^{87a} S. V. Addepalli²⁷ M. J. Addison¹⁰³ J. Adelman¹¹⁸
 A. Adiguzel^{22c} T. Adye¹³⁷ A. A. Affolder¹³⁹ Y. Afik⁴⁰ M. N. Agaras¹³ J. Agarwala^{74a,74b} A. Aggarwal¹⁰²
 C. Agheorghiesei^{28c} F. Ahmadov^{39,b} W. S. Ahmed¹⁰⁶ S. Ahuja⁹⁷ X. Ai^{63e} G. Aielli^{77a,77b} A. Aikot¹⁶⁶
 M. Ait Tamlihat^{36e} B. Aitbenchikh^{36a} M. Akbiyik¹⁰² T. P. A. Åkesson¹⁰⁰ A. V. Akimov³⁸ D. Akiyama¹⁷¹
 N. N. Akolkar²⁵ S. Aktas^{22a} K. Al Khoury⁴² G. L. Alberghi^{24b} J. Albert¹⁶⁸ P. Albicocco⁵⁴ G. L. Albouy⁶¹
 S. Alderweireldt⁵³ Z. L. Alegria¹²⁴ M. Aleksa³⁷ I. N. Aleksandrov³⁹ C. Alexa^{28b} T. Alexopoulos¹⁰
 F. Alfonsi^{24b} M. Algren⁵⁷ M. Alhroob¹⁷⁰ B. Ali¹³⁵ H. M. J. Ali^{93,c} S. Ali³² S. W. Alibocus⁹⁴ M. Aliev^{34c}
 G. Alimonti^{72a} W. Alkakhi⁵⁶ C. Allaire⁶⁷ B. M. M. Allbrooke¹⁵⁰ J. F. Allen⁵³ C. A. Allendes Flores^{140f}
 P. P. Allport²¹ A. Aloisio^{73a,73b} F. Alonso⁹² C. Alpigiani¹⁴² Z. M. K. Alsolami⁹³ M. Alvarez Estevez¹⁰¹
 A. Alvarez Fernandez¹⁰² M. Alves Cardoso⁵⁷ M. G. Alviggi^{73a,73b} M. Aly¹⁰³ Y. Amaral Coutinho^{84b}
 A. Ambler¹⁰⁶ C. Amelung³⁷ M. Amerl¹⁰³ C. G. Ames¹¹¹ D. Amidei¹⁰⁸ B. Amini⁵⁵ K. J. Amirie¹⁵⁸
 S. P. Amor Dos Santos^{133a} K. R. Amos¹⁶⁶ D. Amperiadou¹⁵⁶ S. An⁸⁵ V. Ananiev¹²⁸ C. Anastopoulos¹⁴³
 T. Andeen¹¹ J. K. Anders³⁷ A. C. Anderson⁶⁰ S. Y. Andrean^{48a,48b} A. Andreazza^{72a,72b} S. Angelidakis⁹
 A. Angerami⁴² A. V. Anisenkov³⁸ A. Annovi^{75a} C. Antel⁵⁷ E. Antipov¹⁴⁹ M. Antonelli⁵⁴ F. Anulli^{76a}
 M. Aoki⁸⁵ T. Aoki¹⁵⁷ M. A. Aparo¹⁵⁰ L. Aperio Bella⁴⁹ C. Appelt¹⁹ A. Apyan²⁷ S. J. Arbiol Val⁸⁸
 C. Arcangeletti⁵⁴ A. T. H. Arce⁵² J-F. Arguin¹¹⁰ S. Argyropoulos⁵⁵ J.-H. Arling⁴⁹ O. Arnaez⁴ H. Arnold¹⁴⁹
 G. Artoni^{76a,76b} H. Asada¹¹³ K. Asai¹²¹ S. Asai¹⁵⁷ N. A. Asbah³⁷ R. A. Ashby Pickering¹⁷⁰ K. Assamagan³⁰
 R. Astalos^{29a} K. S. V. Astrand¹⁰⁰ S. Atashi¹⁶² R. J. Atkin^{34a} M. Atkinson¹⁶⁵ H. Atmani^{36f} P. A. Atmasiddha¹³¹
 K. Augsten¹³⁵ S. Auricchio^{73a,73b} A. D. Auriol²¹ V. A. Austrup¹⁰³ G. Avolio³⁷ K. Axiotis⁵⁷ G. Azuelos^{110,d}
 D. Babal^{29b} H. Bachacou¹³⁸ K. Bachas^{156,e} A. Bachiu³⁵ F. Backman^{48a,48b} A. Badea⁴⁰ T. M. Baer¹⁰⁸
 P. Bagnaia^{76a,76b} M. Bahmani¹⁹ D. Bahner⁵⁵ K. Bai¹²⁶ J. T. Baines¹³⁷ L. Baines⁹⁶ O. K. Baker¹⁷⁵
 E. Bakos¹⁶ D. Bakshi Gupta⁸ L. E. Balabram Filho^{84b} V. Balakrishnan¹²³ R. Balasubramanian⁴ E. M. Baldin³⁸
 P. Balek^{87a} E. Ballabene^{24b,24a} F. Balli¹³⁸ L. M. Baltes^{64a} W. K. Balunas³³ J. Balz¹⁰² I. Bamwidhi^{119b}
 E. Banas⁸⁸ M. Bandieramonte¹³² A. Bandyopadhyay²⁵ S. Bansal²⁵ L. Barak¹⁵⁵ M. Barakat⁴⁹
 E. L. Barberio¹⁰⁷ D. Barberis^{58b,58a} M. Barbero¹⁰⁴ M. Z. Barel¹¹⁷ T. Barillari¹¹² M.-S. Barisits³⁷
 T. Barklow¹⁴⁷ P. Baron¹²⁵ D. A. Baron Moreno¹⁰³ A. Baroncelli^{63a} A. J. Barr¹²⁹ J. D. Barr⁹⁸ F. Barreiro¹⁰¹
 J. Barreiro Guimarães da Costa¹⁴ U. Barron¹⁵⁵ M. G. Barros Teixeira^{133a} S. Barsov³⁸ F. Bartels^{64a}
 R. Bartoldus¹⁴⁷ A. E. Barton⁹³ P. Bartos^{29a} A. Basan¹⁰² M. Baselga⁵⁰ A. Bassalat^{67,f} M. J. Basso^{159a}
 S. Bataju⁴⁵ R. Bate¹⁶⁷ R. L. Bates⁶⁰ S. Batlamous¹⁰¹ B. Batool¹⁴⁵ M. Battaglia¹³⁹ D. Battulga¹⁹
 M. Bauce^{76a,76b} M. Bauer⁸⁰ P. Bauer²⁵ L. T. Bazzano Hurrell³¹ J. B. Beacham⁵² T. Beau¹³⁰ J. Y. Beaucamp⁹²

- P. H. Beauchemin^b,¹⁶¹ P. Bechtle^b,²⁵ H. P. Beck^b,^{20,g} K. Becker^b,¹⁷⁰ A. J. Beddall^b,⁸³ V. A. Bednyakov^b,³⁹ C. P. Bee^b,¹⁴⁹ L. J. Beemster^b,¹⁶ T. A. Beermann^b,³⁷ M. Begalli^b,^{84d} M. Begel^b,³⁰ A. Behera^b,¹⁴⁹ J. K. Behr^b,⁴⁹ J. F. Beirer^b,³⁷ F. Beisiegel^b,²⁵ M. Belfkir^b,^{119b} G. Bella^b,¹⁵⁵ L. Bellagamba^b,^{24b} A. Bellerive^b,³⁵ P. Bellos^b,²¹ K. Beloborodov^b,³⁸ D. Benchekroun^b,^{36a} F. Bendebba^b,^{36a} Y. Benhammou^b,¹⁵⁵ K. C. Benkendorfer^b,⁶² L. Beresford^b,⁴⁹ M. Beretta^b,⁵⁴ E. Bergeas Kuutmann^b,¹⁶⁴ N. Berger^b,⁴ B. Bergmann^b,¹³⁵ J. Beringer^b,^{18a} G. Bernardi^b,⁵ C. Bernius^b,¹⁴⁷ F. U. Bernlochner^b,²⁵ F. Bernon^b,^{37,104} A. Berrocal Guardia^b,¹³ T. Berry^b,⁹⁷ P. Berta^b,¹³⁶ A. Berthold^b,⁵¹ S. Bethke^b,¹¹² A. Betti^b,^{76a,76b} A. J. Bevan^b,⁹⁶ N. K. Bhalla^b,⁵⁵ S. Bhatta^b,¹⁴⁹ D. S. Bhattacharya^b,¹⁶⁹ P. Bhattacharai^b,¹⁴⁷ K. D. Bhide^b,⁵⁵ V. S. Bhopatkar^b,¹²⁴ R. M. Bianchi^b,¹³² G. Bianco^b,^{24b,24a} O. Bibel^b,¹¹¹ R. Bielski^b,¹²⁶ M. Biglietti^b,^{78a} C. S. Billingsley^b,⁴⁵ Y. Bimgni^b,^{36f} M. Bindi^b,⁵⁶ A. Bingul^b,^{22b} C. Bini^b,^{76a,76b} G. A. Bird^b,³³ M. Birman^b,¹⁷² M. Biros^b,¹³⁶ S. Biryukov^b,¹⁵⁰ T. Bisanz^b,⁵⁰ E. Bisceglie^b,^{44b,44a} J. P. Biswal^b,¹³⁷ D. Biswas^b,¹⁴⁵ I. Bloch^b,⁴⁹ A. Blue^b,⁶⁰ U. Blumenschein^b,⁹⁶ J. Blumenthal^b,¹⁰² V. S. Bobrovnikov^b,³⁸ M. Boehler^b,⁵⁵ B. Boehm^b,¹⁶⁹ D. Bogavac^b,³⁷ A. G. Bogdanchikov^b,³⁸ L. S. Boggia^b,¹³⁰ C. Bohm^b,^{48a} V. Boisvert^b,⁹⁷ P. Bokan^b,³⁷ T. Bold^b,^{87a} M. Bomben^b,⁵ M. Bona^b,⁹⁶ M. Boonekamp^b,¹³⁸ C. D. Booth^b,⁹⁷ A. G. Borbely^b,⁶⁰ I. S. Bordulev^b,³⁸ G. Borissov^b,⁹³ D. Bortoletto^b,¹²⁹ D. Boscherini^b,^{24b} M. Bosman^b,¹³ J. D. Bossio Sola^b,³⁷ K. Bouaouda^b,^{36a} N. Bouchhar^b,¹⁶⁶ L. Boudet^b,⁴ J. Boudreau^b,¹³² E. V. Bouhova-Thacker^b,⁹³ D. Boumediene^b,⁴¹ R. Bouquet^b,^{58b,58a} A. Boveia^b,¹²² J. Boyd^b,³⁷ D. Boye^b,³⁰ I. R. Boyko^b,³⁹ L. Bozianu^b,⁵⁷ J. Bracinik^b,²¹ N. Brahimi^b,⁴ G. Brandt^b,¹⁷⁴ O. Brandt^b,³³ F. Braren^b,⁴⁹ B. Brau^b,¹⁰⁵ J. E. Brau^b,¹²⁶ R. Brener^b,¹⁷² L. Brenner^b,¹¹⁷ R. Brenner^b,¹⁶⁴ S. Bressler^b,¹⁷² G. Brianti^b,^{79a,79b} D. Britton^b,⁶⁰ D. Britzger^b,¹¹² I. Brock^b,²⁵ R. Brock^b,¹⁰⁹ G. Brooijmans^b,⁴² E. M. Brooks^b,^{159b} E. Brost^b,³⁰ L. M. Brown^b,¹⁶⁸ L. E. Bruce^b,⁶² T. L. Bruckler^b,¹²⁹ P. A. Bruckman de Renstrom^b,⁸⁸ B. Brüers^b,⁴⁹ A. Bruni^b,^{24b} G. Bruni^b,^{24b} M. Bruschi^b,^{24b} N. Bruscino^b,^{76a,76b} T. Buanes^b,¹⁷ Q. Buat^b,¹⁴² D. Buchin^b,¹¹² A. G. Buckley^b,⁶⁰ O. Bulekov^b,³⁸ B. A. Bullard^b,¹⁴⁷ S. Burdin^b,⁹⁴ C. D. Burgard^b,⁵⁰ A. M. Burger^b,³⁷ B. Burghgrave^b,⁸ O. Burlayenko^b,⁵⁵ J. Burleson^b,¹⁶⁵ J. T. P. Burr^b,³³ J. C. Burzynski^b,¹⁴⁶ E. L. Busch^b,⁴² V. Büscher^b,¹⁰² P. J. Bussey^b,⁶⁰ J. M. Butler^b,²⁶ C. M. Buttari^b,⁶⁰ J. M. Butterworth^b,⁹⁸ W. Buttinger^b,¹³⁷ C. J. Buxo Vazquez^b,¹⁰⁹ A. R. Buzykaev^b,³⁸ S. Cabrera Urbán^b,¹⁶⁶ L. Cadamuro^b,⁶⁷ D. Caforio^b,⁵⁹ H. Cai^b,¹³² Y. Cai^b,^{14,114c} Y. Cai^b,^{114a} V. M. M. Cairo^b,³⁷ O. Cakir^b,^{3a} N. Calace^b,³⁷ P. Calafuria^b,^{18a} G. Calderini^b,¹³⁰ P. Calfayan^b,⁶⁹ G. Callea^b,⁶⁰ L. P. Caloba,^{84b} D. Calvet^b,⁴¹ S. Calvet^b,⁴¹ M. Calvetti^b,^{75a,75b} R. Camacho Toro^b,¹³⁰ S. Camarda^b,³⁷ D. Camarero Munoz^b,²⁷ P. Camarri^b,^{77a,77b} M. T. Camerlingo^b,^{73a,73b} D. Cameron^b,³⁷ C. Camincher^b,¹⁶⁸ M. Campanelli^b,⁹⁸ A. Camplani^b,⁴³ V. Canale^b,^{73a,73b} A. C. Canbay^b,^{3a} E. Canonero^b,⁹⁷ J. Cantero^b,¹⁶⁶ Y. Cao^b,¹⁶⁵ F. Capocasa^b,²⁷ M. Capua^b,^{44b,44a} A. Carbone^b,^{72a,72b} R. Cardarelli^b,^{77a} J. C. J. Cardenas^b,⁸ G. Carducci^b,^{44b,44a} T. Carli^b,³⁷ G. Carlino^b,^{73a} J. I. Carlotto^b,¹³ B. T. Carlson^b,^{132,h} E. M. Carlson^b,^{168,159a} J. Carmignani^b,⁹⁴ L. Carminati^b,^{72a,72b} A. Carnelli^b,¹³⁸ M. Carnesale^b,^{76a,76b} S. Caron^b,¹¹⁶ E. Carquin^b,^{140f} I. B. Carr^b,¹⁰⁷ S. Carrá^b,^{72a} G. Carratta^b,^{24b,24a} A. M. Carroll^b,¹²⁶ T. M. Carter^b,⁵³ M. P. Casado^b,^{13,i} M. Caspar^b,⁴⁹ F. L. Castillo^b,⁴ L. Castillo Garcia^b,¹³ V. Castillo Gimenez^b,¹⁶⁶ N. F. Castro^b,^{133a,133e} A. Catinaccio^b,³⁷ J. R. Catmore^b,¹²⁸ T. Cavalieri^b,⁴ V. Cavalieri^b,³⁰ N. Cavalli^b,^{24b,24a} L. J. Caviedes Betancourt^b,^{23b} Y. C. Cekmecelioglu^b,⁴⁹ E. Celebi^b,⁸³ S. Cella^b,³⁷ F. Celli^b,¹²⁹ M. S. Centonze^b,^{71a,71b} V. Cepaitis^b,⁵⁷ K. Cerny^b,¹²⁵ A. S. Cerqueira^b,^{84a} A. Cerri^b,¹⁵⁰ L. Cerrito^b,^{77a,77b} F. Cerutti^b,^{18a} B. Cervato^b,¹⁴⁵ A. Cervelli^b,^{24b} G. Cesarini^b,⁵⁴ S. A. Cetin^b,⁸³ D. Chakraborty^b,¹¹⁸ J. Chan^b,^{18a} W. Y. Chan^b,¹⁵⁷ J. D. Chapman^b,³³ E. Chapron^b,¹³⁸ B. Chargeishvili^b,^{153b} D. G. Charlton^b,²¹ M. Chatterjee^b,²⁰ C. Chauhan^b,¹³⁶ Y. Che^b,^{114a} S. Chekanov^b,⁶ S. V. Chekulaev^b,^{159a} G. A. Chelkov^b,^{39,j} A. Chen^b,¹⁰⁸ B. Chen^b,¹⁵⁵ B. Chen^b,¹⁶⁸ H. Chen^b,^{114a} H. Chen^b,³⁰ J. Chen^b,^{63c} J. Chen^b,¹⁴⁶ M. Chen^b,¹²⁹ S. Chen^b,⁸⁹ S. J. Chen^b,^{114a} X. Chen^b,^{63c} X. Chen^b,^{15,k} Y. Chen^b,^{63a} C. L. Cheng^b,¹⁷³ H. C. Cheng^b,^{65a} S. Cheong^b,¹⁴⁷ A. Cheplakov^b,³⁹ E. Cheremushkina^b,⁴⁹ E. Cherepanova^b,¹¹⁷ R. Cherkaoui El Moursli^b,^{36e} E. Cheu^b,⁷ K. Cheung^b,⁶⁶ L. Chevalier^b,¹³⁸ V. Chiarella^b,⁵⁴ G. Chiarelli^b,^{75a} N. Chiedde^b,¹⁰⁴ G. Chiodini^b,^{71a} A. S. Chisholm^b,²¹ A. Chitan^b,^{28b} M. Chitishvili^b,¹⁶⁶ M. V. Chizhov^b,^{39,1} K. Choi^b,¹¹ Y. Chou^b,¹⁴² E. Y. S. Chow^b,¹¹⁶ K. L. Chu^b,¹⁷² M. C. Chu^b,^{65a} X. Chu^b,^{14,114c} Z. Chubinidze^b,⁵⁴ J. Chudoba^b,¹³⁴ J. J. Chwastowski^b,⁸⁸ D. Cieri^b,¹¹² K. M. Ciesla^b,^{87a} V. Cindro^b,⁹⁵ A. Ciocio^b,^{18a} F. Cirotto^b,^{73a,73b} Z. H. Citron^b,¹⁷² M. Citterio^b,^{72a} D. A. Ciubotaru,^{28b} A. Clark^b,⁵⁷ P. J. Clark^b,⁵³ N. Clarke Hall^b,⁹⁸ C. Clarry^b,¹⁵⁸ J. M. Clavijo Columbie^b,⁴⁹ S. E. Clawson^b,⁴⁹ C. Clement^b,^{48a,48b} Y. Coadou^b,¹⁰⁴ M. Cobal^b,^{70a,70c} A. Coccoaro^b,^{58b} R. F. Coelho Barre^b,^{133a} R. Coelho Lopes De Sa^b,¹⁰⁵ S. Coelli^b,^{72a} B. Cole^b,⁴² J. Collot^b,⁶¹ P. Conde Muiño^b,^{133a,133g} M. P. Connell^b,^{34c} S. H. Connell^b,^{34c} E. I. Conroy^b,¹²⁹ F. Conventi^b,^{73a,m} H. G. Cooke^b,²¹ A. M. Cooper-Sarkar^b,¹²⁹ F. A. Corchia^b,^{24b,24a} A. Cordeiro Oudot Choi^b,¹³⁰ L. D. Corpe^b,⁴¹ M. Corradi^b,^{76a,76b} F. Corriveau^b,^{106,n} A. Cortes-Gonzalez^b,¹⁹ M. J. Costa^b,¹⁶⁶ F. Costanza^b,⁴ D. Costanzo^b,¹⁴³ B. M. Cote^b,¹²² J. Couthures^b,⁴ G. Cowan^b,⁹⁷ K. Cranmer^b,¹⁷³ L. Cremer^b,⁵⁰ D. Cremonini^b,^{24b,24a} S. Crépé-Renaudin^b,⁶¹ F. Crescioli^b,¹³⁰ M. Cristinziani^b,¹⁴⁵ M. Cristoforetti^b,^{79a,79b} V. Croft^b,¹¹⁷ J. E. Crosby^b,¹²⁴ G. Crosetti^b,^{44b,44a} A. Cueto^b,¹⁰¹ H. Cui^b,⁹⁸ Z. Cui^b,⁷ W. R. Cunningham^b,⁶⁰ F. Curcio^b,¹⁶⁶ J. R. Curran^b,⁵³ P. Czodrowski^b,³⁷ M. J. Da Cunha Sargedas De Sousa^b,^{58b,58a} J. V. Da Fonseca Pinto^b,^{84b} C. Da Via^b,¹⁰³ W. Dabrowski^b,^{87a} T. Dado^b,³⁷ S. Dahabi^b,¹⁵² T. Dai^b,¹⁰⁸ D. Dal Santo^b,²⁰ C. Dallapiccola^b,¹⁰⁵ M. Dam^b,⁴³ G. D'amen^b,³⁰ V. D'Amico^b,¹¹¹ J. Damp^b,¹⁰² J. R. Dandoy^b,³⁵ D. Dannheim^b,³⁷ M. Danninger^b,¹⁴⁶ V. Dao^b,¹⁴⁹ G. Darbo^b,^{58b} S. J. Das^b,³⁰ F. Dattola^b,⁴⁹ S. D'Auria^b,^{72a,72b} A. D'Avanzo^b,^{73a,73b} C. David^b,^{34a} T. Davidek^b,¹³⁶ I. Dawson^b,⁹⁶ H. A. Day-hall^b,¹³⁵ K. De^b,⁸ R. De Asmundis^b,^{73a} N. De Biase^b,⁴⁹ S. De Castro^b,^{24b,24a} N. De Groot^b,¹¹⁶ P. de Jong^b,¹¹⁷ H. De la Torre^b,¹¹⁸ A. De Maria^b,^{114a} A. De Salvo^b,^{76a} U. De Sanctis^b,^{77a,77b} F. De Santis^b,^{71a,71b}

- A. De Santo ¹⁵⁰ J. B. De Vivie De Regie ⁶¹ J. Debevc ⁹⁵ D. V. Dedovich, ³⁹ J. Degens ⁹⁴ A. M. Deiana ⁴⁵
 F. Del Corso ^{24b,24a} J. Del Peso ¹⁰¹ L. Delagrange ¹³⁰ F. Deliot ¹³⁸ C. M. Delitzsch ⁵⁰ M. Della Pietra ^{73a,73b}
 D. Della Volpe ⁵⁷ A. Dell'Acqua ³⁷ L. Dell'Asta ^{72a,72b} M. Delmastro ⁴ P. A. Delsart ⁶¹ S. Demers ¹⁷⁵
 M. Demichev ³⁹ S. P. Denisov ³⁸ L. D'Eramo ⁴¹ D. Derendarz ⁸⁸ F. Derue ¹³⁰ P. Dervan ⁹⁴ K. Desch ²⁵
 C. Deutsch ²⁵ F. A. Di Bello ^{58b,58a} A. Di Ciaccio ^{77a,77b} L. Di Ciaccio ⁴ A. Di Domenico ^{76a,76b}
 C. Di Donato ^{73a,73b} A. Di Girolamo ³⁷ G. Di Gregorio ³⁷ A. Di Luca ^{79a,79b} B. Di Micco ^{78a,78b} R. Di Nardo ^{78a,78b}
 K. F. Di Petrillo ⁴⁰ M. Diamantopoulou ³⁵ F. A. Dias ¹¹⁷ T. Dias Do Vale ¹⁴⁶ M. A. Diaz ^{140a,140b}
 F. G. Diaz Capriles ²⁵ A. R. Didenko ³⁹ M. Didenko ¹⁶⁶ E. B. Diehl ¹⁰⁸ S. Díez Cornell ⁴⁹ C. Diez Pardos ¹⁴⁵
 C. Dimitriadi ¹⁶⁴ A. Dimitrieva ²¹ J. Dingfelder ²⁵ T. Dingley ¹²⁹ I-M. Dinu ^{28b} S. J. Dittmeier ^{64b} F. Dittus ³⁷
 M. Divisek ¹³⁶ B. Dixit ⁹⁴ F. Djama ¹⁰⁴ T. Djobava ^{153b} C. Doglioni ^{103,100} A. Dohnalova ^{29a} J. Dolejsi ¹³⁶
 Z. Dolezal ¹³⁶ K. Domijan ^{87a} K. M. Dona ⁴⁰ M. Donadelli ^{84d} B. Dong ¹⁰⁹ J. Donini ⁴¹ A. D'Onofrio ^{73a,73b}
 M. D'Onofrio ⁹⁴ J. Dopke ¹³⁷ A. Doria ^{73a} N. Dos Santos Fernandes ^{133a} P. Dougan ¹⁰³ M. T. Dova ⁹²
 A. T. Doyle ⁶⁰ M. A. Draguet ¹²⁹ E. Dreyer ¹⁷² I. Drivas-koulouris ¹⁰ M. Drnevich ¹²⁰ M. Drozdova ⁵⁷ D. Du ^{63a}
 T. A. du Pree ¹¹⁷ F. Dubinin ³⁸ M. Dubovsky ^{29a} E. Duchovni ¹⁷² G. Duckeck ¹¹¹ O. A. Ducu ^{28b} D. Duda ⁵³
 A. Dudarev ³⁷ E. R. Duden ²⁷ M. D'uffizi ¹⁰³ L. Duflot ⁶⁷ M. Dührssen ³⁷ I. Dumitrica ^{28g} A. E. Dumitriu ^{28b}
 M. Dunford ^{64a} S. Dungs ⁵⁰ K. Dunne ^{48a,48b} A. Duperrin ¹⁰⁴ H. Duran Yildiz ^{3a} M. Düren ⁵⁹ A. Durglishvili ^{153b}
 B. L. Dwyer ¹¹⁸ G. I. Dyckes ^{18a} M. Dyndal ^{87a} B. S. Dziedzic ³⁷ Z. O. Earnshaw ¹⁵⁰ G. H. Eberwein ¹²⁹
 B. Eckerova ^{29a} S. Eggebrecht ⁵⁶ E. Egidio Purcino De Souza ^{84e} L. F. Ehrke ⁵⁷ G. Eigen ¹⁷ K. Einsweiler ^{18a}
 T. Ekelof ¹⁶⁴ P. A. Ekman ¹⁰⁰ S. El Farkh ^{36b} Y. El Ghazali ^{63a} H. El Jarrari ³⁷ A. El Moussaouy ^{36a}
 V. Ellajosyula ¹⁶⁴ M. Ellert ¹⁶⁴ F. Ellinghaus ¹⁷⁴ N. Ellis ³⁷ J. Elmsheuser ³⁰ M. Elsawy ^{119a} M. Elsing ³⁷
 D. Emeliyanov ¹³⁷ Y. Enari ⁸⁵ I. Ene ^{18a} S. Epari ¹³ P. A. Erland ⁸⁸ D. Ernani Martins Neto ⁸⁸ M. Errenst ¹⁷⁴
 M. Escalier ⁶⁷ C. Escobar ¹⁶⁶ E. Etzion ¹⁵⁵ G. Evans ^{133a} H. Evans ⁶⁹ L. S. Evans ⁹⁷ A. Ezhilov ³⁸
 S. Ezzarqtouni ^{36a} F. Fabbri ^{24b,24a} L. Fabbri ^{24b,24a} G. Facini ⁹⁸ V. Fadeyev ¹³⁹ R. M. Fakhrutdinov ³⁸
 D. Fakoudis ¹⁰² S. Falciano ^{76a} L. F. Falda Ulhoa Coelho ³⁷ F. Fallavollita ¹¹² G. Falsetti ^{44b,44a} J. Faltova ¹³⁶
 C. Fan ¹⁶⁵ K. Y. Fan ^{65b} Y. Fan ¹⁴ Y. Fang ^{14,114c} M. Fanti ^{72a,72b} M. Faraj ^{70a,70b} Z. Farazpay ⁹⁹ A. Farbin ⁸
 A. Farilla ^{78a} T. Farooque ¹⁰⁹ S. M. Farrington ⁵³ F. Fassi ^{36e} D. Fassouliotis ⁹ M. Fauci Giannelli ^{77a,77b}
 W. J. Fawcett ³³ L. Fayard ⁶⁷ P. Federic ¹³⁶ P. Federicova ¹³⁴ O. L. Fedin ^{38,j} M. Feickert ¹⁷³ L. Feligioni ¹⁰⁴
 D. E. Fellers ¹²⁶ C. Feng ^{63b} Z. Feng ¹¹⁷ M. J. Fenton ¹⁶² L. Ferencz ⁴⁹ R. A. M. Ferguson ⁹³
 S. I. Fernandez Luengo ^{140f} P. Fernandez Martinez ⁶⁸ M. J. V. Fernoux ¹⁰⁴ J. Ferrando ⁹³ A. Ferrari ¹⁶⁴
 P. Ferrari ^{117,116} R. Ferrari ^{74a} D. Ferrere ⁵⁷ C. Ferretti ¹⁰⁸ D. Fiacco ^{76a,76b} F. Fiedler ¹⁰² P. Fiedler ¹³⁵
 S. Filimonov ³⁸ A. Filipčič ⁹⁵ E. K. Filmer ¹ F. Filthaut ¹¹⁶ M. C. N. Fiolhais ^{133a,133c,o} L. Fiorini ¹⁶⁶
 W. C. Fisher ¹⁰⁹ T. Fitschen ¹⁰³ P. M. Fitzhugh ¹³⁸ I. Fleck ¹⁴⁵ P. Fleischmann ¹⁰⁸ T. Flick ¹⁷⁴ M. Flores ^{34d,p}
 L. R. Flores Castillo ^{65a} L. Flores Sanz De Acedo ³⁷ F. M. Follega ^{79a,79b} N. Fomin ³³ J. H. Foo ¹⁵⁸ A. Formica ¹³⁸
 A. C. Forti ¹⁰³ E. Fortin ³⁷ A. W. Fortman ^{18a} M. G. Foti ^{18a} L. Fountas ^{9,q} D. Fournier ⁶⁷ H. Fox ⁹³
 P. Francavilla ^{75a,75b} S. Francescato ⁶² S. Franchellucci ⁵⁷ M. Franchini ^{24b,24a} S. Franchino ^{64a} D. Francis ³⁷
 L. Franco ¹¹⁶ V. Franco Lima ³⁷ L. Franconi ⁴⁹ M. Franklin ⁶² G. Frattari ²⁷ Y. Y. Frid ¹⁵⁵ J. Friend ⁶⁰
 N. Fritzsche ³⁷ A. Froch ⁵⁵ D. Froidevaux ³⁷ J. A. Frost ¹²⁹ Y. Fu ^{63a} S. Fuenzalida Garrido ^{140f} M. Fujimoto ¹⁰⁴
 K. Y. Fung ^{65a} E. Furtado De Simas Filho ^{84e} M. Furukawa ¹⁵⁷ J. Fuster ¹⁶⁶ A. Gaa ⁵⁶ A. Gabrielli ^{24b,24a}
 A. Gabrielli ¹⁵⁸ P. Gadow ³⁷ G. Gagliardi ^{58b,58a} L. G. Gagnon ^{18a} S. Gaid ¹⁶³ S. Galantzan ¹⁵⁵ J. Gallagher ¹
 E. J. Gallas ¹²⁹ B. J. Gallop ¹³⁷ K. K. Gan ¹²² S. Ganguly ¹⁵⁷ Y. Gao ⁵³ F. M. Garay Walls ^{140a,140b} B. Garcia ³⁰
 C. García ¹⁶⁶ A. Garcia Alonso ¹¹⁷ A. G. Garcia Caffaro ¹⁷⁵ J. E. García Navarro ¹⁶⁶ M. Garcia-Sciveres ^{18a}
 G. L. Gardner ¹³¹ R. W. Gardner ⁴⁰ N. Garelli ¹⁶¹ D. Garg ⁸¹ R. B. Garg ¹⁴⁷ J. M. Gargan ⁵³ C. A. Garner ¹⁵⁸
 C. M. Garvey ^{34a} V. K. Gassmann ¹⁶¹ G. Gaudio ^{74a} V. Gautam ¹³ P. Gauzzi ^{76a,76b} J. Gavranovic ⁹⁵
 I. L. Gavrilenco ³⁸ A. Gavriluky ³⁸ C. Gay ¹⁶⁷ G. Gaycken ¹²⁶ E. N. Gazis ¹⁰ A. A. Geanta ^{28b} C. M. Gee ¹³⁹
 A. Gekow ¹²² C. Gemme ^{58b} M. H. Genest ⁶¹ A. D. Gentry ¹¹⁵ S. George ⁹⁷ W. F. George ²¹ T. Geralis ⁴⁷
 P. Gessinger-Befurt ³⁷ M. E. Geyik ¹⁷⁴ M. Ghani ¹⁷⁰ K. Ghorbanian ⁹⁶ A. Ghosal ¹⁴⁵ A. Ghosh ¹⁶² A. Ghosh ¹⁷
 B. Giacobbe ^{24b} S. Giagu ^{76a,76b} T. Giani ¹¹⁷ A. Giannini ^{63a} S. M. Gibson ⁹⁷ M. Gignac ¹³⁹ D. T. Gil ^{87b}
 A. K. Gilbert ^{87a} B. J. Gilbert ⁴² D. Gillberg ³⁵ G. Gilles ¹¹⁷ L. Ginabat ¹³⁰ D. M. Gingrich ^{2,d}
 M. P. Giordani ^{70a,70c} P. F. Giraud ¹³⁸ G. Giugliarelli ^{70a,70c} D. Giugni ^{72a} F. Giulia ³⁷ I. Gkialas ^{9,q}
 L. K. Gladilin ³⁸ C. Glasman ¹⁰¹ G. R. Gledhill ¹²⁶ G. Glemža ⁴⁹ M. Glisic ¹²⁶ I. Gnesi ^{44b} Y. Go ³⁰
 M. Goblirsch-Kolb ³⁷ B. Gocke ⁵⁰ D. Godin ¹¹⁰ B. Gokturk ^{22a} S. Goldfarb ¹⁰⁷ T. Golling ⁵⁷ M. G. D. Gololo ^{34g}
 D. Golubkov ³⁸ J. P. Gombas ¹⁰⁹ A. Gomes ^{133a,133b} G. Gomes Da Silva ¹⁴⁵ A. J. Gomez Delegido ¹⁶⁶
 R. Gonçalo ^{133a} L. Gonella ²¹ A. Gongadze ^{153c} F. Gonnella ²¹ J. L. Gonski ¹⁴⁷ R. Y. González Andana ⁵³
 S. González de la Hoz ¹⁶⁶ R. Gonzalez Lopez ⁹⁴ C. Gonzalez Renteria ^{18a} M. V. Gonzalez Rodrigues ⁴⁹
 R. Gonzalez Suarez ¹⁶⁴ S. Gonzalez-Sevilla ⁵⁷ L. Goossens ³⁷ B. Gorini ³⁷ E. Gorini ^{71a,71b} A. Gorišek ⁹⁵
 T. C. Gosart ¹³¹ A. T. Goshaw ⁵² M. I. Gostkin ³⁹ S. Goswami ¹²⁴ C. A. Gottardo ³⁷ S. A. Gotz ¹¹¹
 M. Gouighri ^{36b} V. Goumarre ⁴⁹ A. G. Goussiou ¹⁴² N. Govender ^{34c} R. P. Grabarczyk ¹²⁹ I. Grabowska-Bold ^{87a}
 K. Graham ³⁵ E. Gramstad ¹²⁸ S. Grancagnolo ^{71a,71b} C. M. Grant, ^{1,138} P. M. Gravila ^{28f} F. G. Gravili ^{71a,71b}

- H. M. Gray^{18a} M. Greco^{71a,71b} M. J. Green¹ C. Grefe²⁵ A. S. Grefsrud¹⁷ I. M. Gregor⁴⁹ K. T. Greif¹⁶²
 P. Grenier¹⁴⁷ S. G. Grewe¹¹² A. A. Grillo¹³⁹ K. Grimm³² S. Grinstein^{13,r} J.-F. Grivaz⁶⁷ E. Gross¹⁷²
 J. Grossé-Knetter⁵⁶ L. Guan¹⁰⁸ J. G. R. Guerrero Rojas¹⁶⁶ G. Guerrieri³⁷ R. Gugel¹⁰² J. A. M. Guhit¹⁰⁸
 A. Guida¹⁹ E. Guilloton¹⁷⁰ S. Guindon³⁷ F. Guo^{14,114c} J. Guo^{63c} L. Guo⁴⁹ Y. Guo¹⁰⁸ A. Gupta⁵⁰
 R. Gupta¹³² S. Gurbuz²⁵ S. S. Gurdasani⁵⁵ G. Gustavino^{76a,76b} P. Gutierrez¹²³ L. F. Gutierrez Zagazeta¹³¹
 M. Gutsche⁵¹ C. Gutschow⁹⁸ C. Gwenlan¹²⁹ C. B. Gwilliam⁹⁴ E. S. Haaland¹²⁸ A. Haas¹²⁰ M. Habedank⁴⁹
 C. Haber^{18a} H. K. Hadavand⁸ A. Hadef⁵¹ S. Hadzic¹¹² A. I. Hagan⁹³ J. J. Hahn¹⁴⁵ E. H. Haines⁹⁸
 M. Haleem¹⁶⁹ J. Haley¹²⁴ J. J. Hall¹⁴³ G. D. Hallewell¹⁰⁴ L. Halser²⁰ K. Hamano¹⁶⁸ M. Hamer²⁵
 G. N. Hamity⁵³ E. J. Hampshire⁹⁷ J. Han^{63b} K. Han^{63a} L. Han^{114a} L. Han^{63a} S. Han^{18a} Y. F. Han¹⁵⁸
 K. Hanagaki⁸⁵ M. Hance¹³⁹ D. A. Hangal⁴² H. Hanif¹⁴⁶ M. D. Hank¹³¹ J. B. Hansen⁴³ P. H. Hansen⁴³
 D. Harada⁵⁷ T. Harenberg¹⁷⁴ S. Harkusha³⁸ M. L. Harris¹⁰⁵ Y. T. Harris²⁵ J. Harrison¹³ N. M. Harrison¹²²
 P. F. Harrison¹⁷⁰ N. M. Hartman¹¹² N. M. Hartmann¹¹¹ R. Z. Hasan^{97,137} Y. Hasegawa¹⁴⁴ F. Haslbeck¹²⁹
 S. Hassan¹⁷ R. Hauser¹⁰⁹ C. M. Hawkes²¹ R. J. Hawkings³⁷ Y. Hayashi¹⁵⁷ D. Hayden¹⁰⁹ C. Hayes¹⁰⁸
 R. L. Hayes¹¹⁷ C. P. Hays¹²⁹ J. M. Hays⁹⁶ H. S. Hayward⁹⁴ F. He^{63a} M. He^{14,114c} Y. He⁴⁹ Y. He⁹⁸
 N. B. Heatley⁹⁶ V. Hedberg¹⁰⁰ A. L. Heggelund¹²⁸ N. D. Hehir^{96,s} C. Heidegger⁵⁵ K. K. Heidegger⁵⁵
 J. Heilman³⁵ S. Heim⁴⁹ T. Heim^{18a} J. G. Heinlein¹³¹ J. J. Heinrich¹²⁶ L. Heinrich^{112,t} J. Hejbal¹³⁴
 A. Held¹⁷³ S. Hellesund¹⁷ C. M. Helling¹⁶⁷ S. Hellman^{48a,48b} R. C. W. Henderson⁹³ L. Henkelmann³³
 A. M. Henriques Correia³⁷ H. Herde¹⁰⁰ Y. Hernández Jiménez¹⁴⁹ L. M. Herrmann²⁵ T. Herrmann⁵¹ G. Herten⁵⁵
 R. Hertenberger¹¹¹ L. Hervas³⁷ M. E. Hespingle¹⁰² N. P. Hessey^{159a} J. Hessler¹¹² M. Hidaoui^{36b} N. Hidic¹³⁶
 E. Hill¹⁵⁸ S. J. Hillier²¹ J. R. Hinds¹⁰⁹ F. Hinterkeuser²⁵ M. Hirose¹²⁷ S. Hirose¹⁶⁰ D. Hirschbuehl¹⁷⁴
 T. G. Hitchings¹⁰³ B. Hiti⁹⁵ J. Hobbs¹⁴⁹ R. Hobincu^{28e} N. Hod¹⁷² M. C. Hodgkinson¹⁴³ B. H. Hodgkinson¹²⁹
 A. Hoecker³⁷ D. D. Hofer¹⁰⁸ J. Hofer¹⁶⁶ T. Holm²⁵ M. Holzbock³⁷ L. B. A. H. Hommels³³ B. P. Honan¹⁰³
 J. J. Hong⁶⁹ J. Hong^{63c} T. M. Hong¹³² B. H. Hooberman¹⁶⁵ W. H. Hopkins⁶ M. C. Hoppesch¹⁶⁵ Y. Horii¹¹³
 M. E. Horstmann¹¹² S. Hou¹⁵² A. S. Howard⁹⁵ J. Howarth⁶⁰ J. Hoya⁶ M. Hrabovsky¹²⁵ A. Hrynevich⁴⁹
 T. Hrynová⁴ P. J. Hsu⁶⁶ S.-C. Hsu¹⁴² T. Hsu⁶⁷ M. Hu^{18a} Q. Hu^{63a} S. Huang^{65b} X. Huang^{14,114c}
 Y. Huang¹⁴³ Y. Huang¹⁰² Y. Huang¹⁴ Z. Huang¹⁰³ Z. Hubacek¹³⁵ M. Huebner²⁵ F. Huegging²⁵
 T. B. Huffman¹²⁹ C. A. Hugli⁴⁹ M. Huhtinen³⁷ S. K. Huiberts¹⁷ R. Hulsken¹⁰⁶ N. Huseynov^{12,u} J. Huston¹⁰⁹
 J. Huth¹⁰ R. Hyneman¹⁴⁷ G. Iacobucci⁵⁷ G. Iakovidis³⁰ L. Iconomidou-Fayard⁶⁷ J. P. Iddon³⁷ P. Iengo¹⁰
 R. Iguchi¹⁵⁷ Y. Iiyama¹⁵⁷ T. Iizawa¹²⁹ Y. Ikegami⁸⁵ N. Ilic¹⁵⁸ H. Imam^{84c} G. Inacio Goncalves^{84d}
 M. Ince Lezki⁵⁷ T. Ingebretsen Carlson^{48a,48b} J. M. Inglis⁹⁶ G. Introzzi^{74a,74b} M. Iodice^{78a} V. Ippolito^{76a,76b}
 R. K. Irwin⁹⁴ M. Ishino¹⁵⁷ W. Islam¹⁷³ C. Issever^{19,49} S. Istin^{22a,v} H. Ito¹⁷¹ R. Iuppa^{79a,79b} A. Ivina¹⁷²
 J. M. Izen⁴⁶ V. Izzo^{73a} P. Jacka¹³⁴ P. Jackson¹ C. S. Jagfeld¹¹¹ G. Jain^{159a} P. Jain⁴⁹ K. Jakobs⁵⁵
 T. Jakoubek¹⁷² J. Jamieson⁶⁰ W. Jang¹⁵⁷ M. Javurkova¹⁰⁵ P. Jawahar¹⁰³ L. Jeanty¹²⁶ J. Jejelava^{153a,w}
 P. Jenni^{55,x} C. E. Jessiman³⁵ C. Jia^{63b} H. Jia¹⁶⁷ J. Jia¹⁴⁹ X. Jia^{14,114c} Z. Jia^{114a} C. Jiang⁵³ S. Jiggins⁴⁹
 J. Jimenez Pena¹³ S. Jin^{114a} A. Jinaru^{28b} O. Jinnouchi¹⁴¹ P. Johansson¹⁴³ K. A. Johns⁷ J. W. Johnson¹³⁹
 F. A. Jolly⁴⁹ D. M. Jones¹⁵⁰ E. Jones⁴⁹ K. S. Jones⁸ P. Jones³³ R. W. L. Jones⁹³ T. J. Jones⁹⁴ H. L. Joos^{56,37}
 R. Joshi¹²² J. Jovicevic¹⁶ X. Ju^{18a} J. J. Junggeburth¹⁰⁵ T. Junkermann^{64a} A. Juste Rozas^{13,r} M. K. Juzek⁸⁸
 S. Kabana^{140e} A. Kaczmarska⁸⁸ M. Kado¹¹² H. Kagan¹²² M. Kagan¹⁴⁷ A. Kahn¹³¹ C. Kahra¹⁰² T. Kaji¹⁵⁷
 E. Kajomovitz¹⁵⁴ N. Kakati¹⁷² I. Kalaitzidou⁵⁵ C. W. Kalderon³⁰ N. J. Kang¹³⁹ D. Kar^{34g} K. Karava¹²⁹
 M. J. Kareem^{159b} E. Karentzos⁵⁵ O. Karkout¹¹⁷ S. N. Karpov³⁹ Z. M. Karpova³⁹ V. Kartvelishvili⁹³
 A. N. Karyukhin³⁸ E. Kasimi¹⁵⁶ J. Katzy⁴⁹ S. Kaur³⁵ K. Kawade¹⁴⁴ M. P. Kawale¹²³ C. Kawamoto⁸⁹
 T. Kawamoto^{63a} E. F. Kay³⁷ F. I. Kaya¹⁶¹ S. Kazakos¹⁰⁹ V. F. Kazanin³⁸ Y. Ke¹⁴⁹ J. M. Keaveney^{34a}
 R. Keeler¹⁶⁸ G. V. Kehris⁶² J. S. Keller³⁵ A. S. Kelly⁹⁸ J. J. Kempster¹⁵⁰ P. D. Kennedy¹⁰² O. Kepka¹³⁴
 B. P. Kerridge¹³⁷ S. Kersten¹⁷⁴ B. P. Kerševan⁹⁵ L. Keszeghova^{29a} S. Ketaibchi Haghhighat¹⁵⁸ R. A. Khan¹³²
 A. Khanov¹²⁴ A. G. Kharlamov³⁸ T. Kharlamova³⁸ E. E. Khoda¹⁴² M. Kholodenko^{133a} T. J. Khoo¹⁹
 G. Khoriauli¹⁶⁹ J. Khubua^{153b,s} Y. A. R. Khwaira¹³⁰ B. Kibirige^{34g} D. Kim⁶ D. W. Kim^{48a,48b} Y. K. Kim⁴⁰
 N. Kimura⁹⁸ M. K. Kingston⁵⁶ A. Kirchhoff⁵⁶ C. Kirfel²⁵ F. Kirfel²⁵ J. Kirk¹³⁷ A. E. Kiryunin¹¹²
 S. Kita¹⁶⁰ C. Kitsaki¹⁰ O. Kivernyk²⁵ M. Klassen¹⁶¹ C. Klein³⁵ L. Klein¹⁶⁹ M. H. Klein⁴⁵ S. B. Klein⁵⁷
 U. Klein⁹⁴ P. Klimek³⁷ A. Klimentov³⁰ T. Klioutchnikova³⁷ P. Kluit¹¹⁷ S. Kluth¹¹² E. Kneringer⁸⁰
 T. M. Knight¹⁵⁸ A. Knue⁵⁰ D. Kobylanski¹⁷² S. F. Koch¹²⁹ M. Kocian¹⁴⁷ P. Kodyš¹³⁶ D. M. Koeck¹²⁶
 P. T. Koenig²⁵ T. Koffas³⁵ O. Kolay⁵¹ I. Koletsou⁴ T. Komarek⁸⁸ K. Köneke⁵⁵ A. X. Y. Kong¹ T. Kono¹²¹
 N. Konstantinidis⁹⁸ P. Kontaxakis⁵⁷ B. Konya¹⁰⁰ R. Kopeliansky⁴² S. Koperny^{87a} K. Korcyl⁸⁸ K. Kordas^{156,y}
 A. Korn⁹⁸ S. Korn⁵⁶ I. Korolkov¹³ N. Korotkova³⁸ B. Kortman¹¹⁷ O. Kortner¹¹² S. Kortner¹¹²
 W. H. Kostecka¹¹⁸ V. V. Kostyukhin¹⁴⁵ A. Kotsokechagia³⁷ A. Kotwal⁵² A. Koulouris³⁷
 A. Kourkoumelis-Charalampidi^{74a,74b} C. Kourkoumelis⁹ E. Kourlitis^{112,t} O. Kovanda¹²⁶ R. Kowalewski¹⁶⁸
 W. Kozanecki¹²⁶ A. S. Kozhin³⁸ V. A. Kramarenko³⁸ G. Kramberger⁹⁵ P. Kramer¹⁰² M. W. Krasny¹³⁰
 A. Krasznahorkay³⁷ A. C. Kraus¹¹⁸ J. W. Kraus¹⁷⁴ J. A. Kremer⁴⁹ T. Kresse⁵¹ L. Kretschmann¹⁷⁴
 J. Kretzschmar⁹⁴ K. Kreul¹⁹ P. Krieger¹⁵⁸ M. Krivos¹³⁶ K. Krizka²¹ K. Kroeninger⁵⁰ H. Kroha¹¹²

- J. Kroll ¹³⁴ J. Kroll ¹³¹ K. S. Krownman ¹⁰⁹ U. Kruchonak ³⁹ H. Krüger ²⁵ N. Krumnack, ⁸² M. C. Kruse ⁵²
O. Kuchinskaia ³⁸ S. Kuday ^{3a} S. Kuehn ³⁷ R. Kuesters ⁵⁵ T. Kuhl ⁴⁹ V. Kukhtin ³⁹ Y. Kulchitsky ^{38,j}
S. Kuleshov ^{140d,140b} M. Kumar ^{34g} N. Kumari ⁴⁹ P. Kumari ^{159b} A. Kupco ¹³⁴ T. Kupfer, ⁵⁰ A. Kupich ³⁸
O. Kuprash ⁵⁵ H. Kurashige ⁸⁶ L. L. Kurchaninov ^{159a} O. Kurdysh ⁶⁷ Y. A. Kurochkin ¹³⁴ A. Kurova ³⁸
M. Kuze ¹⁴¹ A. K. Kvam ¹⁰⁵ J. Kvita ¹²⁵ T. Kwan ¹⁰⁶ N. G. Kyriacou ¹⁰⁸ L. A. O. Laatu ¹⁰⁴ C. Lacasta ¹⁶⁶
F. Lacava ^{76a,76b} H. Lacker ¹⁹ D. Lacour ¹³⁰ N. N. Lad ⁹⁸ E. Ladygin ³⁹ A. Lafarge ⁴¹ B. Laforge ¹³⁰
T. Lagouri ¹⁷⁵ F. Z. Lahbabii ^{36a} S. Lai ⁵⁶ J. E. Lambert ¹⁶⁸ S. Lammers ⁶⁹ W. Lampl ⁷ C. Lampoudis ^{156,y}
G. Lamprinoudis ¹⁰² A. N. Lancaster ¹¹⁸ E. Lançon ³⁰ U. Landgraf ⁵⁵ M. P. J. Landon ⁹⁶ V. S. Lang ⁵⁵
O. K. B. Langrekken ¹²⁸ A. J. Lankford ¹⁶² F. Lanni ³⁷ K. Lantsch ²⁵ A. Lanza ^{74a} M. Lanzac Berrocal ¹⁶⁶
J. F. Laporte ¹³⁸ T. Lari ^{72a} F. Lasagni Manghi ^{24b} M. Lassnig ³⁷ V. Latonova ¹³⁴ A. Laurier ¹⁵⁴ S. D. Lawlor ¹⁴³
Z. Lawrence ¹⁰³ R. Lazaridou, ¹⁷⁰ M. Lazzaroni ^{72a,72b} B. Le, ¹⁰³ H. D. M. Le ¹⁰⁹ E. M. Le Boulicaut ¹⁷⁵
L. T. Le Pottier ^{18a} B. Leban ^{24b,24a} A. Lebedev ⁸² M. LeBlanc ¹⁰³ F. Ledroit-Guillon ⁶¹ S. C. Lee ¹⁵²
S. Lee ^{48a,48b} T. F. Lee ⁹⁴ L. L. Leeuw ^{34c} H. P. Lefebvre ⁹⁷ M. Lefebvre ¹⁶⁸ C. Leggett ^{18a} G. Lehmann Miotto ³⁷
M. Leigh ⁵⁷ W. A. Leight ¹⁰⁵ W. Leinonen ¹¹⁶ A. Leisos ^{156,z} M. A. L. Leite ^{84c} C. E. Leitgeb ¹⁹ R. Leitner ¹³⁶
K. J. C. Leney ⁴⁵ T. Lenz ²⁵ S. Leone ^{75a} C. Leonidopoulos ⁵³ A. Leopold ¹⁴⁸ R. Les ¹⁰⁹ C. G. Lester ³³
M. Levchenko ³⁸ J. Levêque ⁴ L. J. Levinson ¹⁷² G. Levрini ^{24b,24a} M. P. Lewicki ⁸⁸ C. Lewis ¹⁴² D. J. Lewis ⁴
L. Lewitt ¹⁴³ A. Li ³⁰ B. Li ^{63b} C. Li ^{63a} C.-Q. Li ¹¹² H. Li ^{63a} H. Li ^{63b} H. Li ^{114a} H. Li ¹⁵ H. Li ^{63b} J. Li ^{63c}
K. Li ¹⁴ L. Li ^{63c} M. Li ^{14,114c} S. Li ^{14,114c} S. Li ^{63d,63c} T. Li ⁵ X. Li ¹⁰⁶ Z. Li ¹²⁹ Z. Li ¹⁵⁷ Z. Li ^{14,114c}
Z. Li ^{63a} S. Liang ^{14,114c} Z. Liang ¹⁴ M. Liberatore ¹³⁸ B. Liberti ^{77a} K. Lie ^{65c} J. Lieber Marin ^{84e}
H. Lien ⁶⁹ H. Lin ¹⁰⁸ K. Lin ¹⁰⁹ R. E. Lindley ⁷ J. H. Lindon ² J. Ling ⁶² E. Lipelies ¹³¹ A. Lipniacka ¹⁷
A. Lister ¹⁶⁷ J. D. Little ⁶⁹ B. Liu ¹⁴ B. X. Liu ^{114b} D. Liu ¹⁴ E. H. L. Liu ²¹ J. B. Liu ^{63a} J. K. K. Liu ³³
K. Liu ^{63d} K. Liu ^{63d,63c} M. Liu ^{63a} M. Y. Liu ^{63a} P. Liu ¹⁴ Q. Liu ^{63d,142,63c} X. Liu ^{63a} X. Liu ^{63b}
Y. Liu ^{114b,114c} Y. L. Liu ^{63b} Y. W. Liu ^{63a} S. L. Lloyd ⁹⁶ E. M. Lobodzinska ⁴⁹ P. Loch ⁷ E. Lodhi ¹⁵⁸
T. Lohse ¹⁹ K. Lohwasser ¹⁴³ E. Loiacono ⁴⁹ M. Lokajicek ^{134,s} J. D. Lomas ²¹ J. D. Long ⁴² I. Longarini ¹⁶²
R. Longo ¹⁶⁵ I. Lopez Paz ⁶⁸ A. Lopez Solis ⁴⁹ N. A. Lopez-canelas ⁷ N. Lorenzo Martinez ⁴ A. M. Lory ¹¹¹
M. Losada ^{119a} G. Löschke Centeno ¹⁵⁰ O. Loseva ³⁸ X. Lou ^{48a,48b} X. Lou ^{14,114c} A. Lounis ⁶⁷ P. A. Love ⁹³
G. Lu ^{14,114c} M. Lu ⁶⁷ S. Lu ¹³¹ Y. J. Lu ⁶⁶ H. J. Lubatti ¹⁴² C. Luci ^{76a,76b} F. L. Lucio Alves ^{114a} F. Luehring ⁶⁹
O. Lukianchuk ⁶⁷ B. S. Lunday ¹³¹ O. Lundberg ¹⁴⁸ B. Lund-Jensen ^{148,s} N. A. Luongo ⁶ M. S. Lutz ³⁷
A. B. Lux ²⁶ D. Lynn ³⁰ R. Lysak ¹³⁴ E. Lytken ¹⁰⁰ V. Lyubushkin ³⁹ T. Lyubushkina ³⁹ M. M. Lyukova ¹⁴⁹
M. Firduas M. Soberi ⁵³ H. Ma ³⁰ K. Ma ^{63a} L. L. Ma ^{63b} W. Ma ^{63a} Y. Ma ¹²⁴ J. C. MacDonald ¹⁰²
P. C. Machado De Abreu Farias ^{84e} R. Madar ⁴¹ T. Madula ⁹⁸ J. Maeda ⁸⁶ T. Maeno ³⁰ H. Maguire ¹⁴³
V. Maiboroda ¹³⁸ A. Maio ^{133a,133b,133d} K. Maj ^{87a} O. Majersky ⁴⁹ S. Majewski ¹²⁶ N. Makovec ⁶⁷
V. Maksimovic ¹⁶ B. Malaescu ¹³⁰ Pa. Malecki ⁸⁸ V. P. Maleev ³⁸ F. Malek ^{61,aa} M. Mali ⁹⁵ D. Malito ⁹⁷
U. Mallik ⁸¹ S. Maltezos, ¹⁰ S. Malyukov, ³⁹ J. Mamuzic ¹³ G. Mancini ⁵⁴ M. N. Mancini ²⁷ G. Manco ^{134,74b}
J. P. Mandalia ⁹⁶ S. S. Mandarry ¹⁵⁰ I. Mandić ⁹⁵ L. Manhaes de Andrade Filho ^{84a} I. M. Maniatis ¹⁷²
J. Manjarres Ramos ⁹¹ D. C. Mankad ¹⁷² A. Mann ¹¹¹ S. Manzoni ³⁷ L. Mao ^{63c} X. Mapekula ^{34c}
A. Marantis ^{156,z} G. Marchiori ⁵ M. Marcisovsky ¹³⁴ C. Marcon ^{72a} M. Marinescu ²¹ S. Marium ⁴⁹
M. Marjanovic ¹²³ A. Markhoos ⁵⁵ M. Markovich ⁶⁷ E. J. Marshall ⁹³ Z. Marshall ^{18a} S. Marti-Garcia ¹⁶⁶
J. Martin ⁹⁸ T. A. Martin ¹³⁷ V. J. Martin ⁵³ B. Martin dit Latour ¹⁷ L. Martinelli ^{76a,76b} M. Martinez ^{13,r}
P. Martinez Agullo ¹⁶⁶ V. I. Martinez Outschoorn ¹⁰⁵ P. Martinez Suarez ¹³ S. Martin-Haugh ¹³⁷ G. Martinovicova ¹³⁶
V. S. Martouï ^{28b} A. C. Martyniuk ⁹⁸ A. Marzin ³⁷ D. Mascione ^{79a,79b} L. Masetti ¹⁰² J. Masik ¹⁰³
A. L. Maslennikov ³⁸ S. L. Mason ⁴² P. Massarotti ^{73a,73b} P. Mastrandrea ^{75a,75b} A. Mastroberardino ^{44b,44a}
T. Masubuchi ¹²⁷ T. T. Mathew ¹²⁶ T. Mathisen ¹⁶⁴ J. Matousek ¹³⁶ J. Maurer ^{28b} T. Maurin ⁶⁰ A. J. Maury ⁶⁷
B. Maćek ⁹⁵ D. A. Maximov ³⁸ A. E. May ¹⁰³ R. Mazini ¹⁵² I. Maznas ¹¹⁸ M. Mazza ¹⁰⁹ S. M. Mazza ¹³⁹
E. Mazzeo ^{72a,72b} C. Mc Ginn ³⁰ J. P. Mc Gowan ¹⁶⁸ S. P. Mc Kee ¹⁰⁸ C. C. McCracken ¹⁶⁷ E. F. McDonald ¹⁰⁷
A. E. McDougall ¹¹⁷ J. A. McFayden ¹⁵⁰ R. P. McGovern ¹³¹ R. P. Mckenzie ^{34g} T. C. McLachlan ⁴⁹
D. J. McLaughlin ⁹⁸ S. J. McMahon ¹³⁷ C. M. Mcpartland ⁹⁴ R. A. McPherson ^{168,n} S. Mehlhase ¹¹¹ A. Mehta ⁹⁴
D. Melini ¹⁶⁶ B. R. Mellado Garcia ^{34g} A. H. Melo ⁵⁶ F. Meloni ⁴⁹ A. M. Mendes Jacques Da Costa ¹⁰³
H. Y. Meng ¹⁵⁸ L. Meng ⁹³ S. Menke ¹¹² M. Mentink ³⁷ E. Meoni ^{44b,44a} G. Mercado ¹¹⁸ S. Merianos ¹⁵⁶
C. Merlassino ^{70a,70c} L. Merola ^{73a,73b} C. Meroni ^{72a,72b} J. Metcalfe ⁶ A. S. Mete ⁶ E. Meuser ¹⁰² C. Meyer ⁶⁹
J-P. Meyer ¹³⁸ R. P. Middleton ¹³⁷ L. Mijović ⁵³ G. Mikenberg ¹⁷² M. Mikestikova ¹³⁴ M. Mikuž ⁹⁵
H. Mildner ¹⁰² A. Milic ³⁷ D. W. Miller ⁴⁰ E. H. Miller ¹⁴⁷ L. S. Miller ³⁵ A. Milov ¹⁷² D. A. Milstead, ^{48a,48b}
T. Min, ^{114a} A. A. Minaenko ³⁸ I. A. Minashvili ^{153b} L. Mince ⁶⁰ A. I. Mincer ¹²⁰ B. Mindur ^{87a} M. Mineev ³⁹
Y. Mino ⁸⁹ L. M. Mir ¹³ M. Miralles Lopez ⁶⁰ M. Mironova ^{18a} M. C. Missio ¹¹⁶ A. Mitra ¹⁷⁰ V. A. Mitsou ¹⁶⁶
Y. Mitsumori ¹¹³ O. Miu ¹⁵⁸ P. S. Miyagawa ⁹⁶ T. Mkrtchyan ^{64a} M. Mlinarevic ⁹⁸ T. Mlinarevic ⁹⁸
M. Mlynarikova ³⁷ S. Mobius ²⁰ P. Mogg ¹¹¹ M. H. Mohamed Farook ¹¹⁵ A. F. Mohammed ^{14,114c} S. Mohapatra ⁴²
G. Mokgatitswane ^{34g} L. Moleri ¹⁷² B. Mondal ¹⁴⁵ S. Mondal ¹³⁵ K. Mönig ⁴⁹ E. Monnier ¹⁰⁴
L. Monsonis Romero, ¹⁶⁶ J. Montejo Berlingen ¹³ A. Montella ^{48a,48b} M. Montella ¹²² F. Montereali ^{78a,78b}

- F. Monticelli ⁹², S. Monzani ^{70a,70c}, A. Morancho Tarda ⁴³, N. Morange ⁶⁷, A. L. Moreira De Carvalho ⁴⁹, M. Moreno Llácer ¹⁶⁶, C. Moreno Martinez ⁵⁷, J. M. Moreno Perez ^{23b}, P. Morettini ^{58b}, S. Morgenstern ³⁷, M. Morii ⁶², M. Morinaga ¹⁵⁷, M. Moritsu ⁹⁰, F. Morodei ^{76a,76b}, L. Morvaj ³⁷, P. Moschovakos ³⁷, B. Moser ¹²⁹, M. Mosidze ^{153b}, T. Moskalets ⁴⁵, P. Moskvitina ¹¹⁶, J. Moss ^{32,ab}, P. Moszkowicz ^{87a}, A. Moussa ^{36d}, E. J. W. Moyse ¹⁰⁵, O. Mtintsilana ^{34g}, S. Muanza ¹⁰⁴, J. Mueller ¹³², D. Muenstermann ⁹³, R. Müller ³⁷, G. A. Mullier ¹⁶⁴, A. J. Mullin, ³³, J. J. Mullin, ¹³¹, A. E. Mulski ⁶², D. P. Mungo ¹⁵⁸, D. Munoz Perez ¹⁶⁶, F. J. Munoz Sanchez ¹⁰³, M. Murin ¹⁰³, W. J. Murray ^{170,137}, M. Muškinja ⁹⁵, C. Mwewa ³⁰, A. G. Myagkov ^{38,j}, A. J. Myers ⁸, G. Myers ¹⁰⁸, M. Myska ¹³⁵, B. P. Nachman ^{18a}, O. Nackenhorst ⁵⁰, K. Nagai ¹²⁹, K. Nagano ⁸⁵, R. Nagasaka, ¹⁵⁷, J. L. Nagle ^{30,ac}, E. Nagy ¹⁰⁴, A. M. Nairz ³⁷, Y. Nakahama ⁸⁵, K. Nakamura ⁸⁵, K. Nakkalil ⁵, H. Nanjo ¹²⁷, E. A. Narayanan ¹¹⁵, I. Naryshkin ³⁸, L. Nasella ^{72a,72b}, M. Naseri ³⁵, S. Nasri ^{119b}, C. Nass ²⁵, G. Navarro ^{23a}, J. Navarro-Gonzalez ¹⁶⁶, R. Nayak ¹⁵⁵, A. Nayaz ¹⁹, P. Y. Nechaeva ³⁸, S. Nechaeva ^{24b,24a}, F. Nechansky ¹³⁴, L. Nedic ¹²⁹, T. J. Neep ²¹, A. Negri ^{74a,74b}, M. Negrini ^{24b}, C. Nellist ¹¹⁷, C. Nelson ¹⁰⁶, K. Nelson ¹⁰⁸, S. Nemecek ¹³⁴, M. Nessi ^{37,ad}, M. S. Neubauer ¹⁶⁵, F. Neuhaus ¹⁰², J. Neundorf ⁴⁹, J. Newell ⁹⁴, P. R. Newman ²¹, C. W. Ng ¹³², Y. W. Y. Ng ⁴⁹, B. Ngair ^{119a}, H. D. N. Nguyen ¹¹⁰, R. B. Nickerson ¹²⁹, R. Nicolaïdou ¹³⁸, J. Nielsen ¹³⁹, M. Niemeyer ⁵⁶, J. Niermann ⁵⁶, N. Nikiforou ³⁷, V. Nikolaenko ^{38,j}, I. Nikolic-Audit ¹³⁰, K. Nikolopoulos ²¹, P. Nilsson ³⁰, I. Ninca ⁴⁹, G. Ninio ¹⁵⁵, A. Nisati ^{76a}, N. Nishu ², R. Nisius ¹¹², J.-E. Nitschke ⁵¹, E. K. Nkademeng ^{34g}, T. Nobe ¹⁵⁷, T. Nommensen ¹⁵¹, M. B. Norfolk ¹⁴³, B. J. Norman ³⁵, M. Noury ^{36a}, J. Novak ⁹⁵, T. Novak ⁹⁵, L. Novotny ¹³⁵, R. Novotny ¹¹⁵, L. Nozka ¹²⁵, K. Ntekas ¹⁶², N. M. J. Nunes De Moura Junior ^{84b}, J. Ocariz ¹³⁰, A. Ochi ⁸⁶, I. Ochoa ^{133a}, S. Oerdekk ^{49,ae}, J. T. Offermann ⁴⁰, A. Ogrodnik ¹³⁶, A. Oh ¹⁰³, C. C. Ohm ¹⁴⁸, H. Oide ⁸⁵, R. Oishi ¹⁵⁷, M. L. Ojeda ³⁷, Y. Okumura ¹⁵⁷, L. F. Oleiro Seabra ^{133a}, I. Oleksiyuk ⁵⁷, S. A. Olivares Pino ^{140d}, G. Oliveira Correa ¹³, D. Oliveira Damazio ³⁰, J. L. Oliver ¹⁶², Ö. Ö. Öncel ⁵⁵, A. P. O'Neill ²⁰, A. Onofre ^{133a,133e}, P. U. E. Onyisi ¹¹, M. J. Oreglia ⁴⁰, G. E. Orellana ⁹², D. Orestano ^{78a,78b}, N. Orlando ¹³, R. S. Orr ¹⁵⁸, L. M. Osojnak ¹³¹, R. Ospanov ^{63a}, G. Otero y Garzon ³¹, H. Otono ⁹⁰, P. S. Ott ^{64a}, G. J. Ottino ^{18a}, M. Ouchrif ^{36d}, F. Ould-Saada ¹²⁸, T. Ovsiannikova ¹⁴², M. Owen ⁶⁰, R. E. Owen ¹³⁷, V. E. Ozcan ^{22a}, F. Ozturk ⁸⁸, N. Ozturk ⁸, S. Ozturk ⁸³, H. A. Pacey ¹²⁹, A. Pacheco Pages ¹³, C. Padilla Aranda ¹³, G. Padovano ^{76a,76b}, S. Pagan Griso ^{18a}, G. Palacino ⁶⁹, A. Palazzo ^{71a,71b}, J. Pampel ²⁵, J. Pan ¹⁷⁵, T. Pan ^{65a}, D. K. Panchal ¹¹, C. E. Pandini ¹¹⁷, J. G. Panduro Vazquez ¹³⁷, H. D. Pandya ¹, H. Pang ¹⁵, P. Pani ⁴⁹, G. Panizzo ^{70a,70c}, L. Panwar ¹³⁰, L. Paolozzi ⁵⁷, S. Parajuli ¹⁶⁵, A. Paramonov ⁶, C. Paraskevopoulos ⁵⁴, D. Paredes Hernandez ^{65b}, A. Paret ^{74a,74b}, K. R. Park ⁴², T. H. Park ¹⁵⁸, M. A. Parker ³³, F. Parodi ^{58b,58a}, E. W. Parrish ¹¹⁸, V. A. Parrish ⁵³, J. A. Parsons ⁴², U. Parzefall ⁵⁵, B. Pascual Dias ¹¹⁰, L. Pascual Dominguez ¹⁰¹, E. Pasqualucci ^{76a}, S. Passaggio ^{58b}, F. Pastore ^b, P. Patel ⁹⁷, P. Patel ⁸⁸, U. M. Patel ⁵², J. R. Pater ¹⁰³, T. Pauly ³⁷, F. Pauwels ¹³⁶, C. I. Pazos ¹⁶¹, J. Pearkes ¹⁴⁷, M. Pedersen ¹²⁸, R. Pedro ^{133a}, S. V. Peleganchuk ³⁸, O. Penc ³⁷, E. A. Pender ⁵³, S. Peng ¹⁵, G. D. Penn ¹⁷⁵, K. E. Penski ¹¹¹, M. Penzin ³⁸, B. S. Peralva ^{84d}, A. P. Pereira Peixoto ¹⁴², L. Pereira Sanchez ¹⁴⁷, D. V. Perepelitsa ^{30,ac}, G. Perera ¹⁰⁵, E. Perez Codina ^{159a}, M. Perganti ¹⁰, H. Pernegger ³⁷, S. Perrella ^{76a,76b}, O. Perrin ⁴¹, K. Peters ⁴⁹, R. F. Y. Peters ¹⁰³, B. A. Petersen ³⁷, T. C. Petersen ⁴³, E. Petit ¹⁰⁴, V. Petousis ¹³⁵, C. Petridou ^{156,y}, T. Petru ¹³⁶, A. Petrukhin ¹⁴⁵, M. Pettee ^{18a}, A. Petukhov ³⁸, K. Petukhova ³⁷, R. Pezoa ^{140f}, L. Pezzotti ³⁷, G. Pezzullo ¹⁷⁵, A. J. Pfleger ³⁷, T. M. Pham ¹⁷³, T. Pham ¹⁰⁷, P. W. Phillips ¹³⁷, G. Piacquadio ¹⁴⁹, E. Pianori ^{18a}, F. Piazza ¹²⁶, R. Piegaia ³¹, D. Pietreanu ^{28b}, A. D. Pilkington ¹⁰³, M. Pinamonti ^{70a,70c}, J. L. Pinfold ², B. C. Pinheiro Pereira ^{133a}, J. Pinol Bel ¹³, A. E. Pinto Pinoargote ^{138,138}, L. Pintucci ^{70a,70c}, K. M. Piper ¹⁵⁰, A. Pirttikoski ⁵⁷, D. A. Pizzi ³⁵, L. Pizzimento ^{65b}, A. Pizzini ¹¹⁷, M.-A. Pleier ³⁰, V. Pleskot ¹³⁶, E. Plotnikova ³⁹, G. Poddar ⁹⁶, R. Poettgen ¹⁰⁰, L. Poggioli ¹³⁰, I. Pokharel ⁵⁶, S. Polacek ¹³⁶, G. Polesello ^{74a}, A. Poley ^{146,159a}, A. Polini ^{24b}, C. S. Pollard ¹⁷⁰, Z. B. Pollock ¹²², E. Pompa Pacchi ^{76a,76b}, N. I. Pond ⁹⁸, D. Ponomarenko ⁶⁹, L. Pontecorvo ³⁷, S. Popa ^{28a}, G. A. Popeneiciu ^{28d}, A. Poreba ³⁷, D. M. Portillo Quintero ^{159a}, S. Pospisil ¹³⁵, M. A. Postill ¹⁴³, P. Postolache ^{28c}, K. Potamianos ¹⁷⁰, P. A. Potepa ^{87a}, I. N. Potrap ³⁹, C. J. Potter ³³, H. Potti ¹⁵¹, J. Poveda ¹⁶⁶, M. E. Pozo Astigarraga ³⁷, A. Prades Ibanez ^{77a,77b}, J. Pretel ¹⁶⁸, D. Price ¹⁰³, M. Primavera ^{71a}, L. Primomo ^{70a,70c}, M. A. Principe Martin ¹⁰¹, R. Privara ¹²⁵, T. Procter ⁶⁰, M. L. Proffitt ¹⁴², N. Proklova ¹³¹, K. Prokofiev ^{65c}, G. Proto ¹¹², J. Proudfoot ⁶, M. Przybycien ^{87a}, W. W. Przygoda ^{87b}, A. Psallidas ⁴⁷, J. E. Puddefoot ¹⁴³, D. Pudzha ⁵⁵, D. Pyatiibyzantseva ³⁸, J. Qian ¹⁰⁸, D. Qichen ¹⁰³, Y. Qin ¹³, T. Qiu ⁵³, A. Quadt ⁵⁶, M. Queitsch-Maitland ¹⁰³, G. Quetant ⁵⁷, R. P. Quinn ¹⁶⁷, G. Rabanal Bolanos ⁶², D. Rafanoharana ⁵⁵, F. Raffaeli ^{77a,77b}, F. Ragusa ^{72a,72b}, J. L. Rainbolt ⁴⁰, J. A. Raine ⁵⁷, S. Rajagopalan ³⁰, E. Ramakoti ³⁸, L. Rambelli ^{58b,58a}, I. A. Ramirez-Berend ³⁵, K. Ran ^{49,114c}, D. S. Rankin ¹³¹, N. P. Rapheeza ^{34g}, H. Rasheed ^{28b}, V. Raskina ¹³⁰, D. F. Rassloff ^{64a}, A. Rastogi ^{18a}, S. Rave ¹⁰², S. Ravera ^{58b,58a}, B. Ravina ⁵⁶, I. Ravinovich ¹⁷², M. Raymond ³⁷, A. L. Read ¹²⁸, N. P. Readioff ¹⁴³, D. M. Rebuzzi ^{74a,74b}, G. Redlinger ³⁰, A. S. Reed ¹¹², K. Reeves ²⁷, J. A. Reidelsturz ¹⁷⁴, D. Reikher ¹²⁶, A. Rej ⁵⁰, C. Rembsler ³⁷, M. Renda ^{28b}, F. Renner ⁴⁹, A. G. Rennie ¹⁶², A. L. Rescia ⁴⁹, S. Resconi ^{72a}, M. Ressegotti ^{58b,58a}, S. Rettie ³⁷, J. G. Reyes Rivera ¹⁰⁹, E. Reynolds ^{18a}, O. L. Rezanova ³⁸, P. Reznicek ¹³⁶, H. Riani ^{36d}, N. Ribaric ⁵², E. Ricci ^{79a,79b}, R. Richter ¹¹², S. Richter ^{48a,48b}, E. Richter-Was ^{87b}, M. Ridel ¹³⁰, S. Ridouani ^{36d}, P. Rieck ¹²⁰, P. Riedler ³⁷, E. M. Riefel ^{48a,48b}, J. O. Rieger ¹¹⁷, M. Rijssenbeek ¹⁴⁹, M. Rimoldi ³⁷, L. Rinaldi ^{24b,24a}, P. Rincke ^{56,164}, T. T. Rinn ³⁰, M. P. Rinnagel ¹¹¹, G. Ripellino ¹⁶⁴, I. Riut ¹³, J. C. Rivera Vergara ¹⁶⁸

- F. Rizatdinova ¹²⁴, E. Rizvi ⁹⁶, B. R. Roberts ^{18a}, S. S. Roberts ¹³⁹, S. H. Robertson ^{106,n}, D. Robinson ³³, M. Robles Manzano ¹⁰², A. Robson ⁶⁰, A. Rocchi ^{77a,77b}, C. Roda ^{75a,75b}, S. Rodriguez Bosca ³⁷, Y. Rodriguez Garcia ^{23a}, A. Rodriguez Rodriguez ⁵⁵, A. M. Rodríguez Vera ¹¹⁸, S. Roe ³⁷, J. T. Roemer ³⁷, A. R. Roepe-Gier ¹³⁹, O. Røhne ¹²⁸, R. A. Rojas ¹⁰⁵, C. P. A. Roland ¹³⁰, J. Roloff ³⁰, A. Romaniouk ⁸⁰, E. Romano ^{74a,74b}, M. Romano ^{24b}, A. C. Romero Hernandez ¹⁶⁵, N. Rompotis ⁹⁴, L. Roos ¹³⁰, S. Rosati ^{76a}, B. J. Rosser ⁴⁰, E. Rossi ¹²⁹, E. Rossi ^{73a,73b}, L. P. Rossi ⁶², L. Rossini ⁵⁵, R. Rosten ¹²², M. Rotaru ^{28b}, B. Rottler ⁵⁵, C. Rougier ⁹¹, D. Rousseau ⁶⁷, D. Rousseau ⁴⁹, A. Roy ¹⁶⁵, S. Roy-Garand ¹⁵⁸, A. Rozanov ¹⁰⁴, Z. M. A. Rozario ⁶⁰, Y. Rozen ¹⁵⁴, A. Rubio Jimenez ¹⁶⁶, A. J. Ruby ⁹⁴, V. H. Ruelas Rivera ¹⁹, T. A. Ruggeri ¹, A. Ruggiero ¹²⁹, A. Ruiz-Martinez ¹⁶⁶, A. Rummler ³⁷, Z. Rurikova ⁵⁵, N. A. Rusakovich ³⁹, H. L. Russell ¹⁶⁸, G. Russo ^{76a,76b}, J. P. Rutherford Colmenares ³³, M. Rybar ¹³⁶, E. B. Rye ¹²⁸, A. Ryzhov ⁴⁵, J. A. Sabater Iglesias ⁵⁷, H.-F.-W. Sadrozinski ¹³⁹, F. Safai Tehrani ^{76a}, B. Safarzadeh Samani ¹³⁷, S. Saha ¹, M. Sahinsoy ⁸³, A. Saibel ¹⁶⁶, M. Saimpert ¹³⁸, M. Saito ¹⁵⁷, T. Saito ¹⁵⁷, A. Sala ^{72a,72b}, D. Salamani ³⁷, A. Salnikov ¹⁴⁷, J. Salt ¹⁶⁶, A. Salvador Salas ¹⁵⁵, D. Salvatore ^{44b,44a}, F. Salvatore ¹⁵⁰, A. Salzburger ³⁷, D. Sammel ⁵⁵, E. Sampson ⁹³, D. Sampsonidis ^{156,y}, D. Sampsonidou ¹²⁶, J. Sánchez ¹⁶⁶, V. Sanchez Sebastian ¹⁶⁶, H. Sandaker ¹²⁸, C. O. Sander ⁴⁹, J. A. Sandesara ¹⁰⁵, M. Sandhoff ¹⁷⁴, C. Sandoval ^{23b}, L. Sanfilippo ^{64a}, D. P. C. Sankey ¹³⁷, T. Sano ⁸⁹, A. Sansoni ⁵⁴, L. Santi ^{37,76b}, C. Santoni ⁴¹, H. Santos ^{133a,133b}, A. Santra ¹⁷², E. Sanzani ^{24b,24a}, K. A. Saoucha ¹⁶³, J. G. Saraiva ^{133a,133d}, J. Sardain ⁷, O. Sasaki ⁸⁵, K. Sato ¹⁶⁰, C. Sauer ^{64b}, E. Sauvan ⁴, P. Savard ^{158,d}, R. Sawada ¹⁵⁷, C. Sawyer ¹³⁷, L. Sawyer ⁹⁹, C. Sbarra ^{24b}, A. Sbrizzi ^{24b,24a}, T. Scanlon ⁹⁸, J. Schaarschmidt ¹⁴², U. Schäfer ¹⁰², A. C. Schaffer ^{67,45}, D. Schaile ¹¹¹, R. D. Schamberger ¹⁴⁹, C. Scharf ¹⁹, M. M. Schefer ²⁰, V. A. Schegelsky ³⁸, D. Scheirich ¹³⁶, M. Schernau ¹⁶², C. Scheulen ⁵⁶, C. Schiavi ^{58b,58a}, M. Schioppa ^{44b,44a}, B. Schlag ¹⁴⁷, K. E. Schleicher ⁵⁵, S. Schlenker ³⁷, J. Schmeing ¹⁷⁴, M. A. Schmidt ¹⁷⁴, K. Schmieden ¹⁰², C. Schmitt ¹⁰², N. Schmitt ¹⁰², S. Schmitt ⁴⁹, L. Schoeffel ¹³⁸, A. Schoening ^{64b}, P. G. Scholer ³⁵, E. Schopf ¹²⁹, M. Schott ²⁵, J. Schovancova ³⁷, S. Schramm ⁵⁷, T. Schroer ⁵⁷, H.-C. Schultz-Coulon ^{64a}, M. Schumacher ⁵⁵, B. A. Schumm ¹³⁹, Ph. Schune ¹³⁸, A. J. Schuy ¹⁴², H. R. Schwartz ¹³⁹, A. Schwartzman ¹⁴⁷, T. A. Schwarz ¹⁰⁸, Ph. Schwemling ¹³⁸, R. Schwienhorst ¹⁰⁹, F. G. Sciaccia ²⁰, A. Sciandra ³⁰, G. Sciolla ²⁷, F. Seuri ^{75a}, C. D. Sebastiani ⁹⁴, K. Sedlaczek ¹¹⁸, S. C. Seidel ¹¹⁵, A. Seiden ¹³⁹, B. D. Seidlitz ⁴², C. Seitz ⁴⁹, J. M. Seixas ^{84b}, G. Sekhniaidze ^{73a}, L. Selem ⁶¹, N. Semprini-Cesari ^{24b,24a}, D. Sengupta ⁵⁷, V. Senthilkumar ¹⁶⁶, L. Serin ⁶⁷, M. Sessa ^{77a,77b}, H. Severini ¹²³, F. Sforza ^{58b,58a}, A. Sfyrla ⁵⁷, Q. Sha ¹⁴, E. Shabalina ⁵⁶, A. H. Shah ³³, R. Shaheen ¹⁴⁸, J. D. Shahinian ¹³¹, D. Shaked Renous ¹⁷², L. Y. Shan ¹⁴, M. Shapiro ^{18a}, A. Sharma ³⁷, A. S. Sharma ¹⁶⁷, P. Sharma ⁸¹, P. B. Shatalov ³⁸, K. Shaw ¹⁵⁰, S. M. Shaw ¹⁰³, Q. Shen ^{63c}, D. J. Sheppard ¹⁴⁶, P. Sherwood ⁹⁸, L. Shi ⁹⁸, X. Shi ¹⁴, S. Shimizu ⁸⁵, C. O. Shimmin ¹⁷⁵, J. D. Shinner ⁹⁷, I. P. J. Shipsey ¹²⁹, S. Shirabe ⁹⁰, M. Shiyakova ^{39,af}, M. J. Shochet ⁴⁰, D. R. Shope ¹²⁸, B. Shrestha ¹²³, S. Shrestha ^{122,ag}, I. Shreyber ³⁸, M. J. Shroff ¹⁶⁸, P. Sicho ¹³⁴, A. M. Sickles ¹⁶⁵, E. Sideras Haddad ^{34g}, A. C. Sidley ¹¹⁷, A. Sidoti ^{24b}, F. Siegert ⁵¹, Dj. Sijacki ¹⁶, F. Sili ⁹², J. M. Silva ⁵³, I. Silva Ferreira ^{84b}, M. V. Silva Oliveira ³⁰, S. B. Silverstein ^{48a}, S. Simion ⁶⁷, R. Simoniello ³⁷, E. L. Simpson ¹⁰³, H. Simpson ¹⁵⁰, L. R. Simpson ¹⁰⁸, N. D. Simpson ¹⁰⁰, S. Simsek ⁸³, S. Sindhu ⁵⁶, P. Sinervo ¹⁵⁸, S. Singh ¹⁵⁸, S. Sinha ⁴⁹, S. Sinha ¹⁰³, M. Sioli ^{24b,24a}, I. Siral ³⁷, E. Sitnikova ⁴⁹, J. Sjölin ^{48a,48b}, A. Skaf ⁵⁶, E. Skorda ²¹, P. Skubic ¹²³, M. Slawinska ⁸⁸, V. Smakhtin ¹⁷², B. H. Smart ¹³⁷, S. Yu. Smirnov ³⁸, Y. Smirnov ³⁸, L. N. Smirnova ^{38,j}, O. Smirnova ¹⁰⁰, A. C. Smith ⁴², D. R. Smith ¹⁶², E. A. Smith ⁴⁰, J. L. Smith ¹⁰³, R. Smith ¹⁴⁷, M. Smizanska ⁹³, K. Smolek ¹³⁵, A. A. Snesarev ³⁸, H. L. Snoek ¹¹⁷, S. Snyder ³⁰, R. Sobie ^{168,n}, A. Soffer ¹⁵⁵, C. A. Solans Sanchez ³⁷, E. Yu. Soldatov ³⁸, U. Soldevila ¹⁶⁶, A. A. Solodkov ³⁸, S. Solomon ²⁷, A. Soloshenko ³⁹, K. Solovieva ⁵⁵, O. V. Solovyanov ⁴¹, P. Sommer ⁵¹, A. Sonay ¹³, W. Y. Song ^{159b}, A. Sopczak ¹³⁵, A. L. Sopio ⁵³, F. Sopkova ^{29b}, J. D. Sorenson ¹¹⁵, I. R. Sotarriba Alvarez ¹⁴¹, V. Sothilingam ^{64a}, O. J. Soto Sandoval ^{140c,140b}, S. Sottocornola ⁶⁹, R. Soualah ¹⁶³, Z. Soumaimi ^{36e}, D. South ⁴⁹, N. Soybelman ¹⁷², S. Spagnolo ^{71a,71b}, M. Spalla ¹¹², D. Sperlich ⁵⁵, G. Spigo ³⁷, B. Spisso ^{73a,73b}, D. P. Spiteri ⁶⁰, M. Spousta ¹³⁶, E. J. Staats ³⁵, R. Stamen ^{64a}, A. Stampekitis ²¹, E. Stancka ⁸⁸, W. Stanek-Maslouska ⁴⁹, M. V. Stange ⁵¹, B. Stanislaus ^{18a}, M. M. Stanitzki ⁴⁹, B. Stapf ⁴⁹, E. A. Starchenko ³⁸, G. H. Stark ¹³⁹, J. Stark ⁹¹, P. Staroba ¹³⁴, P. Starovoitov ^{64a}, S. Stärz ¹⁰⁶, R. Staszewski ⁸⁸, G. Stavropoulos ⁴⁷, A. Stefl ³⁷, P. Steinberg ³⁰, B. Stelzer ^{146,159a}, H. J. Stelzer ¹³², O. Stelzer-Chilton ^{159a}, H. Stenzel ⁵⁹, T. J. Stevenson ¹⁵⁰, G. A. Stewart ³⁷, J. R. Stewart ¹²⁴, M. C. Stockton ³⁷, G. Stoica ^{28b}, M. Stolarski ^{133a}, S. Stonjek ¹¹², A. Straessner ⁵¹, J. Strandberg ¹⁴⁸, S. Strandberg ^{48a,48b}, M. Stratmann ¹⁷⁴, M. Strauss ¹²³, T. Strebler ¹⁰⁴, P. Strizenec ^{29b}, R. Ströhmer ¹⁶⁹, D. M. Strom ¹²⁶, R. Stroynowski ⁴⁵, A. Strubig ^{48a,48b}, S. A. Stucci ³⁰, B. Stugu ¹⁷, J. Stupak ¹²³, N. A. Styles ⁴⁹, D. Su ¹⁴⁷, S. Su ^{63a}, W. Su ^{63d}, X. Su ^{63a}, D. Suchy ^{29a}, K. Sugizaki ¹⁵⁷, V. V. Sulin ³⁸, M. J. Sullivan ⁹⁴, D. M. S. Sultan ¹²⁹, L. Sultanaliyeva ³⁸, S. Sultansoy ^{3b}, T. Sumida ⁸⁹, S. Sun ¹⁷³, O. Sunneborn Gudnadottir ¹⁶⁴, N. Sur ¹⁰⁴, M. R. Sutton ¹⁵⁰, H. Suzuki ¹⁶⁰, M. Svatos ¹³⁴, M. Swiatlowski ^{159a}, T. Swirski ¹⁶⁹, I. Sykora ^{29a}, M. Sykora ¹³⁶, T. Sykora ¹³⁶, D. Ta ¹⁰², K. Tackmann ^{49,ae}, A. Taffard ¹⁶², R. Tafirout ^{159a}, J. S. Tafoya Vargas ⁶⁷, Y. Takubo ⁸⁵, M. Talby ¹⁰⁴, A. A. Talyshев ³⁸, K. C. Tam ^{65b}, N. M. Tamir ¹⁵⁵, A. Tanaka ¹⁵⁷, J. Tanaka ¹⁵⁷, R. Tanaka ⁶⁷, M. Tanasini ¹⁴⁹, Z. Tao ¹⁶⁷, S. Tapia Araya ^{140f}, S. Tapprogge ¹⁰², A. Tarek Abouelfadl Mohamed ¹⁰⁹, S. Tarem ¹⁵⁴, K. Tariq ¹⁴, G. Tarna ^{28b}, G. F. Tartarelli ^{72a}, M. J. Tartarin ⁹¹, P. Tas ¹³⁶, M. Tasevsky ¹³⁴, E. Tassi ^{44b,44a}, A. C. Tate ¹⁶⁵, G. Tateno ¹⁵⁷, Y. Tayalati ^{36e,ah}

- G. N. Taylor¹⁰⁷ W. Taylor^{159b} R. Teixeira De Lima¹⁴⁷ P. Teixeira-Dias⁹⁷ J. J. Teoh¹⁵⁸ K. Terashi¹⁵⁷
J. Terron¹⁰¹ S. Terzo¹³ M. Testa⁵⁴ R. J. Teuscher^{158,n} A. Thaler⁸⁰ O. Theiner⁵⁷ T. Theveneaux-Pelzer¹⁰⁴
O. Thielmann¹⁷⁴ D. W. Thomas⁹⁷ J. P. Thomas²¹ E. A. Thompson^{18a} P. D. Thompson²¹ E. Thomson¹³¹
R. E. Thornberry⁴⁵ C. Tian^{63a} Y. Tian⁵⁶ V. Tikhomirov^{38,j} Yu. A. Tikhonov³⁸ S. Timoshenko³⁸ D. Timoshyn¹³⁶
E. X. L. Ting¹ P. Tipton¹⁷⁵ A. Tishelman-Charny³⁰ S. H. Tlou^{34g} K. Todome¹⁴¹ S. Todorova-Nova¹³⁶ S. Todt⁵¹
L. Toffolin^{70a,70c} M. Togawa⁸⁵ J. Tojo⁹⁰ S. Tokár^{29a} K. Tokushuku⁸⁵ O. Toldaiev⁶⁹ M. Tomoto^{185,113}
L. Tompkins^{147,ai} K. W. Topolnicki^{87b} E. Torrence¹²⁶ H. Torres⁹¹ E. Torró Pastor¹⁶⁶ M. Toscani³¹
C. Tosciri⁴⁰ M. Tost¹¹ D. R. Tovey¹⁴³ I. S. Trandafir^{28b} T. Trefzger¹⁶⁹ A. Tricoli³⁰ I. M. Trigger^{159a}
S. Trincaz-Duvold¹³⁰ D. A. Trischuk²⁷ B. Trocmé⁶¹ A. Tropina³⁹ L. Truong^{34c} M. Trzebinski⁸⁸ A. Trzupek⁸⁸
F. Tsai¹⁴⁹ M. Tsai¹⁰⁸ A. Tsiamis¹⁵⁶ P. V. Tsiareshka³⁸ S. Tsigaridas^{159a} A. Tsirigotis^{156,z} V. Tsiskaridze¹⁵⁸
E. G. Tskhadadze^{153a} M. Tsopoulou¹⁵⁶ Y. Tsujikawa⁸⁹ I. I. Tsukerman³⁸ V. Tsulaia^{18a} S. Tsuno⁸⁵ K. Tsuri¹²¹
D. Tsybychev¹⁴⁹ Y. Tu^{65b} A. Tudorache^{28b} V. Tudorache^{28b} A. N. Tuna⁶² S. Turchikhin^{58b,58a} I. Turk Cakir^{3a}
R. Turra^{72a} T. Turtuvshin³⁹ P. M. Tuts⁴² S. Tzamarias^{156,y} E. Tzovara¹⁰² F. Ukegawa¹⁶⁰
P. A. Ulloa Poblete^{140c,140b} E. N. Umaka³⁰ G. Unal³⁷ A. Undrus³⁰ G. Unel¹⁶² J. Urban^{29b} P. Urrejola^{140a}
G. Usai⁸ R. Ushioda¹⁴¹ M. Usman¹¹⁰ F. Ustuner⁵³ Z. Uysal⁸³ V. Vacek¹³⁵ B. Vachon¹⁰⁶ T. Vafeiadis³⁷
A. Vaitkus⁹⁸ C. Valderanis¹¹¹ E. Valdes Santurio^{48a,48b} M. Valente^{159a} S. Valentinetto^{24b,24a} A. Valero¹⁶⁶
E. Valiente Moreno¹⁶⁶ A. Vallier⁹¹ J. A. Valls Ferrer¹⁶⁶ D. R. Van Arneman¹¹⁷ T. R. Van Daalen¹⁴²
A. Van Der Graaf⁵⁰ P. Van Gemmeren⁶ M. Van Rijnbach³⁷ S. Van Stroud⁹⁸ I. Van Vulpen¹¹⁷ P. Vana¹³⁶
M. Vanadia^{77a,77b} W. Vandelli³⁷ E. R. Vandewall¹²⁴ D. Vannicola¹⁵⁵ L. Vannoli⁵⁴ R. Vari^{76a} E. W. Varnes⁷
C. Varni^{18b} T. Varol¹⁵² D. Varouchas⁶⁷ L. Varriale¹⁶⁶ K. E. Varvell¹⁵¹ M. E. Vasile^{28b} L. Vaslin⁸⁵
G. A. Vasquez¹⁶⁸ A. Vasyukov³⁹ L. M. Vaughan¹²⁴ R. Vavricka¹⁰² T. Vazquez Schroeder³⁷ J. Veatch³²
V. Vecchio¹⁰³ M. J. Veen¹⁰⁵ I. Velisek³⁰ L. M. Veloce¹⁵⁸ F. Veloso^{133a,133c} S. Veneziano^{76a} A. Ventura^{71a,71b}
S. Ventura Gonzalez¹³⁸ A. Verbytskyi¹¹² M. Verducci^{75a,75b} C. Vergis⁹⁶ M. Verissimo De Araujo^{84b}
W. Verkerke¹¹⁷ J. C. Vermeulen¹¹⁷ C. Vernieri¹⁴⁷ M. Vessella¹⁰⁵ M. C. Vetterli^{146,d} A. Vgenopoulos¹⁰²
N. Viaux Maira^{140f} T. Vickey¹⁴³ O. E. Vickey Boeriu¹⁴³ G. H. A. Viehhäuser¹²⁹ L. Vigani^{64b} M. Vigl¹¹²
M. Villa^{24b,24a} M. Villaplana Perez¹⁶⁶ E. M. Villhauer⁵³ E. Vilucchi⁵⁴ M. G. Vincter³⁵ A. Visible¹¹⁷ C. Vittori³⁷
I. Vivarelli^{24b,24a} E. Voevodina¹¹² F. Vogel¹¹¹ J. C. Voigt⁵¹ P. Vokac¹³⁵ Yu. Volkotrub^{87b} J. Von Ahnen⁴⁹
E. Von Toerne²⁵ B. Vormwald³⁷ V. Vorobel¹³⁶ K. Vorobej³⁸ M. Vos¹⁶⁶ K. Voss¹⁴⁵ M. Vozak¹¹⁷
L. Vozdecky¹²³ N. Vranjes¹⁶ M. Vranjes Milosavljevic¹⁶ M. Vreeswijk¹¹⁷ N. K. Vu^{63d,63c} R. Vuillermet³⁷
O. Vujinovic¹⁰² I. Vukotic⁴⁰ I. K. Vyas³⁵ S. Wada¹⁶⁰ C. Wagner¹⁰⁵ J. M. Wagner^{18a} W. Wagner¹⁷⁴
S. Wahdan¹⁷⁴ H. Wahlberg⁹² J. Walder¹³⁷ R. Walker¹¹¹ W. Walkowiak¹⁴⁵ A. Wall¹³¹ E. J. Wallin¹⁰⁰
T. Wamorkar⁶ A. Z. Wang¹³⁹ C. Wang¹⁰² C. Wang¹¹ H. Wang^{18a} J. Wang^{65c} P. Wang⁹⁸ R. Wang⁶²
R. Wang⁶ S. M. Wang¹⁵² S. Wang^{63b} S. Wang¹⁴ T. Wang^{63a} W. T. Wang⁸¹ W. Wang¹⁴ X. Wang^{114a}
X. Wang¹⁶⁵ X. Wang^{63c} Y. Wang^{63d} Y. Wang^{114a} Y. Wang^{63a} Z. Wang¹⁰⁸ Z. Wang^{63d,52,63c} Z. Wang¹⁰⁸
A. Warburton¹⁰⁶ R. J. Ward²¹ N. Warrack⁶⁰ S. Waterhouse⁹⁷ A. T. Watson²¹ H. Watson⁵³ M. F. Watson²¹
E. Watton^{60,137} G. Watts¹⁴² B. M. Waugh⁹⁸ J. M. Webb⁵⁵ C. Weber³⁰ H. A. Weber¹⁹ M. S. Weber²⁰
S. M. Weber^{64a} C. Wei^{63a} Y. Wei⁵⁵ A. R. Weidberg¹²⁹ E. J. Weik¹²⁰ J. Weingarten⁵⁰ C. Weiser⁵⁵
C. J. Wells⁴⁹ T. Wenaus³⁰ B. Wendland⁵⁰ T. Wengler³⁷ N. S. Wenke¹¹² N. Wermes²⁵ M. Wessels^{64a}
A. M. Wharton⁹³ A. S. White⁶² A. White⁸ M. J. White¹ D. Whiteson¹⁶² L. Wickremasinghe¹²⁷
W. Wiedenmann¹⁷³ M. Wielers¹³⁷ C. Wiglesworth⁴³ D. J. Wilbern¹²³ H. G. Wilkens³⁷ J. J. H. Wilkinson³³
D. M. Williams⁴² H. H. Williams¹³¹ S. Williams³³ S. Willocq¹⁰⁵ B. J. Wilson¹⁰³ P. J. Windischhofer⁴⁰
F. I. Winkel³¹ F. Winklmeier¹²⁶ B. T. Winter⁵⁵ J. K. Winter¹⁰³ M. Wittgen¹⁴⁷ M. Wobisch⁹⁹ T. Wojtkowski⁶¹
Z. Wolffs¹¹⁷ J. Wollrath¹⁶² M. W. Wolter⁸⁸ H. Wolters^{133a,133c} M. C. Wong¹³⁹ E. L. Woodward⁴² S. D. Worm⁴⁹
B. K. Wosiek⁸⁸ K. W. Woźniak⁸⁸ S. Wozniewski⁵⁶ K. Wraith⁶⁰ C. Wu²¹ M. Wu^{114b} M. Wu¹¹⁶
S. L. Wu¹⁷³ X. Wu⁵⁷ Y. Wu^{63a} Z. Wu⁴ J. Wuerzinger^{112,t} T. R. Wyatt¹⁰³ B. M. Wynne⁵³ S. Xella⁴³
L. Xia^{114a} M. Xia¹⁵ M. Xie^{63a} S. Xin^{14,114c} A. Xiong¹²⁶ J. Xiong^{18a} D. Xu¹⁴ H. Xu^{63a} L. Xu^{63a}
R. Xu¹³¹ T. Xu¹⁰⁸ Y. Xu¹⁵ Z. Xu⁵³ Z. Xu^{114a} B. Yabsley¹⁵¹ S. Yacoob^{34a} Y. Yamaguchi⁸⁵ E. Yamashita¹⁵⁷
H. Yamauchi¹⁶⁰ T. Yamazaki^{18a} Y. Yamazaki⁸⁶ S. Yan⁶⁰ Z. Yan¹⁰⁵ H. J. Yang^{63c,63d} H. T. Yang^{63a}
S. Yang^{63a} T. Yang^{65c} X. Yang³⁷ X. Yang¹⁴ Y. Yang⁴⁵ Y. Yang^{63a} Z. Yang^{63a} W.-M. Yao^{18a} H. Ye^{114a}
H. Ye⁵⁶ J. Ye¹⁴ S. Ye³⁰ X. Ye^{63a} Y. Yeh⁹⁸ I. Yeletskikh³⁹ B. Yeo^{18b} M. R. Yexley⁹⁸ T. P. Yildirim¹²⁹
P. Yin⁴² K. Yorita¹⁶¹ S. Younas^{28b} C. J. S. Young³⁷ C. Young¹⁴⁷ C. Yu^{14,114c} Y. Yu^{63a} J. Yuan^{14,114c}
M. Yuan¹⁰⁸ R. Yuan^{63d,63c} L. Yue⁹⁸ M. Zaazoua^{63a} B. Zabinski⁸⁸ E. Zaid⁵³ Z. K. Zak⁸⁸ T. Zakareishvili¹⁶⁶
S. Zambito⁵⁷ J. A. Zamora Saa^{140d,140b} J. Zang¹⁵⁷ D. Zanzi⁵⁵ O. Zaplatilek¹³⁵ C. Zeitnitz¹⁷⁴ H. Zeng¹⁴
J. C. Zeng¹⁶⁵ D. T. Zenger, Jr.²⁷ O. Zenin³⁸ T. Zeniš^{29a} S. Zenz⁹⁶ S. Zerradi^{36a} D. Zerwas⁶⁷ M. Zhai^{14,114c}
D. F. Zhang¹⁴³ J. Zhang^{63b} J. Zhang⁶ K. Zhang^{14,114c} L. Zhang^{63a} L. Zhang^{114a} P. Zhang^{14,114c} R. Zhang¹⁷³
S. Zhang¹⁰⁸ S. Zhang⁹¹ T. Zhang¹⁵⁷ X. Zhang^{63c} X. Zhang^{63b} Y. Zhang^{63c} Y. Zhang⁹⁸ Y. Zhang^{114a}
Z. Zhang^{18a} Z. Zhang^{63b} Z. Zhang⁶⁷ H. Zhao¹⁴² T. Zhao^{63b} Y. Zhao¹³⁹ Z. Zhao^{63a} Z. Zhao^{63a}
A. Zhemchugov³⁹ J. Zheng^{114a} K. Zheng¹⁶⁵ X. Zheng^{63a} Z. Zheng¹⁴⁷ D. Zhong¹⁶⁵ B. Zhou¹⁰⁸ H. Zhou⁷

N. Zhou^{63c}, Y. Zhou¹⁵, Y. Zhou^{114a}, Y. Zhou,⁷ C. G. Zhu^{63b}, J. Zhu¹⁰⁸, X. Zhu,^{63d} Y. Zhu^{63c}, Y. Zhu^{63a}, X. Zhuang¹⁴, K. Zhukov⁶⁹, N. I. Zimine³⁹, J. Zinsser^{64b}, M. Ziolkowski¹⁴⁵, L. Živković¹⁶, A. Zoccoli^{24b,24a}, K. Zoch⁶², T. G. Zorbas¹⁴³, O. Zormpa⁴⁷, W. Zou⁴², and L. Zwaliński³⁷

(ATLAS Collaboration)

¹Department of Physics, University of Adelaide, Adelaide, Australia

²Department of Physics, University of Alberta, Edmonton Alberta, Canada

^{3a}Department of Physics, Ankara University, Ankara, Türkiye

^{3b}Division of Physics, TOBB University of Economics and Technology, Ankara, Türkiye

⁴LAPP, Université Savoie Mont Blanc, CNRS/IN2P3, Annecy, France

⁵APC, Université Paris Cité, CNRS/IN2P3, Paris, France

⁶High Energy Physics Division, Argonne National Laboratory, Argonne Illinois, USA

⁷Department of Physics, University of Arizona, Tucson Arizona, USA

⁸Department of Physics, University of Texas at Arlington, Arlington Texas, USA

⁹Physics Department, National and Kapodistrian University of Athens, Athens, Greece

¹⁰Physics Department, National Technical University of Athens, Zografou, Greece

¹¹Department of Physics, University of Texas at Austin, Austin Texas, USA

¹²Institute of Physics, Azerbaijan Academy of Sciences, Baku, Azerbaijan

¹³Institut de Física d'Altes Energies (IFAE), Barcelona Institute of Science and Technology, Barcelona, Spain

¹⁴Institute of High Energy Physics, Chinese Academy of Sciences, Beijing, China

¹⁵Physics Department, Tsinghua University, Beijing, China

¹⁶Institute of Physics, University of Belgrade, Belgrade, Serbia

¹⁷Department for Physics and Technology, University of Bergen, Bergen, Norway

^{18a}Physics Division, Lawrence Berkeley National Laboratory, Berkeley California, USA

^{18b}University of California, Berkeley California, USA

¹⁹Institut für Physik, Humboldt Universität zu Berlin, Berlin, Germany

²⁰Albert Einstein Center for Fundamental Physics and Laboratory for High Energy Physics, University of Bern, Bern, Switzerland

²¹School of Physics and Astronomy, University of Birmingham, Birmingham, United Kingdom

^{22a}Department of Physics, Bogazici University, Istanbul, Türkiye

^{22b}Department of Physics Engineering, Gaziantep University, Gaziantep, Türkiye

^{22c}Department of Physics, Istanbul University, Istanbul, Türkiye

^{23a}Facultad de Ciencias y Centro de Investigaciones, Universidad Antonio Nariño, Bogotá, Colombia

^{23b}Departamento de Física, Universidad Nacional de Colombia, Bogotá, Colombia

^{24a}Dipartimento di Fisica e Astronomia A. Righi, Università di Bologna, Bologna, Italy

^{24b}INFN Sezione di Bologna, Italy

²⁵Physikalisches Institut, Universität Bonn, Bonn, Germany

²⁶Department of Physics, Boston University, Boston Massachusetts, USA

²⁷Department of Physics, Brandeis University, Waltham Massachusetts, USA

^{28a}Transilvania University of Brasov, Brasov, Romania

^{28b}Horia Hulubei National Institute of Physics and Nuclear Engineering, Bucharest, Romania

^{28c}Department of Physics, Alexandru Ioan Cuza University of Iasi, Iasi, Romania

^{28d}National Institute for Research and Development of Isotopic and Molecular Technologies, Physics Department, Cluj-Napoca, Romania

^{28e}National University of Science and Technology Politehnica, Bucharest, Romania

^{28f}West University in Timisoara, Timisoara, Romania

^{28g}Faculty of Physics, University of Bucharest, Bucharest, Romania

^{29a}Faculty of Mathematics, Physics and Informatics, Comenius University, Bratislava, Slovak Republic

^{29b}Department of Subnuclear Physics, Institute of Experimental Physics of the Slovak Academy of Sciences, Kosice; Slovak Republic

³⁰Physics Department, Brookhaven National Laboratory, Upton New York, USA

³¹Universidad de Buenos Aires, Facultad de Ciencias Exactas y Naturales, Departamento de Física, y CONICET,

Instituto de Física de Buenos Aires (IFIBA), Buenos Aires, Argentina

³²California State University, California, USA

³³Cavendish Laboratory, University of Cambridge, Cambridge, United Kingdom

^{34a}Department of Physics, University of Cape Town, Cape Town, South Africa

^{34b}iThemba Labs, Western Cape, South Africa

^{34c}Department of Mechanical Engineering Science, University of Johannesburg, Johannesburg, South Africa

- ^{34d}National Institute of Physics, *University of the Philippines Diliman (Philippines)*, South Africa
^{34e}University of South Africa, Department of Physics, Pretoria, South Africa
^{34f}University of Zululand, KwaDlangezwa, South Africa
^{34g}School of Physics, *University of the Witwatersrand*, Johannesburg, South Africa
³⁵Department of Physics, *Carleton University*, Ottawa Ontario, Canada
^{36a}Faculté des Sciences Ain Chock, *Université Hassan II de Casablanca*, Morocco
^{36b}Faculté des Sciences, *Université Ibn-Tofail*, Kénitra, Morocco
^{36c}Faculté des Sciences Semlalia, Université Cadi Ayyad, LPHEA-Marrakech, Morocco
^{36d}LPMR, Faculté des Sciences, *Université Mohamed Premier*, Oujda, Morocco
^{36e}Faculté des sciences, *Université Mohammed V*, Rabat, Morocco
^{36f}Institute of Applied Physics, *Mohammed VI Polytechnic University*, Ben Guerir, Morocco
³⁷CERN, Geneva, Switzerland
³⁸Affiliated with an institute covered by a cooperation agreement with CERN
³⁹Affiliated with an international laboratory covered by a cooperation agreement with CERN
⁴⁰Enrico Fermi Institute, *University of Chicago*, Chicago Illinois, USA
⁴¹LPC, *Université Clermont Auvergne*, CNRS/IN2P3, Clermont-Ferrand, France
⁴²Nevis Laboratory, *Columbia University*, Irvington New York, USA
⁴³Niels Bohr Institute, *University of Copenhagen*, Copenhagen, Denmark
^{44a}Dipartimento di Fisica, *Università della Calabria*, Rende, Italy
^{44b}INFN Gruppo Collegato di Cosenza, Laboratori Nazionali di Frascati, Italy
⁴⁵Physics Department, *Southern Methodist University*, Dallas Texas, USA
⁴⁶Physics Department, *University of Texas at Dallas*, Richardson Texas, USA
⁴⁷National Centre for Scientific Research “Demokritos”, Agia Paraskevi, Greece
^{48a}Department of Physics, Stockholm University, Sweden
^{48b}Oskar Klein Centre, Stockholm, Sweden
⁴⁹Deutsches Elektronen-Synchrotron DESY, Hamburg and Zeuthen, Germany
⁵⁰Fakultät Physik, *Technische Universität Dortmund*, Dortmund, Germany
⁵¹Institut für Kern- und Teilchenphysik, *Technische Universität Dresden*, Dresden, Germany
⁵²Department of Physics, *Duke University*, Durham North Carolina, USA
⁵³SUPA - School of Physics and Astronomy, *University of Edinburgh*, Edinburgh, United Kingdom
⁵⁴INFN e Laboratori Nazionali di Frascati, Frascati, Italy
⁵⁵Physikalisches Institut, *Albert-Ludwigs-Universität Freiburg*, Freiburg, Germany
⁵⁶II. Physikalisches Institut, *Georg-August-Universität Göttingen*, Göttingen, Germany
⁵⁷Département de Physique Nucléaire et Corpusculaire, *Université de Genève*, Genève, Switzerland
^{58a}Dipartimento di Fisica, *Università di Genova*, Genova, Italy
^{58b}INFN Sezione di Genova, Italy
⁵⁹II. Physikalisches Institut, *Justus-Liebig-Universität Giessen*, Giessen, Germany
⁶⁰SUPA - School of Physics and Astronomy, *University of Glasgow*, Glasgow, United Kingdom
⁶¹LPSC, *Université Grenoble Alpes*, CNRS/IN2P3, Grenoble INP, Grenoble, France
⁶²Laboratory for Particle Physics and Cosmology, *Harvard University*, Cambridge Massachusetts, USA
^{63a}Department of Modern Physics and State Key Laboratory of Particle Detection and Electronics,
University of Science and Technology of China, Hefei, China
^{63b}Institute of Frontier and Interdisciplinary Science and Key Laboratory of Particle Physics
and Particle Irradiation (MOE), *Shandong University*, Qingdao, China
^{63c}School of Physics and Astronomy, *Shanghai Jiao Tong University*,
Key Laboratory for Particle Astrophysics and Cosmology (MOE), SKLPPC, Shanghai, China
^{63d}Tsung-Dao Lee Institute, Shanghai, China
^{63e}School of Physics, Zhengzhou University, China
^{64a}Kirchhoff-Institut für Physik, *Ruprecht-Karls-Universität Heidelberg*, Heidelberg, Germany
^{64b}Physikalisches Institut, *Ruprecht-Karls-Universität Heidelberg*, Heidelberg, Germany
^{65a}Department of Physics, *Chinese University of Hong Kong*, Shatin, N. T., Hong Kong, China
^{65b}Department of Physics, *University of Hong Kong*, Hong Kong, China
^{65c}Department of Physics and Institute for Advanced Study, *Hong Kong University of Science and Technology*,
Clear Water Bay, Kowloon, Hong Kong, China
⁶⁶Department of Physics, *National Tsing Hua University*, Hsinchu, Taiwan
⁶⁷IJCLab, *Université Paris-Saclay*, CNRS/IN2P3, 91405, Orsay, France
⁶⁸Centro Nacional de Microelectrónica (IMB-CNM-CSIC), Barcelona, Spain
⁶⁹Department of Physics, *Indiana University*, Bloomington Indiana, USA
^{70a}INFN Gruppo Collegato di Udine, Sezione di Trieste, Udine, Italy

- ^{70b}*ICTP, Trieste, Italy*
- ^{70c}*Dipartimento Politecnico di Ingegneria e Architettura, Università di Udine, Udine, Italy*
- ^{71a}*INFN Sezione di Lecce, Italy*
- ^{71b}*Dipartimento di Matematica e Fisica, Università del Salento, Lecce, Italy*
- ^{72a}*INFN Sezione di Milano, Milano, Italy*
- ^{72b}*Dipartimento di Fisica, Università di Milano, Milano, Italy*
- ^{73a}*INFN Sezione di Napoli, Napoli, Italy*
- ^{73b}*Dipartimento di Fisica, Università di Napoli, Napoli, Italy*
- ^{74a}*INFN Sezione di Pavia, Pavia, Italy*
- ^{74b}*Dipartimento di Fisica, Università di Pavia, Pavia, Italy*
- ^{75a}*INFN Sezione di Pisa, Pisa, Italy*
- ^{75b}*Dipartimento di Fisica E. Fermi, Università di Pisa, Pisa, Italy*
- ^{76a}*INFN Sezione di Roma, Italy*
- ^{76b}*Dipartimento di Fisica, Sapienza Università di Roma, Roma, Italy*
- ^{77a}*INFN Sezione di Roma Tor Vergata, Roma, Italy*
- ^{77b}*Dipartimento di Fisica, Università di Roma Tor Vergata, Roma, Italy*
- ^{78a}*INFN Sezione di Roma Tre, Roma, Italy*
- ^{78b}*Dipartimento di Matematica e Fisica, Università Roma Tre, Roma, Italy*
- ^{79a}*INFN-TIFPA, Trento, Italy*
- ^{79b}*Università degli Studi di Trento, Trento, Italy*
- ⁸⁰*Universität Innsbruck, Department of Astro and Particle Physics, Innsbruck, Austria*
- ⁸¹*University of Iowa, Iowa City IA, United States of America*
- ⁸²*Department of Physics and Astronomy, Iowa State University, Ames Iowa, USA*
- ⁸³*Istinye University, Sarıyer, İstanbul, Türkiye*
- ^{84a}*Departamento de Engenharia Elétrica, Universidade Federal de Juiz de Fora (UFJF), Juiz de Fora, Brazil*
- ^{84b}*Universidade Federal do Rio De Janeiro COPPE/EE/IF, Rio de Janeiro, Brazil*
- ^{84c}*Instituto de Física, Universidade de São Paulo, São Paulo, Brazil*
- ^{84d}*Rio de Janeiro State University, Rio de Janeiro, Brazil*
- ^{84e}*Federal University of Bahia, Bahia, Brazil*
- ⁸⁵*KEK, High Energy Accelerator Research Organization, Tsukuba, Japan*
- ⁸⁶*Graduate School of Science, Kobe University, Kobe, Japan*
- ^{87a}*AGH University of Krakow, Faculty of Physics and Applied Computer Science, Krakow, Poland*
- ^{87b}*Marian Smoluchowski Institute of Physics, Jagiellonian University, Krakow, Poland*
- ⁸⁸*Institute of Nuclear Physics Polish Academy of Sciences, Krakow, Poland*
- ⁸⁹*Faculty of Science, Kyoto University, Kyoto, Japan*
- ⁹⁰*Research Center for Advanced Particle Physics and Department of Physics, Kyushu University, Fukuoka, Japan*
- ⁹¹*L2IT, Université de Toulouse, CNRS/IN2P3, UPS, Toulouse, France*
- ⁹²*Instituto de Física La Plata, Universidad Nacional de La Plata and CONICET, La Plata, Argentina*
- ⁹³*Physics Department, Lancaster University, Lancaster, United Kingdom*
- ⁹⁴*Oliver Lodge Laboratory, University of Liverpool, Liverpool, United Kingdom*
- ⁹⁵*Department of Experimental Particle Physics, Jožef Stefan Institute and Department of Physics, University of Ljubljana, Ljubljana, Slovenia*
- ⁹⁶*School of Physics and Astronomy, Queen Mary University of London, London, United Kingdom*
- ⁹⁷*Department of Physics, Royal Holloway University of London, Egham, United Kingdom*
- ⁹⁸*Department of Physics and Astronomy, University College London, London, United Kingdom*
- ⁹⁹*Louisiana Tech University, Ruston Louisiana, USA*
- ¹⁰⁰*Fysiska institutionen, Lunds universitet, Lund, Sweden*
- ¹⁰¹*Departamento de Física Teórica C-15 and CIAF, Universidad Autónoma de Madrid, Madrid, Spain*
- ¹⁰²*Institut für Physik, Universität Mainz, Mainz, Germany*
- ¹⁰³*School of Physics and Astronomy, University of Manchester, Manchester, United Kingdom*
- ¹⁰⁴*CPPM, Aix-Marseille Université, CNRS/IN2P3, Marseille, France*
- ¹⁰⁵*Department of Physics, University of Massachusetts, Amherst Massachusetts, USA*
- ¹⁰⁶*Department of Physics, McGill University, Montreal Quebec, Canada*
- ¹⁰⁷*School of Physics, University of Melbourne, Victoria, Australia*
- ¹⁰⁸*Department of Physics, University of Michigan, Ann Arbor Michigan, USA*
- ¹⁰⁹*Department of Physics and Astronomy, Michigan State University, East Lansing Michigan, USA*
- ¹¹⁰*Group of Particle Physics, University of Montreal, Montreal Quebec, Canada*
- ¹¹¹*Fakultät für Physik, Ludwig-Maximilians-Universität München, München, Germany*
- ¹¹²*Max-Planck-Institut für Physik (Werner-Heisenberg-Institut), München, Germany*
- ¹¹³*Graduate School of Science and Kobayashi-Maskawa Institute, Nagoya University, Nagoya, Japan*

- ^{114a}*Department of Physics, Nanjing University, Nanjing, China*
^{114b}*School of Science, Shenzhen Campus of Sun Yat-sen University, China*
^{114c}*University of Chinese Academy of Science (UCAS), Beijing, China*
¹¹⁵*Department of Physics and Astronomy, University of New Mexico, Albuquerque New Mexico, USA*
¹¹⁶*Institute for Mathematics, Astrophysics and Particle Physics, Radboud University/Nikhef, Nijmegen, Netherlands*
¹¹⁷*Nikhef National Institute for Subatomic Physics and University of Amsterdam, Amsterdam, Netherlands*
¹¹⁸*Department of Physics, Northern Illinois University, DeKalb Illinois, USA*
^{119a}*New York University Abu Dhabi, Abu Dhabi, United Arab Emirates*
^{119b}*United Arab Emirates University, Al Ain, United Arab Emirates*
¹²⁰*Department of Physics, New York University, New York New York, USA*
¹²¹*Ochanomizu University, Otsuka, Bunkyo-ku, Tokyo, Japan*
¹²²*Ohio State University, Columbus Ohio, USA*
¹²³*Homer L. Dodge Department of Physics and Astronomy, University of Oklahoma, Norman Oklahoma, USA*
¹²⁴*Department of Physics, Oklahoma State University, Stillwater Oklahoma, USA*
¹²⁵*Palacký University, Joint Laboratory of Optics, Olomouc, Czech Republic*
¹²⁶*Institute for Fundamental Science, University of Oregon, Eugene, Oregon, USA*
¹²⁷*Graduate School of Science, Osaka University, Osaka, Japan*
¹²⁸*Department of Physics, University of Oslo, Oslo, Norway*
¹²⁹*Department of Physics, Oxford University, Oxford, United Kingdom*
¹³⁰*LPNHE, Sorbonne Université, Université Paris Cité, CNRS/IN2P3, Paris, France*
¹³¹*Department of Physics, University of Pennsylvania, Philadelphia Pennsylvania, USA*
¹³²*Department of Physics and Astronomy, University of Pittsburgh, Pittsburgh Pennsylvania, USA*
^{133a}*Laboratório de Instrumentação e Física Experimental de Partículas - LIP, Lisboa, Portugal*
^{133b}*Departamento de Física, Faculdade de Ciências, Universidade de Lisboa, Lisboa, Portugal*
^{133c}*Departamento de Física, Universidade de Coimbra, Coimbra, Portugal*
^{133d}*Centro de Física Nuclear da Universidade de Lisboa, Lisboa, Portugal*
^{133e}*Departamento de Física, Universidade do Minho, Braga, Portugal*
^{133f}*Departamento de Física Teórica y del Cosmos, Universidad de Granada, Granada (Spain)*
^{133g}*Departamento de Física, Instituto Superior Técnico, Universidade de Lisboa, Lisboa, Portugal*
¹³⁴*Institute of Physics of the Czech Academy of Sciences, Prague, Czech Republic*
¹³⁵*Czech Technical University in Prague, Prague, Czech Republic*
¹³⁶*Charles University, Faculty of Mathematics and Physics, Prague, Czech Republic*
¹³⁷*Particle Physics Department, Rutherford Appleton Laboratory, Didcot, United Kingdom*
¹³⁸*IRFU, CEA, Université Paris-Saclay, Gif-sur-Yvette, France*
¹³⁹*Santa Cruz Institute for Particle Physics, University of California Santa Cruz, Santa Cruz California, USA*
^{140a}*Departamento de Física, Pontificia Universidad Católica de Chile, Santiago, Chile*
^{140b}*Millennium Institute for Subatomic Physics at High Energy Frontier (SAPHIR), Santiago, Chile*
^{140c}*Instituto de Investigación Multidisciplinario en Ciencia y Tecnología, y Departamento de Física, Universidad de La Serena, Chile*
^{140d}*Universidad Andres Bello, Department of Physics, Santiago, Chile*
^{140e}*Instituto de Alta Investigación, Universidad de Tarapacá, Arica, Chile*
^{140f}*Departamento de Física, Universidad Técnica Federico Santa María, Valparaíso, Chile*
¹⁴¹*Department of Physics, Institute of Science, Tokyo, Japan*
¹⁴²*Department of Physics, University of Washington, Seattle Washington, USA*
¹⁴³*Department of Physics and Astronomy, University of Sheffield, Sheffield, United Kingdom*
¹⁴⁴*Department of Physics, Shinshu University, Nagano, Japan*
¹⁴⁵*Department Physik, Universität Siegen, Siegen, Germany*
¹⁴⁶*Department of Physics, Simon Fraser University, Burnaby British Columbia, Canada*
¹⁴⁷*SLAC National Accelerator Laboratory, Stanford California, USA*
¹⁴⁸*Department of Physics, Royal Institute of Technology, Stockholm, Sweden*
¹⁴⁹*Departments of Physics and Astronomy, Stony Brook University, Stony Brook New York, USA*
¹⁵⁰*Department of Physics and Astronomy, University of Sussex, Brighton, United Kingdom*
¹⁵¹*School of Physics, University of Sydney, Sydney, Australia*
¹⁵²*Institute of Physics, Academia Sinica, Taipei, Taiwan*
^{153a}*E. Andronikashvili Institute of Physics, Iv. Javakhishvili Tbilisi State University, Tbilisi, Georgia*
^{153b}*High Energy Physics Institute, Tbilisi State University, Tbilisi, Georgia*
^{153c}*University of Georgia, Tbilisi, Georgia*
¹⁵⁴*Department of Physics, Technion, Israel Institute of Technology, Haifa, Israel*
¹⁵⁵*Raymond and Beverly Sackler School of Physics and Astronomy, Tel Aviv University, Tel Aviv, Israel*
¹⁵⁶*Department of Physics, Aristotle University of Thessaloniki, Thessaloniki, Greece*

¹⁵⁷*International Center for Elementary Particle Physics and Department of Physics, University of Tokyo, Tokyo, Japan*

¹⁵⁸*Department of Physics, University of Toronto, Toronto Ontario, Canada*

^{159a}*TRIUMF, Vancouver British Columbia, Canada*

^{159b}*Department of Physics and Astronomy, York University, Toronto Ontario, Canada*

¹⁶⁰*Division of Physics and Tomonaga Center for the History of the Universe, Faculty of Pure and Applied Sciences, University of Tsukuba, Tsukuba, Japan*

¹⁶¹*Department of Physics and Astronomy, Tufts University, Medford Massachusetts, USA*

¹⁶²*Department of Physics and Astronomy, University of California Irvine, Irvine California, USA*

¹⁶³*University of Sharjah, Sharjah, United Arab Emirates*

¹⁶⁴*Department of Physics and Astronomy, University of Uppsala, Uppsala, Sweden*

¹⁶⁵*Department of Physics, University of Illinois, Urbana Illinois, USA*

¹⁶⁶*Instituto de Física Corpuscular (IFIC), Centro Mixto Universidad de Valencia - CSIC, Valencia, Spain*

¹⁶⁷*Department of Physics, University of British Columbia, Vancouver British Columbia, Canada*

¹⁶⁸*Department of Physics and Astronomy, University of Victoria, Victoria British Columbia, Canada*

¹⁶⁹*Fakultät für Physik und Astronomie, Julius-Maximilians-Universität Würzburg, Würzburg, Germany*

¹⁷⁰*Department of Physics, University of Warwick, Coventry, United Kingdom*

¹⁷¹*Waseda University, Tokyo, Japan*

¹⁷²*Department of Particle Physics and Astrophysics, Weizmann Institute of Science, Rehovot, Israel*

¹⁷³*Department of Physics, University of Wisconsin, Madison Wisconsin, USA*

¹⁷⁴*Fakultät für Mathematik und Naturwissenschaften, Fachgruppe Physik, Bergische Universität Wuppertal, Wuppertal, Germany*

¹⁷⁵*Department of Physics, Yale University, New Haven Connecticut, USA*

^aAlso at Department of Physics, King's College London, London, United Kingdom.

^bAlso at Institute of Physics, Azerbaijan Academy of Sciences, Baku, Azerbaijan.

^cAlso at Imam Mohammad Ibn Saud Islamic University, Saudi Arabia.

^dAlso at TRIUMF, Vancouver British Columbia, Canada.

^eAlso at Department of Physics, University of Thessaly, Greece.

^fAlso at An-Najah National University, Nablus, Palestine.

^gAlso at Department of Physics, University of Fribourg, Fribourg, Switzerland.

^hAlso at Department of Physics, Westmont College, Santa Barbara, United States of America

ⁱAlso at Departament de Fisica de la Universitat Autònoma de Barcelona, Barcelona, Spain.

^jAlso affiliated with an institute covered by a cooperation agreement with CERN.

^kAlso at The Collaborative Innovation Center of Quantum Matter (CICQM), Beijing, China.

^lAlso at Faculty of Physics, Sofia University, 'St. Kliment Ohridski', Sofia, Bulgaria.

^mAlso at Università di Napoli Parthenope, Napoli, Italy.

ⁿAlso at Institute of Particle Physics (IPP), Canada.

^oAlso at Borough of Manhattan Community College, City University of New York, New York New York, USA.

^pAlso at National Institute of Physics, University of the Philippines Diliman (Philippines), Philippines.

^qAlso at Department of Financial and Management Engineering, University of the Aegean, Chios, Greece.

^rAlso at Institutio Catalana de Recerca i Estudis Avancats, ICREA, Barcelona, Spain.

^sDeceased.

^tAlso at Technical University of Munich, Munich, Germany.

^uAlso at CMD-AC UNEC Research Center, Azerbaijan State University of Economics (UNEC), Azerbaijan.

^vAlso at Yeditepe University, Physics Department, Istanbul, Türkiye

^wAlso at Institute of Theoretical Physics, Ilia State University, Tbilisi, Georgia.

^xAlso at CERN, Geneva, Switzerland.

^yAlso at Center for Interdisciplinary Research and Innovation (CIRI-AUTH), Thessaloniki, Greece.

^zAlso at Hellenic Open University, Patras, Greece.

^{aa}Also at Department of Physics, Stellenbosch University, South Africa.

^{ab}Also at Department of Physics, California State University, Sacramento, United States of America

^{ac}Also at University of Colorado Boulder, Department of Physics, Colorado, United States of America

^{ad}Also at Département de Physique Nucléaire et Corpusculaire, Université de Genève, Genève, Switzerland.

^{ae}Also at Institut für Experimentalphysik, Universität Hamburg, Hamburg, Germany.

^{af}Also at Institute for Nuclear Research and Nuclear Energy (INRNE) of the Bulgarian Academy of Sciences, Sofia, Bulgaria.

^{ag}Also at Washington College, Chestertown, Maryland, USA.

^{ah}Also at Institute of Applied Physics, Mohammed VI Polytechnic University, Ben Guerir, Morocco.

^{ai}Also at Department of Physics, Stanford University, Stanford California, USA.